Study of Low Dimensional Systems with NEGF and RMT Approach

THESIS

Submitted in partial fulfilment

of the requirements for the degree of

DOCTOR OF PHILOSOPHY

by

Surender Pratap

Under the supervision of

Dr. Niladri Sarkar

BITS Pilani
Pilani | Dubai | Goa | Hyderabad

BIRLA INSTITUTE OF TECHNOLOGY & SCIENCE, PILANI

2016

BIRLA INSTITUTE OF TECHNOLOGY & SCIENCE PILANI-333031 (RAJASTHAN) INDIA

CERTIFICATE

This is to certify that the work reported in the Ph.D. thesis entitled **"Study of Low Dimensional Systems with NEGF and RMT Approach"**, submitted by **Surender Pratap**, ID.No. **2011PHXF030P** at Physics Department, BITS-Pilani, Pilani Campus for the award of the degree of Doctor of Philosophy (Ph.D.), is a bonafide record of his original work carried out under my supervision. This work has not been submitted elsewhere for any other degree or diploma.

Signature: ....

Dr. Niladri Sarkar

Assistant Professor,

Department of Physics,

BITS-Pilani, Pilani Campus

Date: ....

Dedicated to My family

Acknowledgements

I feel privileged to thank first and foremost my supervisor, Dr. Niladri Sarkar, although not for the common reasons but rather for the uncommon ones. I am most thankful to him for providing a stress-free environment and for his great support during the thesis work. In terms of research, he used to say that I am his supervisor. If this is true, it is only because he unsuspectingly encouraged me to remain on the conventional pathways while doing nonconventional research. I am grateful that he has been fully supportive even when mistakes were made and the progress was slow. He has also put a great amount of time on careful reading of the thesis and valuable comments upon it, for which I am grateful to him.

I would like to offer a special gratitude to the erudite members of my Doctoral Advisory Committee Prof. R.R.Mishra and Prof. Jayendra Nath Bandyopadhyay for their support, critical review and suggestions during the progress review and to review my draft thesis. I sincerely thank Prof. Anshuman Dalvi, Head of Department and Prof. Navin Singh, DRC Convener for their persistent support.

I would like to thank Prof. Asok K. Sen, retired from (SINP), for advising me to the field of localization and Quantum Chaos. Last chapter of this thesis has been done under Prof. Asok K. Sen's guidance. Also, I wish to express my gratitude to all the faculty members of physics department for their kind support time to time. The technical staff of the department, Rajeev Ji, Srikant Ji & Kundan Ji are also gratefully thanked for their help.

I would humbly express my regards to the Vice-Chancellor, Director and Deans of Birla Institute of Technology & Science (BITS), Pilani for providing me the opportunity to pursue my doctoral studies by providing necessary facilities and financial support. I would like to thank Dr. Anshuman, Unit chief Estate management for helping me with a pleasant stay in campus.

I express my gratitude to Prof. S.K Verma (Dean ARD) and Prof. Hemant Jadav (Associate Dean, ARD), for their constant official support in organizing my research work. All other staff members of ARD, Raghuveer Ji and Mahipal Ji are also gratefully thanked for their help. I would like to thank all my friends, V.Bala G, Yogesh, Satish Mohanty and Ashok Sharma. I would like to extend my warm thanks to my labmates Mr. Tridev Mishra, Mr. Ashish Pal and others for their refreshing company and continuous support. I also thank the co-scholars, in particular Mrs. Monika, Mr. Jitendra, Mrs. Keerti, Dr. Amar Singh, Ravi, Ishan Mata and others whom I could not mention for space, for moral support, diversified help, and several light-hearted moments which will always be remembered.

Finally, I owe my heartfelt gratitude to my parents, my brother who have always encouraged me to follow my heart and inspired my inquisitive mind throughout my childhood and study career. I wouldn't be here without my family and their moral support and blessings, I am grateful to them for who I am today.

Surender Pratap

Abstract

Quantum transport has become an emerging field in research day by day. Its pure mesoscopic study. We have used two approaches NEGF & RMT. Quantum transport model is presented using the NEGF(non-equilibrium Green's function) formalism. The non-equilibrium Green's function(NEGF) formalism provides a natural framework for describing quantum transport. The NEGF method originated from the seminal works of Martin and Schwinger (1959), Kadanoff and Baym (1962) and others who used the methods of many-body perturbation theory to describe the distributed entropy generating processes. In our bottom-up approach we have used elastic resistors for which entropy-driven processes are confined to the contacts and problem of our system channel here can be treated within a one-electron picture by connecting contacts to the Schrodinger equation here.

In recent years it has been a revival of interest in Random Matrix Theory (RMT), which has been discussed in second part of the thesis. In this thesis we have studied quantum transport corresponding to different systems like one-dimensional wire, CNT(Carbon Nanotube), GNR(Graphene Nanoribbon) and finally disordered one dimensional wire with Random Matrix Theory (RMT) approach. We have used non-equilibrium Green's function approach in our work also. This thesis has been divided into two parts, in first part we have studied transport corresponding to CNT, GNR and other systems. In second part of the thesis we have studied disordered wire in one-dimensional case, where application wise it leads to high mobility devices. It is pure mesoscopic study and has a lot of applications in spintronic fields. Random Matrix Theory

(RMT) has a lot of applications in different fields like in Quantum mechanics, statistics, condensed matter physics and many more areas like wireless communication etc. It deals with statistical properties of large matrices. In second part of the thesis, we have studied level spacing distributions of finite-sized one-dimensional disordered systems. As the system evolves from a quasi-ballistic to a strongly localized regime, the system crosses over from a strongly non-Wigner-Dyson type level spacing distribution to a universal Poisson distribution in the thermodynamic limit. It goes in between through regimes where the distribution seems to be a mixture of Wigner-Dyson type and Poisson distributions, thus indicating the existence of pre-localized states before the thermodynamic limit sets in.

Preface

About the thesis This thesis presents a theoretical study of the CNT, GNR and level spacing distributions of finite-sized one-dimensional disordered systems. We have used TBH(tight binding Hamiltonian) approach in our work, as well as Random Matrix Theory in our work.

To the reader

The reader is assumed to be associated or working in theoretical condensed matter physics. The main prerequisite for the reader is to have basic knowledge of statistical mechanics, Quantum mechanics and numerical techniques. The thesis requires some basic algebra which may make reader comfortable in relating our studies with the real physical processes.

Thesis outline

This thesis is divided into eight chapters, where the first, respectively are meant as background to the particular fields in devices and physics studied. In chapters (2-8), we discuss the research work that has been carried out. Here is brief discussion about the organization of the thesis.

- In **chapter 1** We discuss the basic structure and dynamics of the devices. A detailed literature review of the theoretical as well as the experimental studies that is related to our work is also present in this chapter.
- The details of the comparison between self-consistent Quantum & Semi-classical methods in **chapter 2**.
- In **chapter 3** We studied certain technologically important Nanoscale MOSFETs as closed & open Quantum systems.

- In **chapter 4** We studied coherent transport with scatterers in low dimensional systems.
- In **chapter 5 & 6** We studied the conductance & transport properties of ZGNR(zigzag graphene nanoribbon) using NEGF method.
- In **chapter 7** Introduction about Random Matrix Theory and Quantum chaos have been discussed.
- In **chapter 8** Mesoscopic Fluctuations, Two parameter Scaling and Concommitant Unusual Level Spacing Distributions in Finite 1D disordered Systems have been discussed.
- Finally, the research work is summarized in chapter "Conclusions and Future work". Here, we outline some conclusions and the future scope of the work.

Contents

List of Figures

Nomenclature

Symbols

ξ	Localization length
μ	Chemical potential
E	Fermionic energy
β	Exponent
L	System size
ρ	Density matrix
E_f	Fermi energy
l_ϕ	Inelastic scattering length
x	Scaled level spacing
V	Hopping parameter
s	Level spacing
σ	Channel conductivity
n	Electron density
H	Channel Hamiltonian

k_B	Boltzmann constant
Γ	Broadening function
T	Transmission function
$\sum_s$	Self energy matrix of source
γ	Scattering rates
V_G	Gate voltage
$\sum_D$	Self energy matrix of drain

Acronyms

W	Strength of disorder
WD	Wigner Dyson
LSD	Level Spacing Distribution
RMT	Random matrix theory
UCF	Universal conductance fluctuation
DOS	Density of States
ZGNR	Zigzag graphene nanoribbon
QW	Quantum well
LDOS	Local Density of States
SCF	Self consistent Field
FET	Field effect transistor
MOSFET	Metal oxide semiconductor field effect transistor

CNT	Carbon nanotube
NEGF	Non equilibrium Green's function
BM	Bulk modes
TBGF	Tight binding Green function
QC	Quantum Chaotic
SWCNT	Single walled carbon nanotube
SCQM	Self Consistent Quantum Methods
DNA	Deoxyribonucleic acid

Chapter 1

Introduction

1.1 Introduction to Nano-scale devices and Approaches

Due to the rapid advancements in the field of Electronics and Computer technologies, it is now possible to incorporate lots of FETs in a Laptop. FET is a three terminal device whose resistance can be controlled. This resistance can be measured by two contacts. So in a nutshell, the resistance is the channel. The two contacts are the source and the drain and the controlling part is the Gate of the FET. There is an insulator between the Gate and the channel which prevents any flow of current. But the applied Gate potential changes the condition of the channel. So we have a Gate voltage which controls the resistance of the channel and a Drain voltage which drives the current in the device. Now, the resistance can be varied between 10KΩ when the device is ON to 100MΩ when it is OFF. Hence, we can use it as a switch. In a laptop, there will be lot of such switches which do all the logical operations. Tremendous progress has occurred in last 50 years in the field of VLSI fabrication technologies. The channel length 'L' is reduced from 10μm in 1960 to of the order of less than 20nm in present day. This allows chip designers to pack

10,000 times more FETs into a chip of a given surface area. This in turn boosts the computing power several folds. What is the limit of the downscaling? Nobody knows but one thing is certain. We have to understand how to model and describe the electronic properties of the futuristic Nano-Scale devices. In order to model the flow of current in a Nano-Scale device. The first step is to draw an equilibrium energy level diagram and locate the electrochemical potential set by the source and drain contacts. To understand the flow of electrons in the channel. The first thing which is of primary importance is the availability of electronic states in the vicinity of the chemical potential. This decides the resistance of the channel. Which can be controlled by the gate voltage. The following figure describes the situation in the channel.

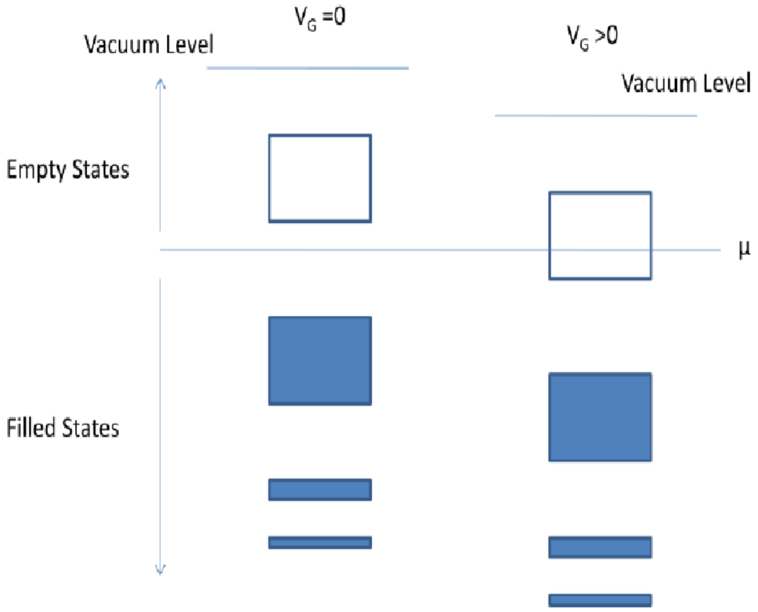

Figure 1.1: *Allowed Energy Levels inside the channel (Active region) of the device. A positive Gate Voltage* V_G *moves the energy levels down and brings the empty energy states in the vicinity of the chemical potential* μ*. The electrochemical potential is fixed by the source and drain contacts. In this case the contacts are under thermal equilibrium.*

If we connect a battery which lowers the energy levels in the drain contact with respect to the source contact. It maintains them at distinct electrochemical potentials separated by qV_D, i.e, μ_1-μ_2=qV_D. We obtain two distinct Fermi functions:

$$f_1(E) = \frac{1}{1 + exp((E - \mu_1)/k_B T)} \tag{1.1}$$

$$f_2(E) = \frac{1}{1 + exp((E - \mu_2)/k_B T)} \tag{1.2}$$

for source and drain contacts. Now, each contact will try to bring the channel into equilibrium with itself. The source will keep on pumping electrons into the channel and the drain will keep pulling out electrons from the channel thereby establishing current in the device.

A nano-scale device is a functional structure with nanoscale dimensions which performs some useful operation, for example a Nano-FET. The schematic of a Nano-FET is shown in the Fig.(1.2). The nature of the transport in such a nano-device depends on the characteristic length scales of the active region of the device. If the scattering events are very frequent as carrier travels through the active region of the device. The carrier transport will be diffusive in nature. This will be reasonably approximated by the semi-classical Boltzmann Transport Equation (BTE) [1]. Energy dissipation occurs throughout the device. The contacts are simply injectors and extractors of carriers under steady-state conditions. In contrast, if there is very little or no scattering from source to drain, the transport is then said to be ballistic. The wave nature of the charge carriers become important in terms of quantum mechanical reflection and interference from the structure itself. The overall description of the transport is given in terms of quantum mechanical fluxes and transmission [2]. The energy is no longer dissipated in the active region of the device. It dissipates at the contacts.

Describing the flow of current in these modern nano-scale devices involves some

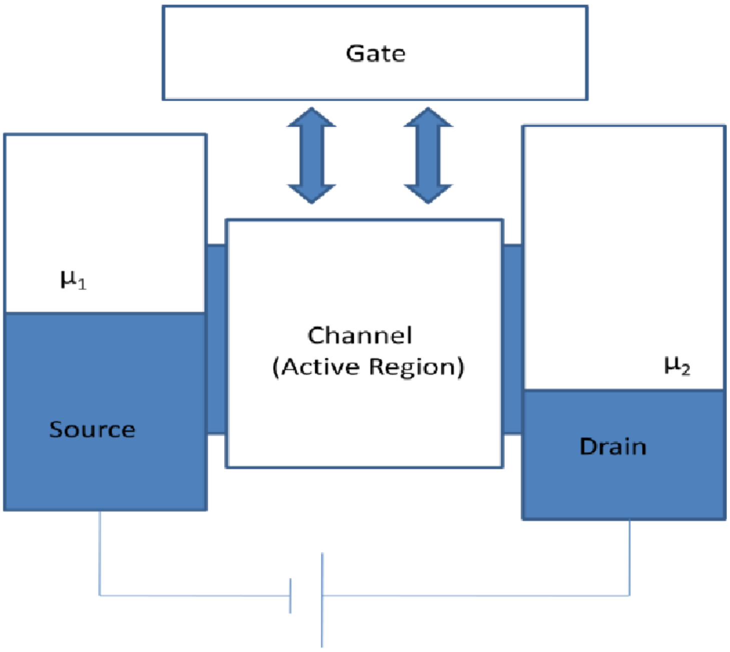

Figure 1.2: *The schematic of a generic Nano-scale FET device consisting of source and drain for charge carriers and a gate which controls the transfer characteristics of the active region.*

of the most advanced concepts of non-equilibrium statistical mechanics. The application of non-equilibrium Green's Function (NEGF) formulation provides a rigorous framework for the development of quantum device models. This actually bridges the gap between the fully coherent quantum transport models to fully incoherent Boltzmann transport models of device physics. It is only with the advent of mesoscopic physics in 1980's. The importance of the contacts in interpreting experiments became widely recognized. Prior to that, it was a common practice to ignore the contacts as minor experimental distractions. A model introduced by Landauer gained increasing popularity [3]. In this model, the conductor itself is assumed to be a wire free of all interactions. And irreversibility and dissipation arise from the connection to the contacts. This Landauer model seems relevant to the modeling of the electronic devices as they scale down to atomic dimensions. A simple quantum mechanical treatment of scattering in nano-transistors has been presented by R. Venugopal et.al [4]. Under this, they have presented a computationally efficient two dimensional quantum mechanical simulation scheme. For modeling dissipative electron transport in thin body, fully depleted, n-channel, silicon-on-insulator transistors. The simulation scheme solves the NEGF self consistently with Poisson's equation. By treating the effects of scattering, we use a simple approximation inspired by Buttiker probes which is often used in mesoscopic physics. Another work by the same group of R. Venugopal et.al. on quantum mechanical analysis of channel access geometry on nano-scale device performance has been carried out. This is based on an expansion of the device Hamiltonian in coupled mode space [5]. An efficient program for all-quantum simulation of nanometer FET using Landauer-Buttiker approach for ultra-thin body FET. The channel imperfection has been developed by V.Vyrurkov et.al. [6]. Recently, a Two-Dimensional Quantum Mechanical simulation to explore the source/drain contacts in Silicon-on Insulator(SOI) MOSFET. The dependencies of the contact resistance on the contact length, Schottky barrier height, doping concentration, SOI thickness have been investigated [7]. The study of quantum transport models for a two-dimensional nano-size double gate(DG) MOSFET using NEGF and Wigner distribution has been studied by Haiyan Jaing and Wei Cai [8]. An elementary introduction of the NEGF method has been given by P. Vogl and T. Kubis [9]. This is extremely important for consistent carrier dynamics calculations of open nanosystems, where quantum effects and incoherent scattering plays a comparable role. A theoretical investigation of the effects of dephasing in molecular junctions using atomistic first principles has been carried out by Jesse Maassen et.al. [10]. Under this, a comparison between Buttiker probe model and a more microscopic dephasing model has been carried out. A Green's function approach to study the transport through a gate-surrounded by Si nanowires with impurity scattering has been carried out by Jung Hyun Oh et.al. [11]. One of the most important work on dephasing in quantum transport using NEGF based model is done by Roksana Golizadeh-Mojarad and Supriyo Datta [12].

Apart from theoretical and simulations of nano-structure devices, there has been a rapid progress over last decade realizing functional nano-scale electronic devices based on self-assembled structures such as semiconductor nano-wires and carbon nano-tubes [13]. Semiconductor nano-wires(NWs) have been studied over the past decade. In terms of their transport properties and for nano-device applications such as resonant tunneling diodes, single electron transistors [14], and FETs. Recently, there has been a dramatic increase in interest in NWs due to the demonstration of directed self-assembly of NWs via in-situ epitaxial growth [15, 16]. Such semiconductor NWs can be epitaxial Si, Ge or III-V semiconductors. Where it has been demonstrated that such wires may be controllably doped during the growth, and abrupt compositional changes can form high-quality 1D hetrojunctions. Nano-wire FETs, bipolar devices and complementary inverters have been synthesized using such techniques. The ability to controllably fabricate heterostructure nano-wires has lead to the demonstration of nanoscale devices such as resonant tunneling diodes and single electron transistors. The scalability of arrays of such nano-wires to circuits and architectures have also been addressed. However, the primary difficulty at present is in the ability to grow and orient NWs with desired location and direction.

Another material which is very useful for fabrication of nano-scale devices is carbon nanotubes. Singled-walled (SW) carbon nano-tubes(CNTs) are a tubular form of carbon with diameters as small as 1nm and lengths of a few nm to microns. Due to their remarkable electronic and mechanical properties, CNT's are currently of interest. For a number of application including interconnects, CNT-based molecular electronics, AFM based imaging, nanomanipulation, nanotube sensors for force and pressure. The chemical nature, nanotube biosensors, molecular motors, nanoelectromechanical systems, hydrogen and lithium storage, and field emitters for instrumentation including flat panel displays. In terms of transport properties, experiments have demonstrated very high mobilities and nearly ballistic transport

[17, 18]. Complimentary n and p channel transistors have been fabricated from CNTs and basic logic functions have been demonstrated [19]. Again as with semiconductor nanowires, the primary difficulty faced today in a fabrication technology is the directed growth of CNTs with desired chirality and positioning on a semiconductor surface, suitable for large scale production.

1.2 Introduction to NEGF and RMT

1.2.1 NEGF Method

Now, we may begin by considering a small device with one energy level in the channel as shown in Fig.(1.3). If we consider $\frac{\gamma_1}{\hbar}$ and $\frac{\gamma_2}{\hbar}$ as the rates at which an electron placed initially in the level ϵ will escape into the source and drain contacts. The steady current in the one level channel can be given as

$$I = \frac{2q}{\hbar}\frac{\gamma_1\gamma_2}{\gamma_1+\gamma_2}[f_1(E) - f_2(E)] \tag{1.3}$$

We apply a small voltage (V_D) across the contacts which split the electrochemical potential as shown Fig.(1.3). We may write the current through this device by assuming $\mu_1 > \epsilon > \mu_2$. Here, the temperature is low enough so that $f_1(\epsilon) \approx 1$ and $f_1(\epsilon) \approx 0$. Hence, the expression of the current through the channel becomes,

$$I = \frac{2q}{\hbar}\frac{\gamma_1\gamma_2}{\gamma_1+\gamma_2} = \frac{q\gamma_1}{\hbar} \tag{1.4}$$

if γ_1=γ_2. Therefore, we can pump unlimited current through this device by increasing the value of γ_1. However, there is a limit to the maximum value of conductance (G_0) for a one level device [20].

What we have missed is the broadening of the level that is due to the coupling of the channel with the contacts. The broadening causes the part of the energy level

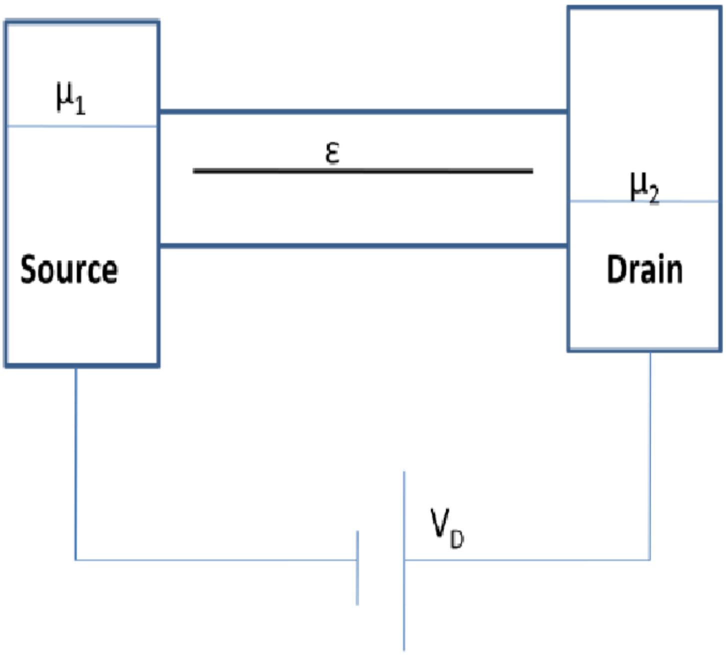

Figure 1.3: *A one-level device channel with energy* ϵ*.*

to spread outside the energy range between μ_1 and μ_2.

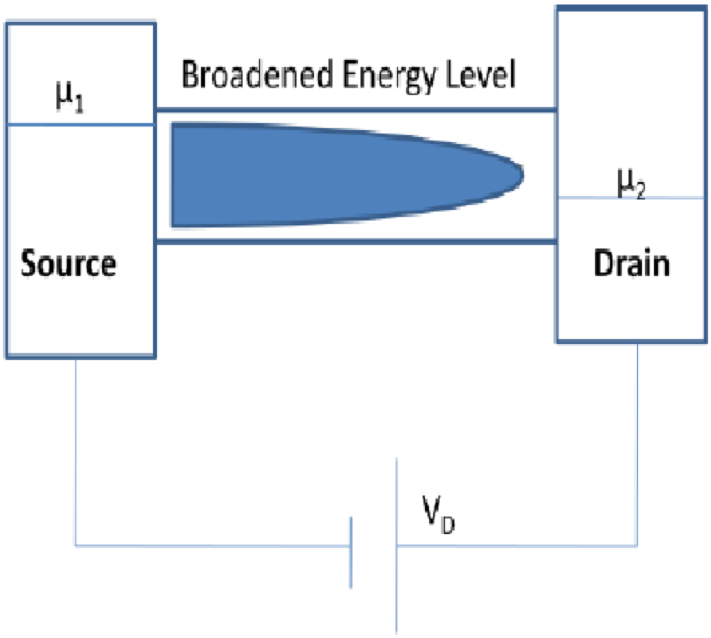

Figure 1.4: *Coupling of channel with the contacts broadens the energy level, thereby spreading part of the energy level outside the range between* μ_1 *and* μ_2*.*

The actual current will now be given as:

$$I = \frac{2q}{\hbar} \int_{-\infty}^{\infty} D_{\epsilon}(E) \frac{\gamma_1 \gamma_2}{\gamma_1 + \gamma_2} [f_1(\epsilon) - f_2(\epsilon)] dE \tag{1.5}$$

where, $D_{\epsilon}(E)$ is the broadened density of states(DOS).

So far we have talked about one-level channel for small conductors. This model helps us to identify important concepts underlying the flow of current through a channel, namely the location of the electrochemical potential relative to the DOS. The broadening of the levels due to coupling with the contacts and existence of a conduction maximum G_0. Now, the challenge will be to make a transition from one-level to multi-level channels with N energy levels. This is bottom-up approach, i.e. from small scale atomistic transport to intermediate ballistic transport to finally diffusive transport.

Under this, we have the following changes. The single energy level ϵ will become N×N Hamiltonian matrix [H]. The term $\gamma_{1,2}$ which is the broadening term will become a broadening matrix, $[\Gamma_{1,2}(\mathrm{E})]$. The effect of the contacts will be described by the 'self energy' matrix, $\sum_{1,2}(\mathrm{E})$. Now, all the above quantities can be worked out using NEGF method which is described and applied in chapter 3 and 4 and 5 of this thesis. The Fig.(1.5) shows a schematic for multilevel channel. There is an enormous amount of physics behind general matrix model. These issues have taken up in this thesis which give an in-depth view of the transport in Nano-Scale devices. Which establishes a bottom up view of the things i.e., from 'Ballistic Transport to Ohms law'.

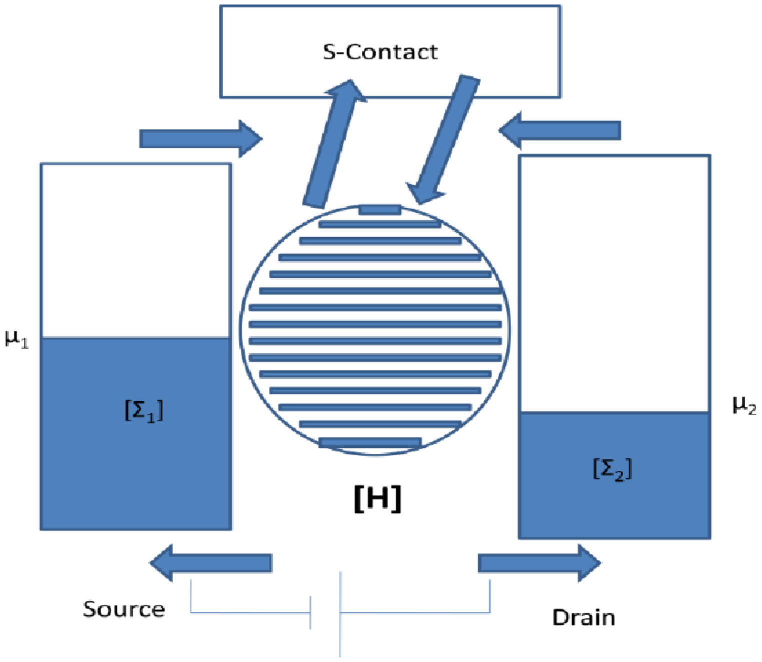

Figure 1.5: *A general matrix model of a multi-level channel. The 's-contact' describes the incoherent scattering processes.*

1.2.2 Random Matrix Theory

Random matrix theory (RMT) was developed in the (1950-1960) by Wigner, Dyson, Mehta and others. In basic statistical mechanics a commensurable renunciation of exact knowledge is made. By surmising all states of a very large ensemble to be equally probable. One can obtain useful information about the over-all behavior of an intricate system, when the observation of the state of the system in all its detail is infeasible. This kind of statistical mechanics is clearly no enough for the discussion of nuclear energy levels. We wish to make verbal expressions about the fine detail of the level structure. Such verbal expressions cannot be made in terms of an ensemble of states. What is here required is an incipient kind of statistical mechanics. In which we renounce exact knowledge, not of the state of the system but of the nature of the system itself. We picture an intricate nucleus as a "black box" in which a large number of particles are interacting according to unknown laws. The problem is then to define in a mathematically precise way an ensemble of systems in which all possible laws of interaction are equally probable [21].

Originally conceived to bring some order into the spectra of complex nuclei. The attraction in random matrix theory was renewed enormously when Bohigas, Giannoni and Schmit conjectured that it should be applicable to the spectra of all chaotic systems [22]. In the following years a lot of evidence has been obtained that this conjecture is true [23].

We study level spacing distributions of finite-sized one-dimensional disordered systems. Density of states of finite-sized one-dimensional disordered system has been discussed for various system sizes and different strength of the disorder system. Disorder effects have started to show up somewhat more prominently in the sense that the level broadening is relatively larger and the overlap between two broadened levels are now enough to rule out any energy-gap between them. One notices that N very prominent peaks therein corresponding to N distinct energy levels in the pure case (disorder is zero). Although the charge carriers are still quasi-ballistic, because the N peaks are quite well-separated except near their bottommost parts. We are putting together the random spectra of many different configurations, not for any averaging process, but just for a clearer visualization of the DOS. For the pure case, the sharp levels at the two ends of the spectrum cause vertical drops of the DOS to zero at the two band edges. But in the impure case, the levels at the ends of the spectrum (just like others) do get broader, and the sharp drop of the density of states is softened by an exponential drop to zero. It is observed in our work that the DOS at the two outer peaks have increased from a value of slightly less than 0.8 (for N=31) to a value of slightly larger than 0.8 (for N=41). Of course, this has happened at the cost of lowering the DOS at the band-centre (E=0) slightly.

As the system evolves from a quasi-ballistic to a strongly localized regime, the system crosses over from a strongly non-Wigner-Dyson type level spacing distribution to a universal Poisson distribution in the thermodynamic (length of the chain approaches to infinity) limit. In between it goes through regimes where the distribution seems to be a mixture of Wigner-Dyson type and Poisson type distributions, thus indicating the existence of prelocalized states before the thermodynamic limit sets in. In the case of a finite, closed quantum system, we did look at the finite number of random energy eigenstates and the corresponding finite number of random nearest level spacings. Kubo formula indicates that the random level spacing distribution should also be unusual in the same regime in which the mesoscopic conductance fluctuations is so, i.e., in the two parameter scaling regime. Introduction of RMT has been briefly explained in Chap.7 and calculation part has been discussed in Chap.8 of the thesis.

1.3 Organization of the Thesis

This thesis is organized into eight chapters. After this chapter on general introduction on Nano-scale devices and approaches, Chap.2 gives a detailed comparison between Self-Consistent Quantum and Semi-classical methods. Under this, a self-consistent scheme is used to solve the Schrodinger-Poisson equations inside the channel of a Nano-Scale dual gate MOSFET. In Chap.3, we study certain technologically important Nano-scale MOSFETs as Closed and Open Quantum systems. Here, we explain and apply NEGF method on SWCNT-based MOSFET. In Chap.4, we studied coherent transport with Scatterers in low dimensional systems. In Chap.5 and Chap.6 we studied the conductance and transport properties of ZGNR under certain conditions using NEGF method. In Chap.7 and Chap.8 we studied level spacing distributions of finite-sized one-dimensional disordered systems.

Chapter 2

Comparison of the Self-Consistent Quantum & Semi-classical Methods & Size Quantization effect in Nano-Scale dual gate-MOSFET

2.1 Introduction

Because of the quick headways in the field of electronics and Computer advancements, it is now possible to incorporate lots and lots of FETs in the core of a tablet [2]. FET is a three terminal device where gate voltage controls the channel resistance. Gate and the channel are separated by insulator that prevents any flow of current which essentially isolates it from the channel. The current-voltage relationship for a MOSFET can be modeled with Ohm's law $j = \sigma \mathrm{E}$, where the channel conductivity is given by $\sigma = q\mu_n n_{3D}$, where μ_n is the electron mobility in the channel and n_{3D} is the electron density in the inversion layer. This model works very well for microelectronic devices with diffusive transport. However, for very clean Nano-Scale devices of the future, the transport properties will be governed by quantum effects [24]. One of the most pronounced effect will be the distribution of the channel electron density as a function of channel thickness and temperature. Since the channel electron density changes as a function of the applied gate voltage, hence it becomes extremely important to study the variation of the channel electron density which will finally dictate the I-V characteristics of the futuristic Nano-Scale devices.

Due to the advancement of high-performance computers, it is now possible to do very advanced simulations using Finite-Difference and Finite Element Methods [24]. Hence, a Self-Consistent scheme for the determination of the channel electron density of a Nano-Scale device is extremely important. Lot of very good work has been done on self-consistent schemes using self-consistent Schrodinger-Poisson and Semi-classical methods. Several of these schemes have been successfully applied on various quantum structures [25]. Also there exist various commercial tools for microelectronic device simulations for the current industrial requirements. Hence, it is of greater academic interest that the codes for the futuristic Nano-Scale devices are developed with a view to serve the future needs. Hence, knowledge of the simulation and the discretization procedures are extremely important for understanding the inner workings and physical viability of these codes. The generic device which we will use for our analysis will be a dual gate MOS capacitor which is shown in Fig.(2.1). For Nano-Scale devices, the channel electron density at room temperature should be calculated from the diagonal elements of the density matrix using Self-Consistent Schrodinger-Poisson method. Another method will be the Semi-Classical approach where the electron density n is given as $n_{3D} = 2(\frac{2m_e^* kT}{2\pi\hbar^2}) f_{1/2}(\frac{E_c - \mu + U(z)}{k_B T})$ where $f_{1/2}$ is the Fermi Dirac integral of the order j=1/2. Similarly, the 2D electron density can be calculated using the Semi-Classical method. Effect of the size quantization is very well reflected when we calculate the electron density using Schrodinger-Poisson approach. However, when we increase the channel thickness, the result obtained by Schrodinger-Poisson approach matches with the Semi-Classical approach. Hence, it is extremely important to understand the strength and weaknesses of these simulation methods as required for calculating the channel electron densities under different regimes. This will be required for the correct interpretation of the I-V characteristics of the futuristic Nano-Scale devices.

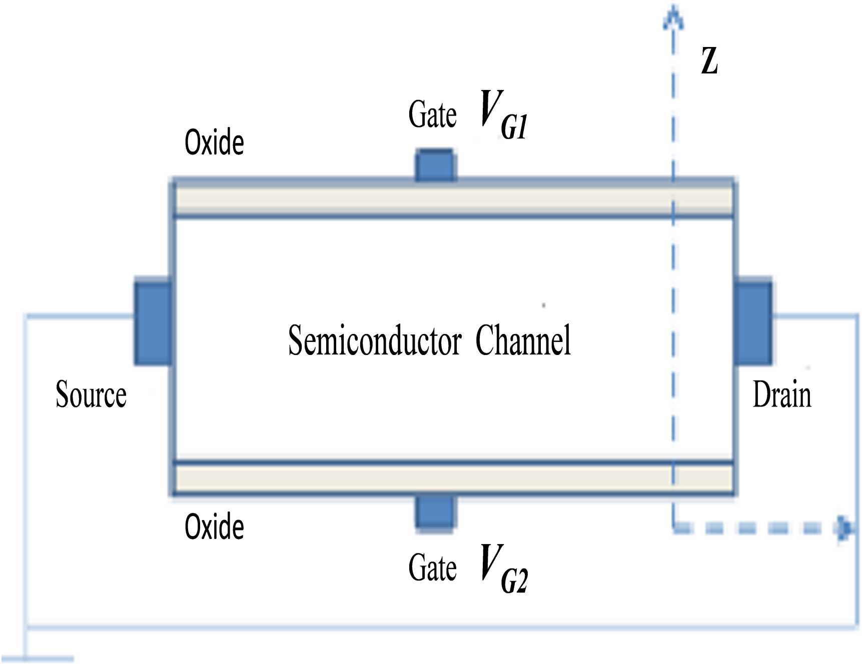

Figure 2.1: *A dual gate Nano-Scale MOSFET with source and drain grounded to zero potential.*

2.2 Theoretical Background

To understand the flow of electrons in a channel, the first thing which is of prime importance is the availability of electronic states in the vicinity of the chemical potential μ [2, 26]. This distinguishes metals from semiconductors. For metals, according to band theory, there is unfilled band which gives a lot of available states for the conduction electrons. On the other hand for a semiconductor there may be fewer or no available states around the chemical potential. Therefore, positive/negative gate voltage is required to bring the empty/filled electronic states in the vicinity of μ. Fig.(2.2) shows the available empty/filled states in the vicinity of the chemical potential. The role of the gate voltage here is to bring the electronic states near the chemical potential μ. This electro-chemical potential is fixed by the source and drain contacts. For this analysis, it is assumed that the contacts are under thermal equilibrium with the channel and are grounded. Although the gate is not under equilibrium with the channel, however the insulator between gate electrode and the channel blocks the flow of electrons from gate to the channel. The gate voltage moves the energy bands up and down around μ to condition the channel resistance. The aim of this work is to calculate the electron distribution, n(z) in the channel as a function of applied gate voltage by using self-consistent Quantum and Semi-Classical simulation methods.

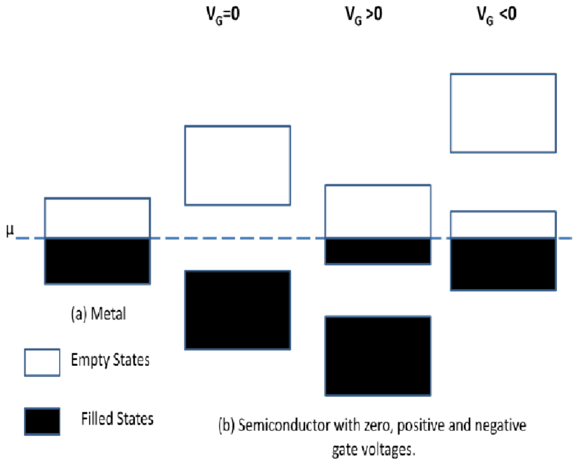

Figure 2.2: *A comparison of the available electronic states in the vicinity of the chemical potential* μ *for (a) metal and (b) Semiconductor channel under zero, positive and negative gate voltages.*

2.3 Self Consistent Quantum and Semi-Classical Simulation Methods

2.3.1 Self Consistent Quantum Methods Using Schrodinger-Poisson Equations

Here, we are modeling a dual gate MOS capacitor with channel thickness of the order of few nanometers. The problem has quantum confinement along z-axis and we apply periodic boundary conditions (PBC) in the x-y plane. This is a good approximation as the channel length and width dimensions are much larger than its thickness. Hence, the eigenfunction in the channel can be given as

$$\psi_N(k_x, k_y, m) = Ae^{ik_x x}e^{ik_y y}\chi_m(z) \tag{2.1}$$

Therefore Schrodinger equation becomes

$$\left(-\frac{\hbar^2}{2m_e^*}\frac{\mathrm{d}^2}{\mathrm{d}x^2} - \frac{\hbar^2}{2m_e^*}\frac{\mathrm{d}^2}{\mathrm{d}y^2} - \frac{\hbar^2}{2m_e^*}\frac{\mathrm{d}^2}{\mathrm{d}z^2} + E_c + U(z)\right)\psi_N = E_N\psi_N \tag{2.2}$$

Here, E_c is the conduction band edge and U(z) is variation of the potential due to applied gate voltages along z-axis. Since, we are applying PBC in the x-y plane, hence, the above equation becomes effectively a 1D problem, where it can be solved using numerical methods for any given values of k_x and k_y, so we can obtain the value of E_N as

$$E_N = E_m + \frac{\hbar^2}{2m_e^*}(k_x^2 + k_y^2) \tag{2.3}$$

Here, E_m is calculated from the 1D version of Eq.(2.2) given as

$$\left(-\frac{\hbar^2}{2m_e^*}\frac{\mathrm{d}^2}{\mathrm{d}z^2} + E_c + U(z)\right)\chi_m = E_m\chi_m \tag{2.4}$$

$$[H_z + U]\chi_m(z) = E_m\chi_m(z) \tag{2.5}$$

So the problem reduces to solving one-dimensional Schrodinger-Poisson equation. Here, 'H_z' is the Hamiltonian for the Oxide/Semiconductor/Oxide material without any gate bias and 'U(z)' is the variation of the potential along z-axis due to the applied gate voltages. Here the device is working at room temperature. Hence, the eigenstates will be partially occupied and the channel electron density at equilibrium can be given as,

$$n_{2D}(z) = \frac{2}{L^2}\sum_m \sum_{k_x,k_y} |\chi_m(z)|^2 f(E_N - \mu) \tag{2.6}$$

where

$$f(E_N - \mu) = \frac{1}{1 + exp(E_N - \mu)/k_BT} \tag{2.7}$$

is the Fermi-Dirac distribution function. Now, the summation over k_x and k_y in the Eq.(2.6) can be reduced to an integral form as

$$\frac{1}{L^2}\sum_{k_x,k_y} f(E_N - \mu) \rightarrow \frac{1}{L^2}\sum_{k_x,k_y} \frac{1}{1 + exp(\Delta/k_BT)} = \int_0^\infty \frac{2\pi k dK}{4\pi^2}\frac{1}{1 + exp(\Delta/k_BT)} \tag{2.8}$$

where, $E_m + \frac{\hbar^2}{2m_e^*}(k_x^2 + k_y^2 - \mu) = \Delta$

$$f_{2D}(E_c + U(z) - \mu) = \frac{m_e^* k_BT}{2\pi\hbar^2} ln\left(1 + exp\left(-\frac{E_c + U(z) - \mu}{k_BT}\right)\right) \tag{2.9}$$

Hence, we have the final form of n(z) as,

$$n_{2D}(z) = 2\sum_m |\chi_m(z)|^2 f_{2D}(E_c + U(z) - \mu) \tag{2.10}$$

Now, this reduces to an interesting electrostatic problem where the solution to the Poisson's equation can be uniquely determined for a given boundary condition [1, 2].

In this case, the gate voltages V_{G_1} and V_{G_2} provide the boundary conditions for this problem. The Poisson's equation will be given as,

$$\nabla^2 U = \frac{-q^2}{\epsilon_r \epsilon_0} \left(n_{2D}(z) - n_0 \right) \tag{2.11}$$

Here, n_0 is the background concentration. Now, the Schrodinger equation and the Poisson equation are to be solved self-consistently for obtaining the channel electron concentration, n(z), Eq.(2.5),(2.10) and Eq.(2.11). Fig.(2.3) shows the self consistent scheme for Quantum method using Schrodinger-Poisson's equations.

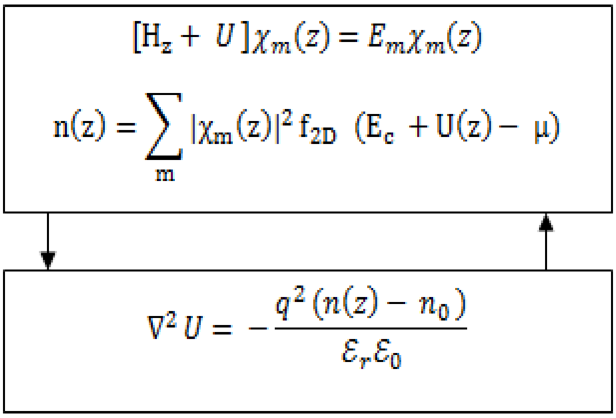

Figure 2.3: *Self-Consistent Procedure for Quantum Method.*

2.4 Self-Consistent Semi-Classical Methods Using Periodic Boundary Conditions (PBC)

Generally PBC's are used for approximating a very large system by small term called unit cell, while here we have assumed that the last point is connected back to the starting point of our system, so that there are no ends now. We are interested in the properties of the interior of structure, so what we are assuming at the boundaries should not affect our results physically [27]. The Semi-Classical approach is used when we assume periodic boundary condition along all the directions. The eigenfunction in the channel can be given as,

$$\psi_N(\vec{k},\vec{r}) = Ae^{i\vec{k}.\vec{r}} \tag{2.12}$$

Now, the electron density will be

$$n_{3D} = \frac{2}{L^3}\sum_{k_x,k_y,k_z} f(E_N-\mu) \tag{2.13}$$

with

$$E_N = E_c + \frac{\hbar^2(k_x^2+k_y^2+k_z^2)}{2m_e^*} + U(z) \tag{2.14}$$

$$\frac{2}{L^3}\sum_{k_x,k_y,k_z} f(E_N-\mu) \to 2\int_0^\infty \frac{4\pi k^2}{8\pi^3}\frac{dk}{1+exp(E_c-\mu+\frac{\hbar^2k^2}{2m_e^*}+U(z))} \tag{2.15}$$

$$\Longrightarrow 2(\frac{m_e^*k_BT}{2\pi\hbar^2})^{3/2}\frac{2}{\sqrt{\pi}}\int_0^\infty \frac{d\zeta\sqrt{\zeta}}{1+exp(E_c-\mu+U(z)/k_BT)}\frac{1}{exp(\zeta)} \tag{2.16}$$

where

$$\zeta = \frac{\hbar^2k^2}{2m_ck_BT} \tag{2.17}$$

which becomes

$$2\left(\frac{m_e^*k_BT}{2\pi\hbar^2}\right)^{3/2} f_{1/2}\left(\frac{E_c-\mu+U(z)}{k_BT}\right) \tag{2.18}$$

The electron density in the channel will vary in the presence of the potential U(z). Fig.(2.4) and Fig.(2.5) represents the scheme for calculating the channel densities using semiclassical methods. Here, the integration is performed over all the three directions in k-space. E_c is the energy of the conduction band edge and $F_{1/2}$ is the Fermi-Dirac integral of the order $j = \frac{1}{2}$. This will be required for calculating the 3D channel electron concentration of the device. It is not possible to solve $f_{1/2}$

analytically.

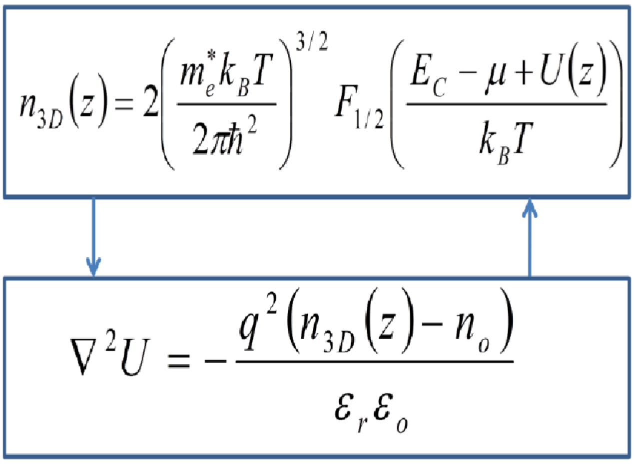

$$n_{3D}(z) = 2\left(\frac{m_e^* k_B T}{2\pi\hbar^2}\right)^{3/2} F_{1/2}\left(\frac{E_C - \mu + U(z)}{k_B T}\right)$$

$$\nabla^2 U = -\frac{q^2\left(n_{3D}(z) - n_o\right)}{\varepsilon_r \varepsilon_o}$$

Figure 2.4: *Self-Consistent Procedure for Semi-Classical Method for determining 3D electron density.*

However, it is very easy to calculate it numerically. The electron density in the channel will vary in the presence of the potential U(z).

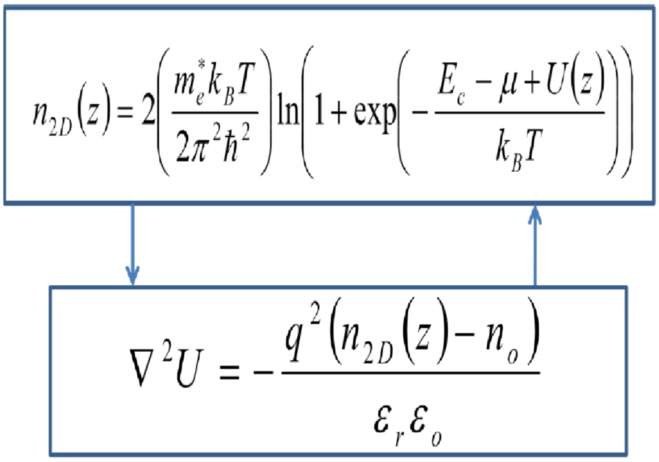

$$n_{2D}(z) = 2\left(\frac{m_e^* k_B T}{2\pi^2\hbar^2}\right)\ln\left(1 + \exp\left(-\frac{E_c - \mu + U(z)}{k_B T}\right)\right)$$

$$\nabla^2 U = -\frac{q^2\left(n_{2D}(z) - n_o\right)}{\varepsilon_r \varepsilon_o}$$

Figure 2.5: *Self Consistent Procedure for Semi-Classical Method for determining 2D electron density.*

2.5 Discretization Techniques

2.5.1 Discretization Procedure for the Self-Consistent Quantum Method

The 1D Schrodinger equation $[H_z + U]\chi_m(z) = E_m\chi_m(z)$, which we obtained in earlier section can be discretized by finite-difference method [28].

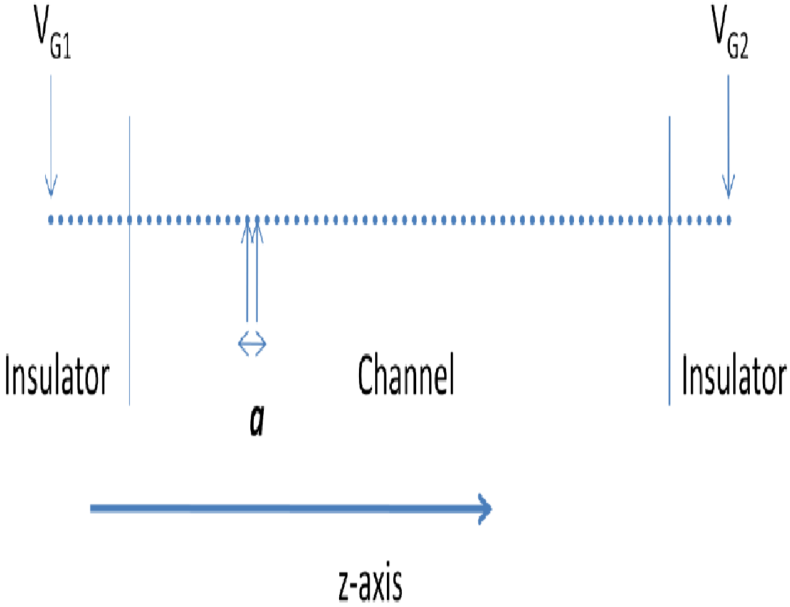

Figure 2.6: *1D discretized picture of the dual gate MOS capacitor along z-axis.*

Fig.(2.6) shows the 1D discretized picture of the dual gate MOS capacitor along z-axis. We use central difference method for calculating the second derivative of the wave function. The space is discretized by n+2 points which is shared between the insulators and the channel thickness of the dual MOS capacitor. The distance between two consecutive points is a and if there are k points inside the channel, then the channel thickness is (k+1)a. The term $H_z + U$ is given as $H_z + U \rightarrow -\frac{\hbar^2}{2m_e^*}\frac{\mathrm{d}^2}{\mathrm{d}z^2} + E_c + U(z)$, where E_c is the energy of the conduction band edge and U(z) is the variation in the potential due to applied gate voltages. Now, by finite-differencing the term

$$\left(-\frac{\hbar^2}{2m_e^*}\frac{\mathrm{d}^2}{\mathrm{d}z^2}+E_c+U(z)\right)\chi_m(z)=E_m\chi_m(z)$$

we obtain a set of 'n' linear equations as shown below [29]

$$\left(-\frac{\hbar^2}{2m_e^*}\frac{\mathrm{d}^2}{\mathrm{d}z^2}+E_c+U(z)\right)\chi_m(z)=E_m\chi_m(z) \tag{2.19}$$

$$\rightarrow \frac{-\hbar^2}{2m_e^*a^2}(\chi_{n+1}-2\chi_n+\chi_{n-1})+E_c\chi_n+U_n\chi_n=E_n\chi_n \tag{2.20}$$

$$\frac{-\hbar^2}{2m_e^*a^2}(\chi_n-2\chi_{n-1}+\chi_{n-2})+E_c\chi_{n-1}+U_{n-1}\chi_{n-1}=E_{n-1}\chi_{n-1} \tag{2.21}$$

- -

$$\frac{-\hbar^2}{2m_e^*a^2}(\chi_k-2\chi_{k-1}+\chi_{k-2})+E_c\chi_{k-1}+U_{k-1}\chi_{k-1}=E_{k-1}\chi_{k-1} \tag{2.22}$$

- -

$$\frac{-\hbar^2}{2m_e^*a^2}(\chi_2-2\chi_1+\chi_0)+E_c\chi_1+U_1\chi_1=E_1\chi_1 \tag{2.23}$$

Now, a $N\times N$ tridiagonal Hamiltonian Matrix [H] can be constructed by truncating χ_{n+1} and χ_0 terms as

$$H=\begin{pmatrix}\frac{\hbar^2}{m_e^*a^2}+E_c+U_n & \frac{-\hbar^2}{2m_e^*a^2} & \dots & 0 & 0\\ \frac{-\hbar^2}{2m_e^*a^2} & \frac{\hbar^2}{m_e^*a^2}+E_c+U_{n-1} & \dots & 0 & 0\\ 0 & \frac{-\hbar^2}{2m_e^*a^2} & \dots & \frac{-\hbar^2}{2m_e^*a^2} & 0\\ \dots & \dots & \dots & \frac{\hbar^2}{m_e^*a^2}+E_c+U_2 & \frac{-\hbar^2}{2m_e^*a^2}\\ 0 & 0 & \dots & \frac{-\hbar^2}{2m_e^*a^2} & \frac{\hbar^2}{m_e^*a^2}+E_c+U_1\end{pmatrix} \tag{2.24}$$

From this Hamiltonian Matrix, the electron density n(z) can be calculated from the diagonal elements of the density matrix given as [1, 30]

$$\rho(z, \acute{z}) = \sum_{m} \chi_m(z) f_{2D}(H - \mu I) \chi_m^*(\acute{z}) \tag{2.25}$$

While solving the above Hamiltonian matrix [H], care must be taken while entering the values of the effective masses. For the two oxide sides, it is m_e^* (oxide) and in between for the channel, it should be m_e^*(channel). However, at the boundary between the oxide and channel, there is an abrupt change in the value of the effective masses. This is reflected as a small peak in the electron density at the oxide/semiconductor interface [31]. Similarly, the Poisson's equation is discretized in the same manner using finite difference method as:

$$\frac{-\mathrm{d}^2 U(z)}{\mathrm{d}z^2} = \frac{q^2}{\epsilon_r \epsilon_0}(n(z) - n_0) \rightarrow \tag{2.26}$$

$$\frac{-1}{a^2}(U_{n+1} - 2U_n + U_{n-1}) = \frac{q^2}{\epsilon_r \epsilon_0}(n_n - n_0) \tag{2.27}$$

$$\frac{-1}{a^2}(U_n - 2U_{n-1} + U_{n-2}) = \frac{q^2}{\epsilon_r \epsilon_0}(n_{n-1} - n_0) \tag{2.28}$$

- -

$$\frac{-1}{a^2}(U_k - 2U_{k-1} + U_{k-2}) = \frac{q^2}{\epsilon_r \epsilon_0}(n_{k-1} - n_0) \tag{2.29}$$

- -

$$\frac{-1}{a^2}(U_2 - 2U_1 + U_0) = \frac{q^2}{\epsilon_r \epsilon_0}(n_1 - n_0) \tag{2.30}$$

Now, by incorporating the boundary conditions i.e., the gate voltages V_{G_1} and V_{G_2} the following matrix equation will determine the solution of the discretized version of the Poisson's equation. The matrix equation is given as

$$\begin{pmatrix} 2\epsilon_r & -\epsilon_r & \dots & 0 & 0 \\ -\epsilon_r & 2\epsilon_r & \dots & 0 & 0 \\ 0 & -\epsilon_r & \dots & -\epsilon_r & 0 \\ \dots & \dots & \dots & 2\epsilon_r & -\epsilon_r \\ 0 & 0 & \dots & -\epsilon_r & 2\epsilon_r \end{pmatrix} \begin{bmatrix} U_n \\ \dots \\ \dots \\ \dots \\ U_1 \end{bmatrix} = \frac{q^2a^2}{\epsilon_0} \begin{pmatrix} n_n - n_0 \\ \dots \\ \dots \\ \dots \\ n_1 - n_0 \end{pmatrix} \tag{2.31}$$

Here we have to enter the values of ϵ_r (oxide) for the oxide layer and ϵ_r (channel) for the channel respectively. This matrix equation will require the electron densities n_i 's as inputs which can be obtained from the diagonal elements of the density matrix $\rho(z, \acute{z})$. Now, by the self-consistent procedure shown in Fig.(2.4-2.5) the values of U_i's and n_i 's at the discrete points in the channel will be obtained.

2.6 Discretization Procedure for the Self-Consistent Semi-Classical Methods

The semi-classical electron density in 3D can be discretized as

$$n_{3D}(z) = 2\left(\frac{m_e^* k_B T}{2\pi\hbar^2}\right)^{3/2} f_{1/2}\left(\frac{E_c - \mu + U(z)}{k_B T}\right) \tag{2.32}$$

$$\rightarrow \begin{pmatrix} n_n \\ \dots \\ n_k \\ \dots \\ n_1 \end{pmatrix} = 2\left(\frac{m_e^* k_B T}{2\pi\hbar^2}\right)^{3/2} \begin{pmatrix} f_{1/2}(\frac{E_c-\mu+U(z)}{k_BT}) \\ \dots \\ f_{1/2}(\frac{E_c-\mu+U(z)}{k_BT}) \\ \dots \\ f_{1/2}(\frac{E_c-\mu+U(z)}{k_BT}) \end{pmatrix} \tag{2.33}$$

Now, the 3D electron density in the channel can be obtained by the self-consistent procedure illustrated in Fig.(2.5). Similarly, the semi-classical electron density in 2D can be discretized as

$$n_{2D}(z) = \left(\frac{m_e^* k_B T}{\pi^2 \hbar^2}\right) ln\left(1 + exp(-\frac{E_c - \mu + U(z)}{k_B T})\right) \tag{2.34}$$

$$\rightarrow \begin{pmatrix} n_n \\ \dots \\ n_k \\ \dots \\ n_1 \end{pmatrix} = \left(\frac{m_e^* k_B T}{\pi^2 \hbar^2}\right) \begin{pmatrix} ln(1 + exp(-\frac{E_c - \mu + U_n}{k_B T})) \\ \dots \\ ln(1 + exp(\frac{-E_c - \mu + U_k}{k_B T})) \\ \dots \\ ln(1 + exp(\frac{-E_c - \mu + U_1}{k_B T})) \end{pmatrix} \tag{2.35}$$

Now, the 2D electron density in the channel can be obtained by using the Self-Consistent procedure for the semi-classical methods illustrated in Fig.(2.7). The discretization procedure for the Poisson's equation will be similar as shown in the section 2.6.

2.7 Results and Discussions

2.7.1 Simulation results for Quantum methods

Fig.(2.7), shows the channel electron density for channel thicknesses of 3nm, 6nm and 9nm respectively under symmetric gate bias. The parameters for the oxide layers are $\epsilon_{ox} = 3.9$ and $m^* = 0.41m_e$. The effective mass of electron in SiO_2 thin film is reported to be about $0.41m_e$ [32]. For the channel, we have taken ϵ to be equal to 11.7 and varied the effective mass of the electron. The simulations were performed for effective masses, $m_e^*{=}m$, $m_e^* = 0.22m_e$, $m_e = 0.12m_e$ and $m_e = 0.067m_e$ respectively. It will be a good idea to vary ϵ for different values of effective masses as well. For 3nm and 6nm thick channels, the electron densities show a V-shaped valley while for 9nm channel the electron density splits into two wide peaks. This anomalous result is due to the fact that we have taken the effective mass of the electron in the channel to be equal to the mass of the free electron.

However, when we vary the effective masses between and we obtain a peak in the middle of the channel. This is related to the size quantization which is reflected well for 3nm and 6nm thick channels. There are two small additional peaks that occur at the boundaries between the oxide/semiconductor interfaces. This occurs due to the abrupt change in the values of ϵ's and at the boundary between the oxide and the semiconductor channel. One may interpret it as the accumulation of charges at the interface. For 9nm thick channel, the size quantization effect begins to disappear and the electron distribution shifts more towards the gates and less in the middle of the channel. This result can also be reproduced by self consistent Semi-Classical simulation. This is shown in the next section which is on Semi-Classical results. Fig.(2.9), shows the variation of the channel electron concentration under asymmetric gate bias. The channel thicknesses are 3nm, 6nm and 9nm respectively. The effective mass of the electron is taken to be equal to $0.22m_e^*$ for 3nm and 9nm channel thicknesses and it is taken to be equal to $0.067m_e^*$ for 6nm thick channel. The effect due to the application of the asymmetric gate bias is seen as a slight shift in the peak for 3nm and 6nm thick channels. However for the 9nm channel, the effect is quite profound as asymmetric gate bias invokes asymmetric electron distribution in the channel. The asymmetric electron distribution for the 9nm case can be reproduced using semi-classical methods as well.

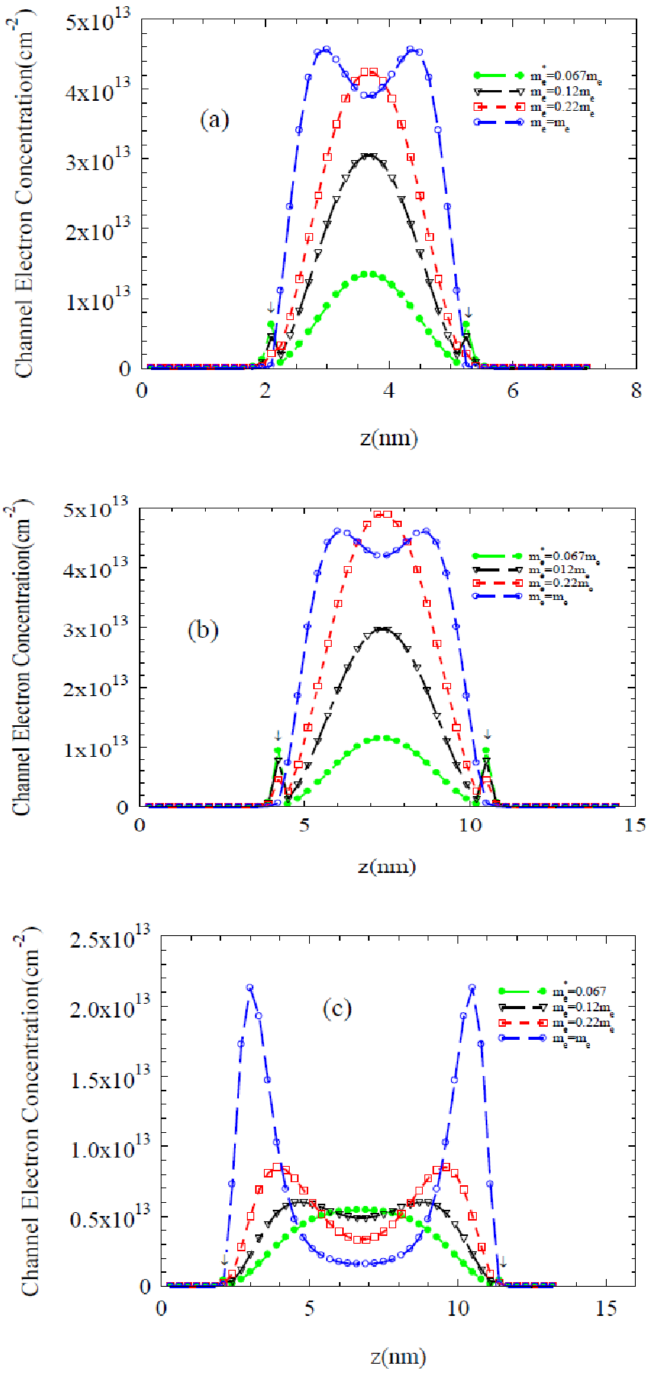

Figure 2.7: *Channel electron concentration for (a) 3nm, (b) 6nm and (c) 9nm channel thicknesses. The calculations are performed using self-consistent Quantum Method for different values of the effective masses of electrons in the channel. The inverted arrows (↓) show two small peaks at the boundary between the oxide/semiconductor interfaces.*

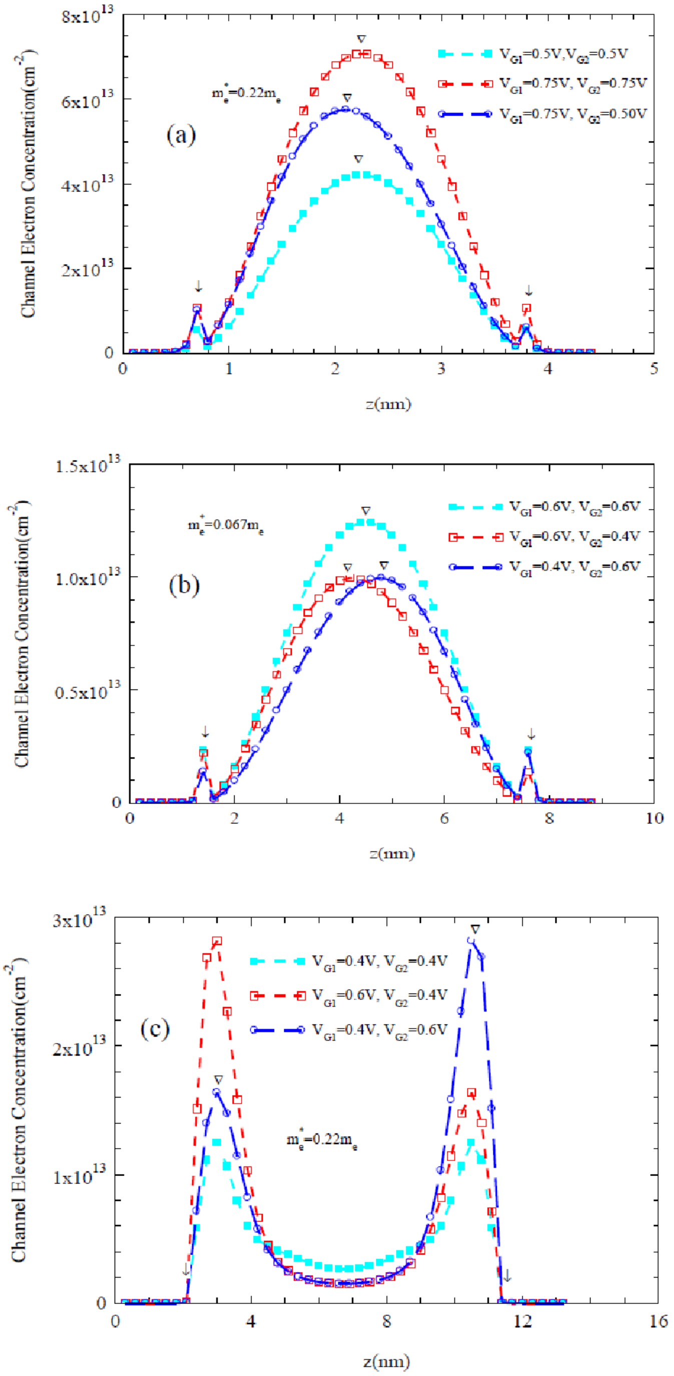

Figure 2.8: *it shows Variation of the channel electron density for (a) 3nm, (b) 6nm and (c) 9nm channel thicknesses under symmetric and asymmetric bias. The calculations are performed using self-consistent Quantum Method. The effective mass for the electron in the channel is taken to be equal to 0.22*m_e *for 3nm and 9nm thick channel and it is taken to be equal to 0.067me for 6nm thick channel. The inverted triangle (*∇*) show the slight shift in the main peak for 3nm and 6nm thick channels under asymmetric bias. For 9nm thick channel, the variation due to asymmetric bias to quite profound.*

2.7.2 Simulation Results for the Semi-Classical Procedure

Fig.(2.7), shows the variation of 2D channel electron density using semi-classical method for channel thicknesses of 3nm, 6nm and 9nm respectively. The effective mass of the channel is taken to be equal to $0.22m_e^*$. The electrons are more accumulated towards the oxide/channel interface for all the three channel widths. The size quantization effect for 3nm and 6nm channel thicknesses which were observed when we used Quantum methods is not observed in this case. Also, the channel electron concentration shows variation with the asymmetric gate bias. On similar lines, Fig.(2.10), shows the variation of 3D channel electron density for channel thicknesses of 3nm, 6nm and 9nm respectively.

Here, again the effective mass of the channel is taken to be equal to $0.22m_e^*$. In this case also, the size-quantization effect is not observed for 3nm and 6nm thick channels. The channel electron concentration varies with the asymmetric gate bias and the electrons are more accumulated towards the oxide/semiconductor interface.

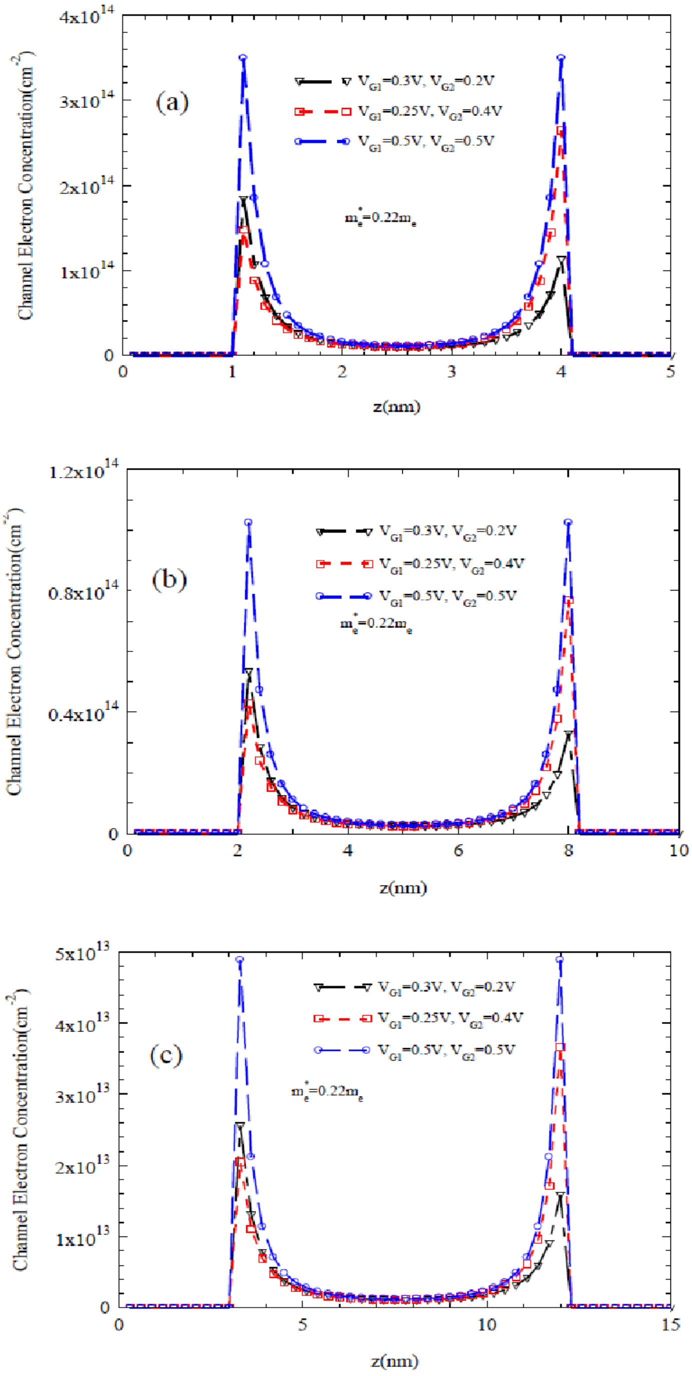

Figure 2.9: *Variation of the 2D channel electron density for (a) 3nm, (b) 6nm and (c) 9nm channel thicknesses under symmetric and asymmetric bias. The calculations are performed using self-consistent Semi-Classical Method. The effective mass for the electron in the channel is taken to be equal to 0.22*m_e^* *for all the cases.*

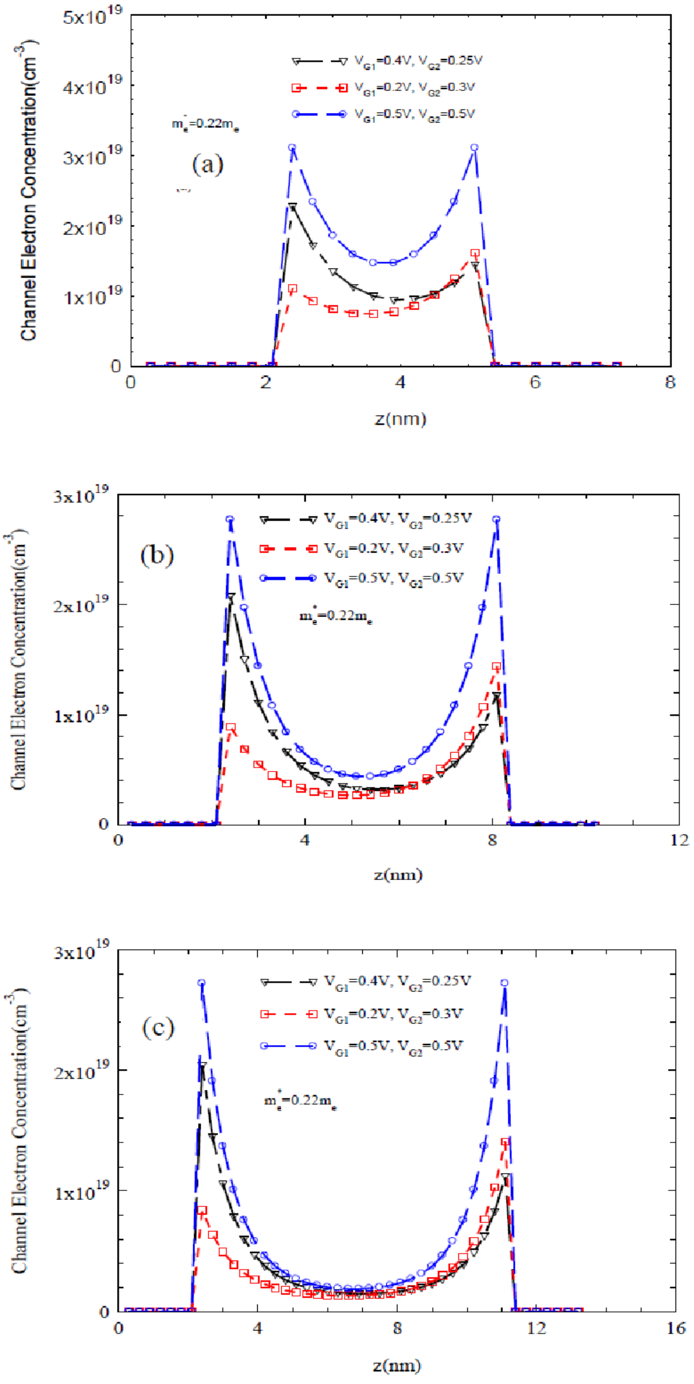

Figure 2.10: *Variation of the 3D channel electron density for (a) 3nm, (b) 6nm and (c) 9nm channel thicknesses under symmetric and asymmetric bias. The calculations are performed using self-consistent Semi-Classical Method. The effective mass for the electron in the channel is taken to be equal to 0.22*m_e^* *for all the cases.*

2.8 Conclusions

We have applied Self-Consistent Quantum and Semi-Classical methods for determining the channel electron density of Nano-Scale MOSFETs. The thickness of the channel was varied between 3nm to 9nm. The size quantization effect is observed for 3nm and 6nm thick channels, but it slowly disappears as the channel thickness is increased to 9nm and further. This effect could be seen, when we apply the self-consistent Quantum method. The size quantization effect is not seen, when we apply the Semi-Classical methods. However, the results of the Quantum and Semi-Classical methods begin to match, when the channel thickness is increased to 9nm and above. The results of the Quantum Method for thin channels between 3nm to 6nm are quite sensitive to the values of the electron effective masses in the channel. The channel electron concentration varies with asymmetric gate voltages. This variation is more for thicker channels, when the size quantization effect disappears with the increase of the channel thickness. Self-Consistent Quantum methods have been used for simulating the channel electron density of a Nano-Scale MOSFET. The size quantization effect is seen for 6nm thick device but it slowly disappears as we increase the channel width. The simulations obtained from the Quantum methods are compared with the Semi-Classical methods. The semi-classical methods fail to capture the size quantization effect in 3nm thick devices. Hence, the Quantum method based on determining the channel electron concentration from the density matrix of the device Hamiltonian is best suitable for the Nano-Scale devices. The semiclassical method fails to capture size effects because we have taken $n_{3D}(z) = 2\left(\frac{m_e^* k_B T}{2\pi\hbar^2}\right)^{3/2} f_{1/2}\left(\frac{E_c-\mu+U(z)}{k_B T}\right)$. This comes from the fact that we treat the system as a free electron gas in 3D, where the eigenfunction is taken as $\psi_N(\vec{k},\vec{r}) = Ae^{i\vec{k}.\vec{r}} = Ae^{ik_x x}e^{ik_y y}e^{ik_z z}$. Whereas in the case of quantum approach, the eigenfunction in the channel is taken to be equal to $\psi_N(k_x,k_y,m) = Ae^{ik_x x}e^{ik_y y}\chi_m(z)$.

Chapter 3

Study of Certain Technologically Important Nano-Scale MOSFETs as Closed and Open Quantum Systems

3.1 Introduction

Rapid advancements in the miniaturization of integrated circuits in the field of Electronics and Computer technologies have shrunk the Gate length of the present day MOSFET to an order of 25 nm or so. In device simulation of CNTFETs a lot of research has been extensively done. After the discovery of CNTs by Iijima in 1991, lot of progress has been done in engineering application. As the overall dimensions of the FET decrease, the role of the MOSFET channel and the interesting physics of source and drain contacts and the scattering issues due to electron-phonon interaction in the channel affecting the overall device performance has become an important area of research in Nano-Scale device physics [1, 2, 24, 26]. Several studies have been performed on various gate geometries starting from a planar single and dual gate MOSFET to SWCNT based MOSFETs [25, 27]. The reason for such rigorous studies which involve advanced concepts of quantum and non-equilibrium statistical mechanics is due to the very fundamental nature of the bottom up approach which is applied here to study the device physics from the atomic scale to the molecular scale which will be the possible length scales of the futuristic devices [33–36].

Up to now, the present devices are modeled with the drift-diffusive transport theory. This is because the development of the devices happened in the top down manner. It is shown experimentally that the gate length can be reduced to the molecular level by the substitution of silicon with CNT and DNA based structures [36–39]. As we know that CNT is basically a rolled up graphene sheet only [19] and honeycomb lattice rolled into a cylinder. Since the diameter of the CNTs are of the order of nanometer size while the length of the nanotube can be more than 1μm. Diameter of the nanotube is very much smaller in size than the most of the semiconductor devices so far, so the CNT plays very important role in semiconductor physics due to very special electronic properties [40]. The most important property of the CNT is the electronic structure and dependence lies on geometry.

We have discussed here in this chapter on SWCNT. Most of the observed single-wall CNTs have diameters less than 2nm. The interesting thing about the structure of CNT is the orientation of six membered carbon ring, so called hexagon in the honeycomb lattice relative to the axis of nanotubes [40]. CNTs are either metallic or semiconducting depends upon the diameter and chirality is defined by single vector called the chirality vector and its shape is in helical geometry. Energy gap of semiconducting CNT can varies between 1 eV to 0 eV by varying the nanotube diameter [40]. Under such circumstances, the nature of the carrier transport and the device performance cannot be understood properly from the present Ohm's law based on

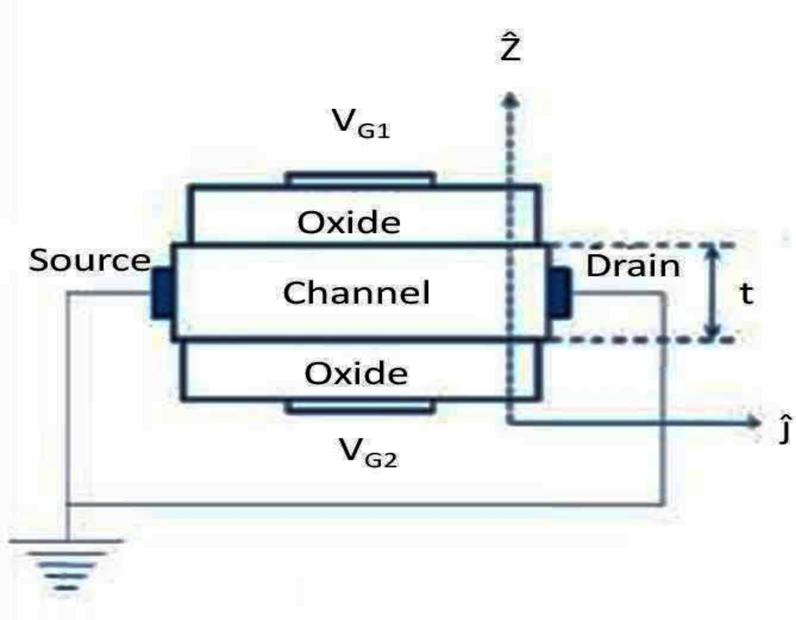

Figure 3.1: *Schematic diagrams for Dual Gate Nano-MOSFET.*

drift-diffusive transport models.

In order to develop the understanding and the theory for these futuristic devices, NEGF procedure is followed, where the role of the source and drain contacts with the device is understood in terms of the self-energy matrices [2, 24, 26]. Under this approach the modeling is done by treating the device as an open quantum system where the Schrodinger equation in the channel is given as $[E - H - \Sigma]\,|\psi\rangle$=[S], where S is the source term and Σ is the self-energy term in the Hamiltonian. Here, we apply an effective simulation procedure to study the Physics of the Nano-Scale devices using Self Consistent Quantum Methods (SCQM) and Non-Equilibrium Green's Function (NEGF) method [28, 30, 32, 41–52]. We calculate the channel densities of a dual gate Nano-Scaled MOSFET and the output characteristics of a Nano-Scaled Single-Walled Carbon Nano Tube (SWCNT) based Transistor.

The first device we study is a dual gate MOSFET, which is shown in Fig.(3.1). In this case, the size quantization effect is observed as a peak in the electron density for ultra thin channels, where the thicknesses are of the order of (3-6)nm. However, this peak begins to disappear as we increase the effective mass of the electron in the

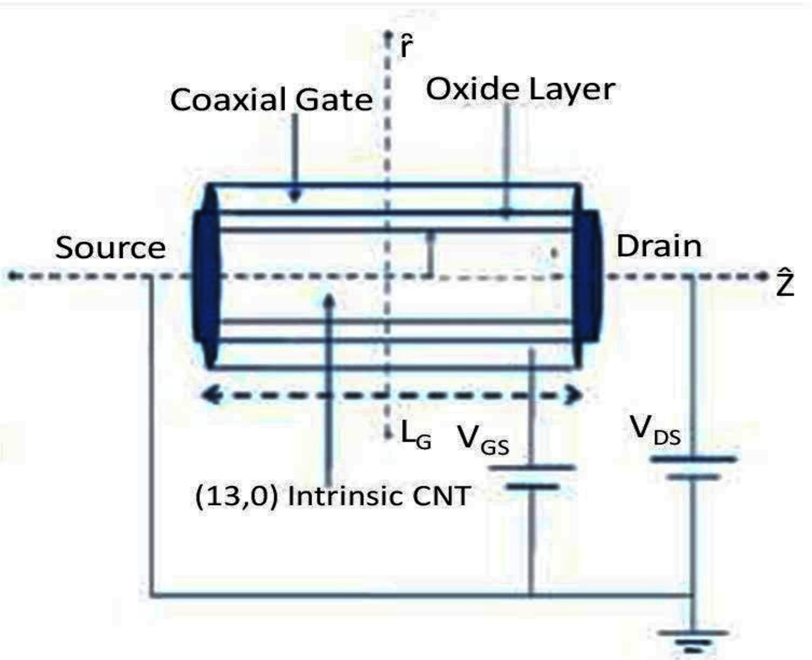

Figure 3.2: *Schematic diagrams for SWCNT-Based Coaxially Gated Nano-MOSFET*

channel.

The second device we study here is a SWCNT based MOSFET which is shown in Fig.(3.2). We study the output characteristics of this device using the self-consistent NEGF procedure. When we combine Newton mechanics with entropy driven processes it becomes Boltzman equation which is widely accepted in semi-classical transport theory [39], similarly when quantum dynamics is combined with entropy driven processes, it will be solved with NEGF and some times called as Quantum Boltzman equation [53]. The idea behind the development of the NEGF was the metal-insulator-metal tunneling experiments, which got a lot of attention in the 1960s [39]. The non-equilibrium Green's function solves Schrodinger equation under non-equilibrium conditions [2] until self-consistency is obtained. NEGF can be used to model flow of current. This method originated basically from the contribution of Martin and Schwinger (1959), Kadanoff and Baym (1962), Keyldish (1965) and many more who used the methods of many-body perturbation theory to describe processes along the channel [53]. NEGF is believed to be an esoteric tool for researchers. NEGF goes beyond ballistic approach of Landauer, where electrons are not interacting to just add inelastic scattering and also correlation effects at an molecular level. For a more discussion one can follow the Green's function method by Supriyo Datta [54]. We have used bottom-up approach in our work, since the validity of top-down approach is questionable at molecular level [55]. It was started with elastic resistors for which entropy driven processes are confined to the contacts of source with channel and drain with channel. Now the problem of resistance can be tackled with a one electron picture by connecting contacts to the Schrodinger equation [56].

Also the first two sub-bands responsible for the carrier transport in the CNT channel are calculated by simulating the potential profile. When we vary V_{DS} from 0 to 1V, the device almost replicates the behavior of a normal MOSFET showing the ON-OFF and saturation regimes. The sub-bands are modulated according to the applied bias. Application of positive gate bias lowers the overall sub-band energies. This work is divided into the five sections. Section(3.2) present the theory, discretization scheme and the self-consistent procedures. Section(3.2.1) present the simulation results when the device is treated as a closed quantum system. Section(3.7) presents simulation results when the device is treated as an open quantum system. Section(3.8) summaries the results.

3.2 Theoretical Background and the Discretization Schemes

3.2.1 Modeling of the Nano-MOSFET as a Closed System

For modeling the device as a closed system, the drain and the gate electrodes are grounded to zero potential [57–59]. There is no flow of current in the device. Only the gate voltage is varied. Positive gate bias lowers the overall energy states in the channel. The channel thickness is taken to be of the order of few nm. We apply periodic boundary conditions (PBC) for the x-y plane and neglect all the boundary effects. This is a valid for ultrathin devices where the planar dimensions are much larger than the lateral dimension. The channel eigenvalue equation is written as,

$$\left[-\frac{\hbar^2}{2m}\nabla.\left(\frac{1}{m(r)}\nabla\right)+E_c(r)+U(r)\right]\psi_N(r)=E_N\psi_N(r) \tag{3.1}$$

$$H\psi_N(r)=E_N\psi_N(r) \tag{3.2}$$

Here, we apply finite difference procedure on the eigenvalue equation and obtain a $N \times N$ block diagonal matrix for the Hamiltonian which is given as:

$$[H]=\begin{pmatrix} \alpha_1 & \beta & \dots & 0 \\ \beta & \alpha_2 & \dots & \dots \\ \dots & \dots & \dots & \beta \\ 0 & \dots & \beta & \alpha_n \end{pmatrix} \tag{3.3}$$

where $[\alpha_i]$ and $[\beta_i]$ are the matrices representing the discretization of the device in the computational domain. The finite difference method can be used on a differential operator $\left(\frac{\partial^2 f}{\partial x^2}\right)_{x=x_n}$ as $\frac{1}{a^2}\left(f(x_{n+1})-2f(x_n)+f(x_{n-1})\right)$. Here, ‘a’ is the distance between the two discrete points. The discretization procedure for the device can be understood from Fig.(3.3). The matrix $[\alpha_i]$ is the discretization of the device as

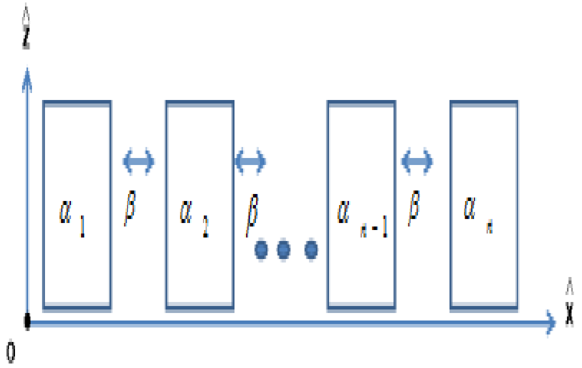

Figure 3.3: *Discretization scheme for the Nano-Scale device.*

along z-axis and it is given as

$$[\alpha_i] = \begin{pmatrix} \frac{\hbar^2}{m_e^* a^2} + E_c + U_n & \frac{-\hbar^2}{2m_e^* a^2} & \dots & 0 & 0 \\ \frac{-\hbar^2}{2m_e^* a^2} & \frac{\hbar^2}{m_e^* a^2} + E_c + U_{n-1} & \dots & 0 & 0 \\ 0 & \frac{-\hbar^2}{m_e^* a^2} & \dots & \frac{-\hbar^2}{m_e^* a^2} & 0 \\ \dots & \dots & \dots & \frac{\hbar^2}{m_e^* a^2} + E_c + U_2 & \frac{-\hbar^2}{m_e^* a^2} \\ 0 & 0 & \dots & \frac{-\hbar^2}{2m_e^* a^2} & \frac{\hbar^2}{m_e^* a^2} + E_c + U_1 \end{pmatrix} \tag{3.4}$$

The matrix $[\beta]$ is the coupling term between the slices of $[\alpha_i]$ and it is given as

$$[\beta] = \begin{pmatrix} \frac{-\hbar^2}{2m_e^* a^2} & 0 & \dots & 0 \\ 0 & \frac{-\hbar^2}{2m_e^* a^2} & \dots & \dots \\ \dots & \dots & \dots & 0 \\ 0 & 0 & 0 & \frac{-\hbar^2}{2m_e^* a^2} \end{pmatrix} \tag{3.5}$$

$[\alpha_i]$ gives the local electron density along the z-axis for a particular value x (see Fig.(3.2)) in the channel. It is calculated from the diagonal elements of the density matrix $[\rho_i]$ which is given as

$$[\rho_i] = \frac{1}{1 + exp(\beta(\alpha_i - \mu))} \tag{3.6}$$

This is the Fermi function of the Hamiltonian Matrix for $[\alpha_i]$.

Now, to satisfy the charge-neutrality condition in the channel, the Schrodinger equation is solved in tandem with the Poisson's equation. The gate voltages V_{G1} and V_{G2} impose the boundary conditions on the system which insures the convergence.

3.3 Open systems

The more active, and thus the more interesting, product of technology are systems that operate far from thermal equilibrium [60]. Few examples of such systems shows that they are generally open, in the sense that they exchange matter with their environment. There are many established techniques for dealing with open systems in fields such as fluid dynamics, neutron transport, and electronics. All these fields are concerned with the transport of (usually) conserved particles. People have used different theoretical approaches to open quantum systems. By far the most common approach to define the boundary conditions on a transport problem is to circumvent the issue entirely. Applications of the Boltzmann equation have most often been restricted to the case of uniform driving fields [61, 62]. When the Boltzmann equation has been applied to nonuniform systems [63–65], techniques requiring that the equation be recast in terms of the Lagrange variables have generally been employed [60]. Our objective here is to obtain an equation of the form

$$E[\psi] = [H + \Sigma][\psi] + [S] \tag{3.7}$$

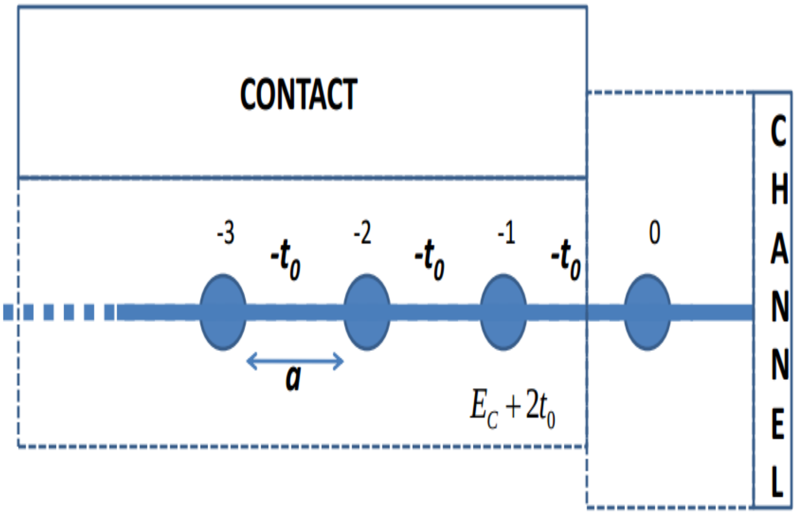

Figure 3.4: *A semi-infinite wire described by a one-band effective mass Hamiltonian. The first point "0" is treated as the channel and the rest as the contact*

.

which describes an open system, unlike the equation $E\psi = H\psi$ that we have used for closed system. As shown in Fig.(3.4), we have a semi-infinite 1D wire described by a one-band effective mass Hamiltonian.

We treat the first point of the wire by giving name "0" as our channel and rest of the wire labeled n, n < 0, as the contact [2]. When the channel is decoupled from the contact it would be described by

$$E\psi = (E_c + 2t_0)\psi \tag{3.8}$$

When we couple the channel with contact, equation becomes

$$E\psi = (E_c + 2t_0)\psi - t_0\phi_{-1} \tag{3.9}$$

where the contact wavefunctions ϕ_n satisfy an infinite series of equations

$$E\psi_n = -t_0\phi_{n-1} + (E_c + 2t_0)\psi_n - t_0\phi_{n+1} \tag{3.10}$$

The solution of these equations consist of an incident wave from the contact and a reflected wave back from the channel, so we have

$$\phi_n = Be^{iKna} + Ce^{-iKna} \tag{3.11}$$

where

$$E = E_c + 2t_0(1 - cosKa) \tag{3.12}$$

From Eq.(3.11) we can write

$$\psi \equiv \phi_0 = B + C \tag{3.13}$$

$$\phi_{-1} = Be^{-iKa} + Ce^{iKa} \tag{3.14}$$

Now, we have

$$\phi_{-1} = \psi e^{iKa} + B[e^{iKa} - e^{-iKa}] \tag{3.15}$$

By using in Eq.(3.9) we have

$$E\psi = (E_c + 2t_0)\psi - t_0 e^{iKa}\psi + t_0 B[e^{iKa} - e^{-iKa}] \tag{3.16}$$

Now comparing Eq.(3.16) with Eq.(3.7) we get

$$\Sigma = t_0 e^{iKa} \tag{3.17}$$

$$S = i2t_0 BsinKa \tag{3.18}$$

The self-energy Σ is non-hermitian and is independent of the amplitudes B, C of the contact wavefunction. The channel wavefunction can leak out into the contact. The source term S, on the other hand, represents the excitation of the channel by the contact and is proportional to B.

3.4 General formulation

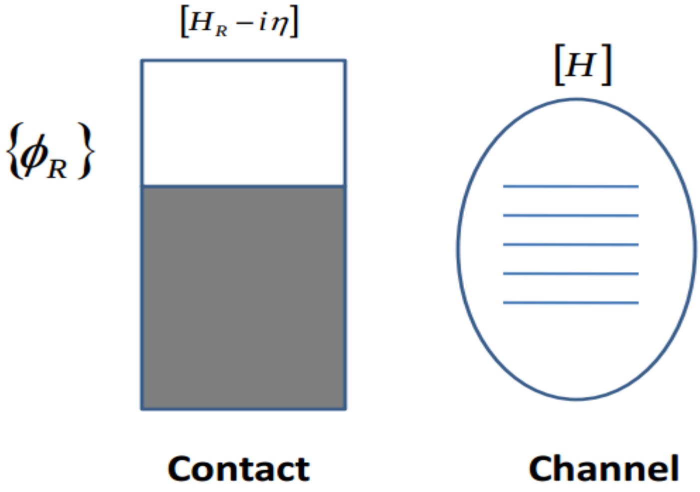

Figure 3.5: *Channel contains no electrons and is disconnected from the contact where the electrons occupy the states described by* ϕ_R*.*

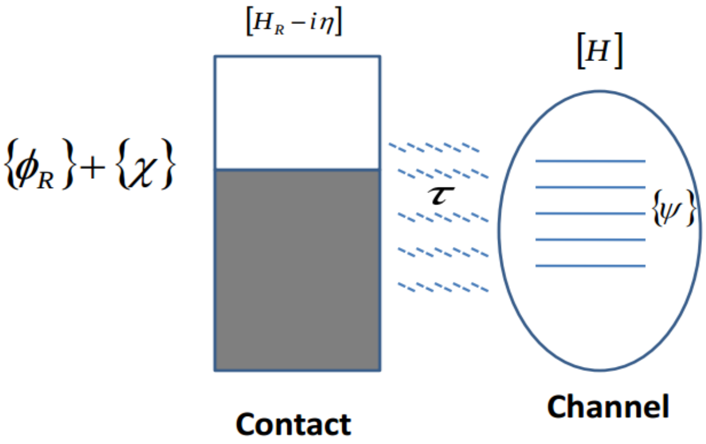

Figure 3.6: *On connecting to the contact, the contact wavefunctions ϕ_R "spill over " into the device giving rise to a wavefunction ψ in the channel which in turn generates a scattered wave χ in the contact.*

First consider a channel with no electrons and it is disconnected from the contacts as shown in Fig.(3.5). The electrons in the contact have wavefunction ϕ_R that obey the Schrodinger equation for the isolated contact

$$[EI_R - H_R][\phi_R] = [0] \tag{3.19}$$

where H_R is the contact Hamiltonian and I_R is an identity matrix of the same size as H_R . Now we may modify the above equation as

$$[EI_R - H_R + i\eta][\phi_R] = [S_R] \tag{3.20}$$

where η=$0^+ I_R$ is a small positive infinitesimal times identity matrix. The term i$[\eta]\phi_R$ on the left of Eq.(3.20) represents the extraction of electrons from the contact while the term S_R on the right of Eq.(3.20) represents the reinjection of electrons from external sources: such extraction and reinjection are essential to maintain the contact at a constant electrochemical potential. The transition from the Schrodinger equation to Eq.(3.20) represents a fundamental change in viewpoint. E is no longer an eigen energy, but an independent variable representing the energy of excitation from external sources. With the Schrodinger equation, the ϕ_R are essentially the eigen- functions of $[H_R]$ that are non-zero only when the energy E matches one of the eigen- energies of $[H_R]$. On the other hand, the ϕ_R in Eq.(3.20) are non-zero for all energies E with peaks around the eigenenergies of $[H_R]$, whose sharpness depends on the infinitesimal 0^+. When coupling is done the contact wavefunctions will "spill over" giving rise to a wavefunction ψ inside the device which in turn will excite scattered waves χ. Full wavefunction will satisfy Schrodinger's equation.

$$\begin{pmatrix} EI_R - H_R + i\eta & -\tau^+ \\ -\tau & EI - H \end{pmatrix} \begin{pmatrix} \phi_R + \chi \\ \psi \end{pmatrix} = \begin{pmatrix} S_R \\ 0 \end{pmatrix} \tag{3.21}$$

where [H] is the device Hamiltonian. The different quantities appearing in Eq.(3.21) are not numbers(except for the energy E). They are matrices of different sizes: Contact Hamiltonian $[H_R]$, identity matrix $[I_R\ ]$, damping $[\eta]$: (R×R). Channel Hamiltonian [H], identity matrix [I]: (d×d). Coupling Hamiltonian (τ): (d×R), (τ^+): (R×d). Column vectors: Contact wavefunction ϕ_R, χ, source S_R : (R×1). Going from Eq.(3.20) to Eq.(3.21), the term S_R on the right-hand side, representing the reinjection of electrons from external sources, is assumed to remain unchanged. It allows us to make use of Eq.(3.20) to eliminate S_R from Eq.(3.21) to write

$$[EI_R - H_R + i\eta][\chi] - [\tau^+][\psi] = [0] \tag{3.22}$$

$$[EI - H][\psi] - [\tau][\chi] = [\tau][\phi_R] \tag{3.23}$$

χ can be written in terms of ψ from the first equation

$$[\chi] = G_R \tau^{+} [\psi] \tag{3.24}$$

where

$$G_R \equiv [EI_R - H_R + i\eta]^{-1} \tag{3.25}$$

$$[\eta] = 0^{+}[I_R] \tag{3.26}$$

so, we have

$$[EI - H - \Sigma][\psi] = [S] \tag{3.27}$$

where $\Sigma \equiv \tau G_R \tau^{+}$ and S$\equiv$ ϕ_R. G_R represents a property of the isolated contact since it only involves the contact Hamiltonian H_R.

3.5 Modeling of the SWCNT-based MOSFET as an Open Quantum System

The problem we address here is the modeling of the device as an open quantum system. The device we study for this is a coaxially gated SWCNT based transistor. In this device, the diameter of the CNT is varied between 1-2 nm. The width of the dielectric layer is taken to be equal to 2nm. The gate length is taken to be equal to 25 nm. Schrodinger equation for the device under active operation becomes

$$[E - H - \Sigma_s - \Sigma_D - \Sigma_{sc}] \left|\psi\right\rangle = [S] \tag{3.28}$$

The Schrodinger equation of the channel which is for the closed system gets modified under device operation. The Green's function [G] for channel is obtained from

Eq.(3.28)

$$[E - H - \Sigma_s - \Sigma_D - \Sigma_{sc}]\,|\psi\rangle = [S] \tag{3.29}$$

$$|\psi\rangle = [E - H_0 - U - \Sigma_s - \Sigma_D - \Sigma_{sc}]^{-1}[S] \tag{3.30}$$

$$|\psi\rangle = [G][S] \tag{3.31}$$

Σ_S, Σ_D, and Σ_{SC} are the self-energy matrices for the source contact, drain contact and the electron-phonon scattering in the device channel. The transmission function, T(E) for the channel is given as $T(E) = Trace(\Gamma_1 G \Gamma_2 G^\dagger)$. Here, Γ_1 and Γ_2 are the broadening terms which arise due to the coupling between the contacts and the device channel. Using the above expressions, the output characteristics of the device is calculated from the following relation

$$I = \int_{-\infty}^{\infty} dE T(E)[f_S(E) - f_D(E)] \tag{3.32}$$

Here f_S(E) and f_D(E) are the Fermi-functions for the source and drain which differs by an amount qV_{DS} for low bias. I-V characteristics of device are finally obtained from the self-consistent procedure where we solve the quantum transport and the Poisson's equations in an iterative manner. The device current and the local electron density of the channel are obtained from the transport equation and the diagonal elements of the density matrix, $[\rho]$. We have already seen the calculation for $[\rho]$ in section(3.2). Now, when the device is ON, the density matrix for the device is calculated from the correlation function $G^n(E)$, which is the electron density per unit energy in the channel. The density matrix is now given as

$$[\rho] = \frac{1}{2\pi}\int dE G^n(E) \tag{3.33}$$

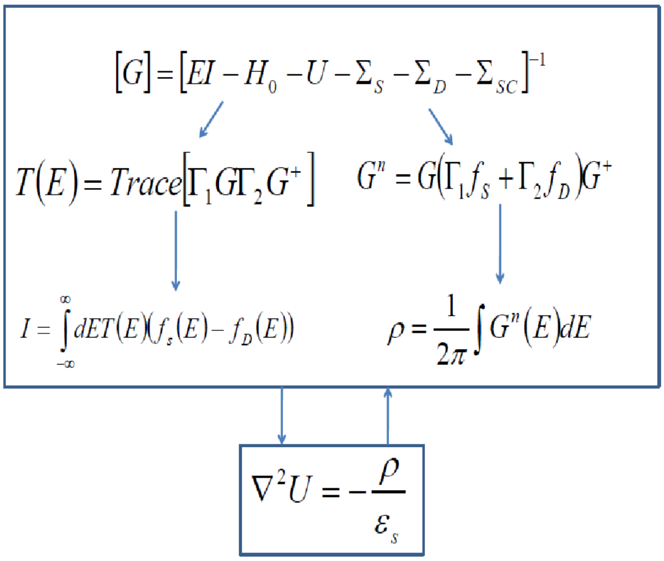

Figure 3.7: *Self-consistent procedure for calculating output characteristics of SWCNT-based MOSFET using NEGF procedure.*

Here, $G^n(E)$ is given as

$$G^n = G(\Gamma_1 f_S(E) + \Gamma_2 f_D(E))G^\dagger \tag{3.34}$$

3.6 Simulation results for the Ultra Thin Channel Density of the Dual Gate Nano MOSFET

The channel electron densities are calculated for the ultra-thin channel using the self-consistent procedure. Fig.(3.5) shows the electron concentration for 3nm thin channel for different effective masses which is varied from $m^* = 0.11m_e$ to $m^* = m_e$. For the effective mass of $0.11m_e$, $0.22m_e$ and $0.33m_e$, the channel density peaks up in the middle.

This is due to the quantum confinement of the carriers. However, when the effective mass is taken to be equal to the free electron mass, the size quantization effect begins to disappear as the distribution of the electrons shifts towards the oxide/channel interface. This effect also can be explained in terms of the conduction

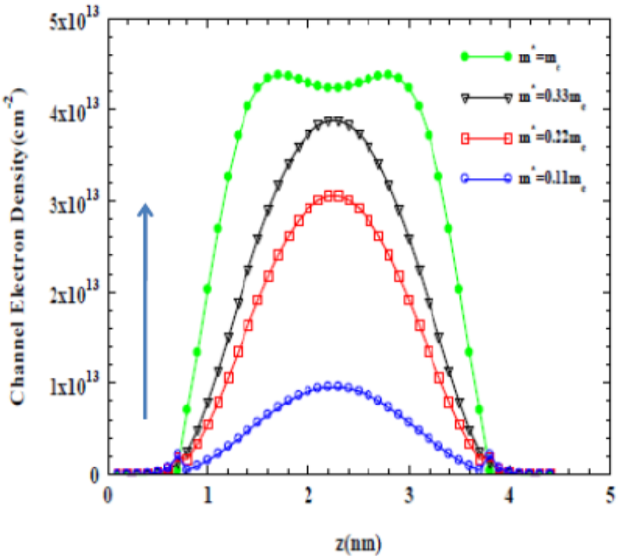

Figure 3.8: *Channel electron concentration for a 3nm thin channel for different electron effective masses. The arrow (↑) points toward increasing effective mass.*

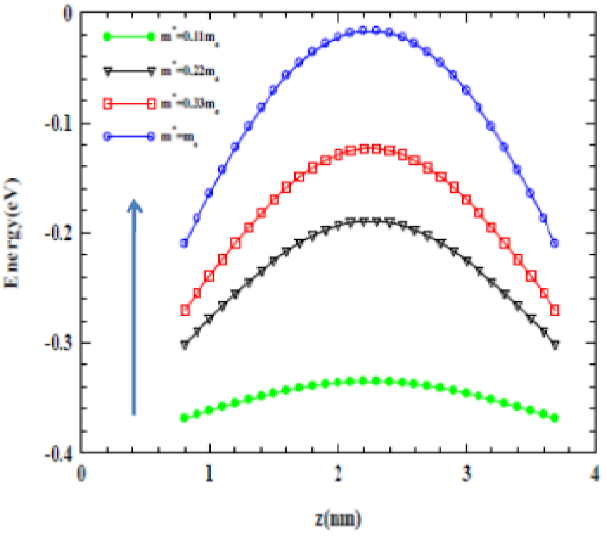

Figure 3.9: *The Conduction Band Profiles inside the channel for different electron effective masses. The arrow (↑) points toward increasing effective mass.*

band profile. Fig.(3.6) shows the conduction band profile inside the channel for different effective masses in real space. From the band profiles, it is quite evident that the electrons with higher effective masses will tend to localize more towards the oxide/channel interface since the slope of the downhill for the band profile is more for the higher effective masses.

3.7 Simulation Results for SWCNT-based MOSFET as an Open Quantum System

This section presents the simulation results for SWCNT-based MOSFET. Fig.(3.5) show the Channel Electron concentration of the SWCNT-based MOSFET for 25nm Gate length. The inset of the Fig.(3.7) shows the sub-band profiles (1 and 2) under zero drain bias. Fig.(3.8) shows the lowering of sub-band 1, when a positive gate bias is applied. The energy bands are lowered as the gate voltage is varied from -0.6V to 0.3V. The lowering of the bands plays an important role in the conductivity of the channel. The conductivity of the channel gets enhanced as lowering of the bands bring more available energy states in the vicinity of the Fermi-level for conduction. The position of the Fermi-Level is fixed here by the Drain voltage. If the Drain voltage, V_{DS} is fixed at zero voltage, then it would be an equilibrium condition. However, if V_{DS} is non-zero, then the difference in the Fermi functions would be equal to qV_{DS} in this case under low bias.

Fig.(3.9) shows the plot of the Sub-Bands responsible for current flow in the CNT based MOSFET device of 25nm gate length. The Gate voltage is fixed at 0.3 V while the Drain Voltage is fixed at 0.4V. The sub-bands are modulated according to the applied drain bias. The barrier for the electrons gets lowered in the source side leading to an increase in the transmission T(E) which results in higher current values. Fig.(3.10) shows output characteristics of the device, when it is treated as

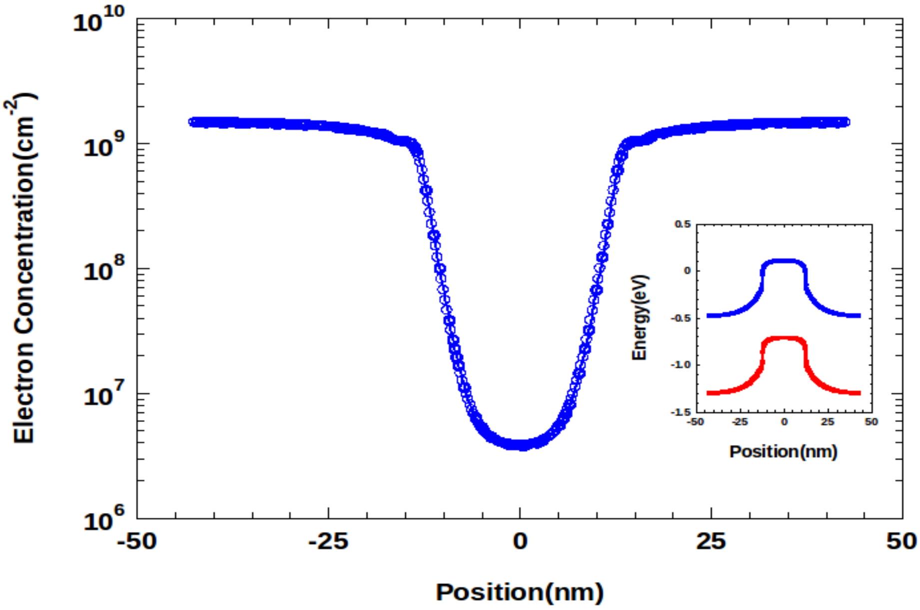

Figure 3.10: *Channel Electron Concentration when the device is OFF under zero drain bias. The inset of the figure shows the sub-band (1 and 2) profile of the CNT channel under OFF condition. The gate length of the device is taken to be 25nm in our simulation.*

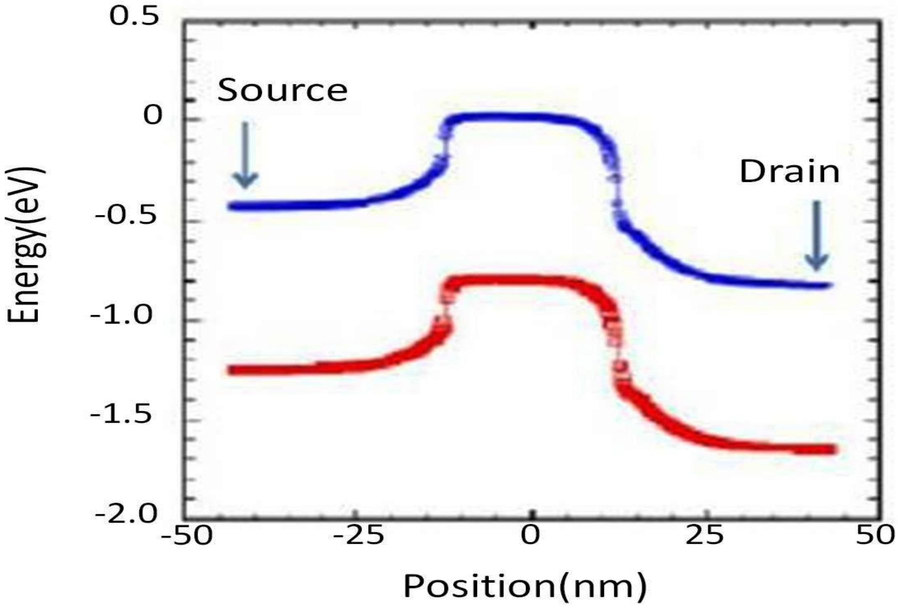

Figure 3.11: *Modulation of sub-bands under applied drain voltages 0.4V. The lowering of the barrier in the source side increases the transmission T(E) for the electrons in the channel.*

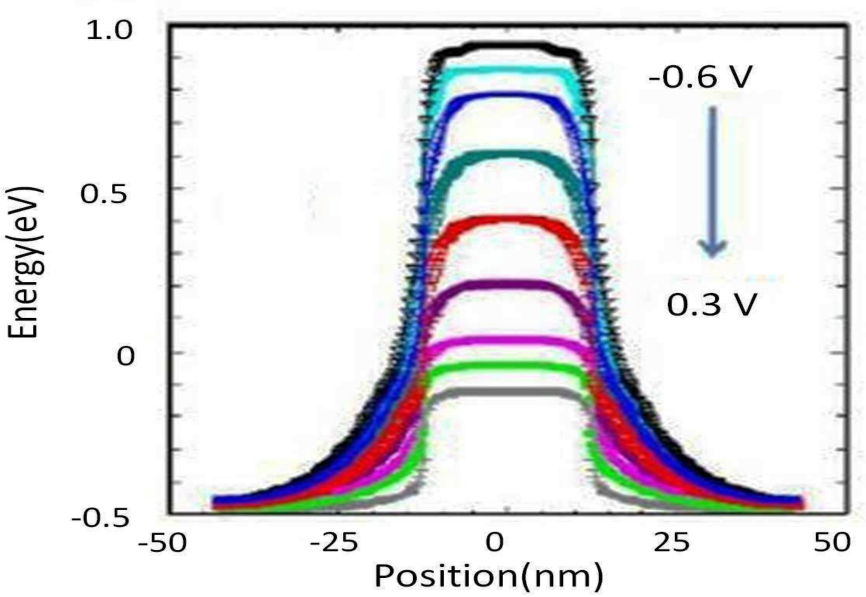

Figure 3.12: *Sub-band 1 profiles (CB) for the channel of the device under the applied gate bias from -0.6V to 0.3V. The device is in OFF state. The lowering of the bands due to the applied gate bias will increase the channel conductivity and will lower the turn-on voltage of the device.*

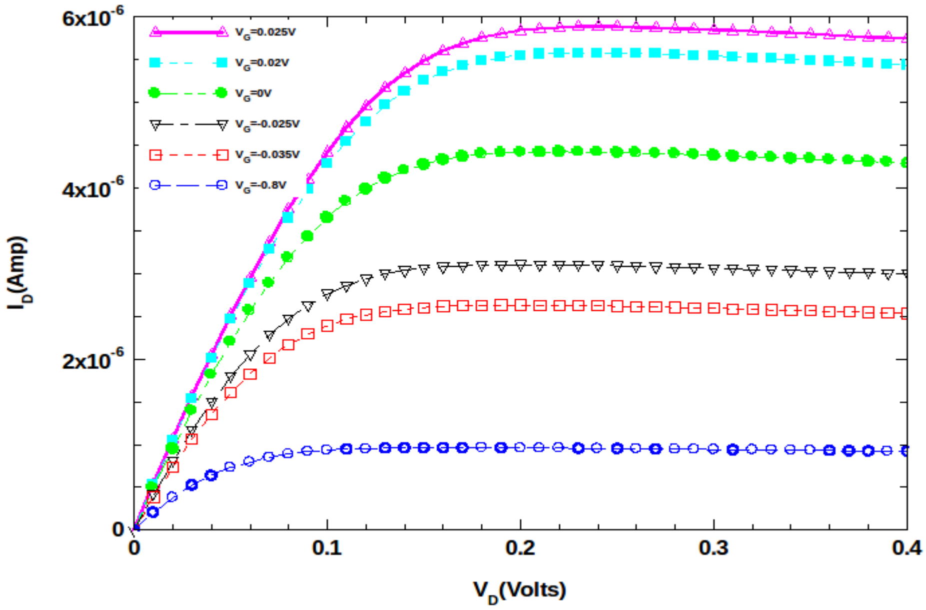

Figure 3.13: *The output characteristics of Nano-Scale MOSFET under low drain bias.*

an open quantum system. The behavior of the device is similar to the conventional MOSFETs with ON-OFF and saturation regions.

3.8 Conclusions

The devices under operation are discretized using finite-difference method and represented as block diagonal matrices in the computational domain and are modeled as a closed and open quantum system. This gives a lot of insight into the Physics and the modeling of these technologically important Nano-scale devices. The size quantization for thin channels is seen here. The output characteristics are obtained from NEGF procedure using a self-consistent method where the transport and the Poisson's equation are solved. This procedure simulates the I-V curve for device showing the ON-OFF and saturation regime. We get a clearer picture of the sub-bands responsible for the transport in the device. These sub-bands get modulated according to the applied drain voltage and get lowered in energy when positive gate voltage is applied on it. Quantum effects have been captured in the work. Current non-equilibrium approach is constrained to work in single particle picture and also a mean field theory. The field of graphene(CNT) has benifited a lot from the rapid progress of experiments in last century. The self energies for the general inelastic scattering procedure in the channel are given as : $\sum_{sc}^{in}(E) = \int_0^\infty \frac{d(\hbar\omega)}{2\pi}\{D^{em}(\hbar\omega).G^n(E+\hbar\omega) + D^{ab}(\hbar\omega).G^n(E-\hbar\omega)\}$, where D^{em} & D^{ab} are the phonon-emission & absorption function. In our calculation for the I-V characterstics of the Nano-scale MOSFETs [66, 67], we have taken $\sum_{sc}$ to be equal to zero. We have done calculation for coherent transport only.

Chapter 4

Self-Consistent NEGF Procedure to Study the Coherent Transport with Scattering in Low Dimensional Systems

4.1 Introduction

Most of the theory based work in these days has been based on the Landauer approach [68] assuming coherent transport. In order to study Quantum Transport in Low-Dimensional Systems, the first device we take into our consideration is a Single-Moded Nanowire with two or more scatterers. For a single moded nanowire, if the scatterers are separated by a quarter of a wavelength, then it will lead to a destructive interference and peak in the transmission in the reflections of the electron waves and if the scatterers are separated by half of a wavelength then it will lead to a constructive interference and dip in the transmission. The aim of this work is to understand the coherent transport in the presence of scatterers in low dimensional

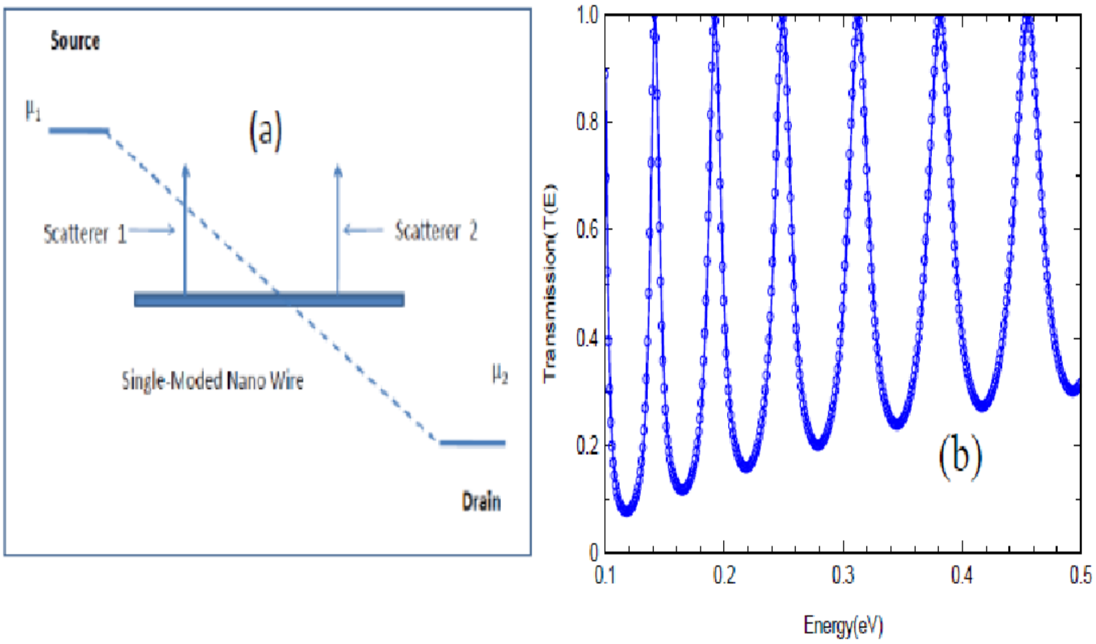

Figure 4.1: *(a) A Schematic of a Single-Moded Nano-Scale Device with Scatterers at "1" and "2". (b) Transmission, T(E) for the device which is obtained from the NEGF procedure.*

systems. Here, we have applied a self consistent NEGF procedure to calculate the transmission, T(E) for this single-moded system. In this chapter we have shown that how the Quantum transport equations can be used to model conductors with phase breaking processes [2].

Fig.(4.1(a)) shows a schematic of a single-moded low dimensional small Nanowire device with two scatterers. A small bias is being applied across the device and we assume that the potential due to the applied bias varies linearly across the device [69]. This is just one particular case with two scatterers as localized impurity potentials. Fig.(4.1(b)) shows the Transmission function, T(E) which has been obtained from the self-consistent NEGF procedure for the device shown in Fig.(4.1(a)). The dip and the peak in the transmission correspond to the destructive and constructive interference from the reflected electron waves in the device.

We can generalize this for many scatterers and also for Multi-Moded low dimensional

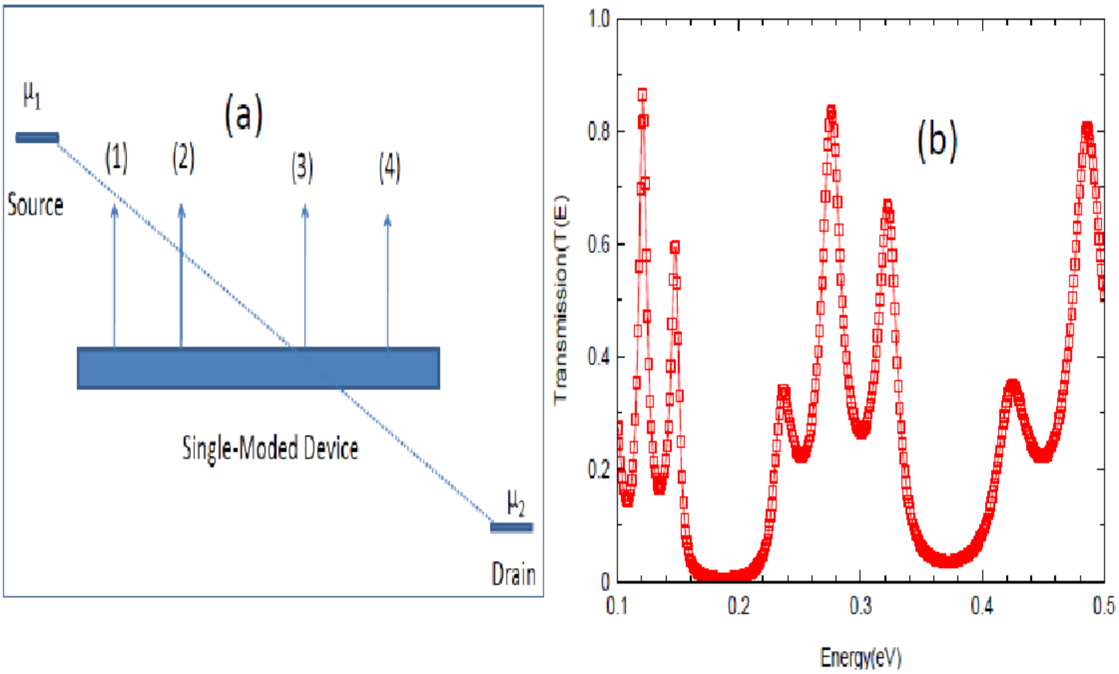

Figure 4.2: *(a) A Schematic of a Single-Moded Nano-scale Device with Scatterers at "1", "2", "3" and "4" (b)Transmission, T(E) for the device which is obtained from the NEGF procedure.*

devices with Phase-Breaking Scatterers. Fig.(4.2(a)) shows a schematic of a single-moded low dimensional small Nanowire device with four scatterers. A small bias is being applied across the device and it is again assumed that the potential due to the applied bias varies linearly across the device. Fig.(4.2(b)) shows the Transmission function, T(E) which has been obtained from the self-consistent NEGF procedure for the device shown in Fig.(4.2(a)). The dips and the peaks in the transmission function again correspond to the destructive and constructive interference from the reflected electron waves in the device. In this case, the Transmittance T(E) has the maximum value of 0.8657 which corresponds to an electron energy of 0.121eV.

In both the cases, we have applied a self-consistent NEGF procedure to calculate T(E). This procedure which involves an iterative calculation of the "Non-Equilibrium Green's Function" for the device is described in the next section.

4.2 Self-Consistent Non-Equilibrium Green's Function Method (NEGF) for Calculating the Transmission Function T(E)

The device is discretized and the Hamiltonian Matrix for the device is constructed using a tight binding method [69]. Fig.(4.3) shows the discretized single-moded wire device with scattering centers at the lattice sites 1, 2, 3 and 4 respectively. Presently, we are treating the device as a two terminal device with an applied V_{DS}. We assume that the potential across the device varies linearly. The self-energies of the source and drain contacts are given as Σ_S and Σ_D. The device is treated here as an open-quantum system and the Schrodinger equation in the device will be given as [12]:

$$[EI - H_0 - U(z) - \Sigma_S - \Sigma_D][\psi] = [S] \tag{4.1}$$

Now, the solution to the above inhomogeneous equation will be given as:

$$[\psi] = [EI - H_0 - U(z) - \Sigma_S - \Sigma_D]^{-1}[S] \tag{4.2}$$

Here, the solution can further be written in a compact form as:

$$[\psi] = [G][S] \tag{4.3}$$

The factor [G] is the Green's function for the device. We calculate the broadening matrices Γ_1 and Γ_2 from the following relation [70] which is given as:

$$\Gamma_1 = i[\Sigma_S - \Sigma_S^\dagger] \tag{4.4}$$

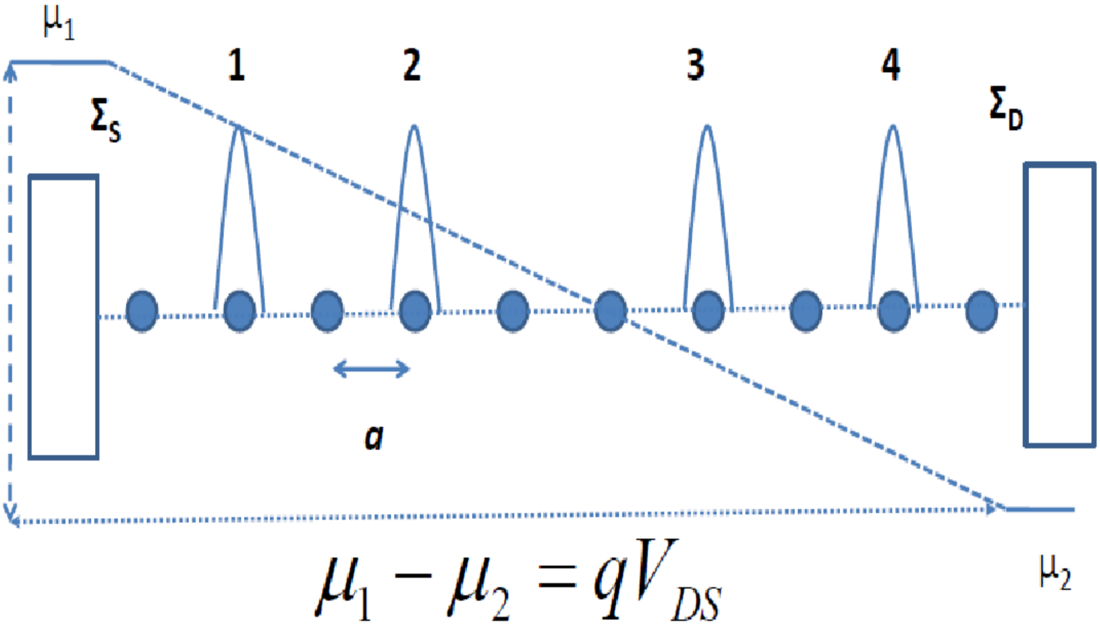

Figure 4.3: *The Schematics for the discretization of the single-moded device with scatterers at lattice sites 1, 2, 3, and 4 respectively. The Hamiltonian for the device can be constructed using the tight-binding method. The self-energies* Σ_S *and* Σ_D *and the broadening terms* Γ_1 *and* Γ_2 *will be required for the calculation of [G] and T(E).*

$$\Gamma_2 = i[\Sigma_D - \Sigma_D^\dagger] \tag{4.5}$$

The Transmission function T(E) is finally worked out using the flowchart shown in Fig.(4.4) which describes the NEGF procedure. Here, Γ_1 and Γ_2 are the broadening terms which describe the ease with which carriers can flow from the contact electrodes to the device and Σ_S and Σ_D are the self energies for the source and drain contacts. The Green's Function [G] for the device is obtained in a self-consistent iterative manner [71] with the Poisson equation. The transmission function T(E) is given as:

$$T(E) = Trace(\Gamma_1 G \Gamma_2 G^\dagger) \tag{4.6}$$

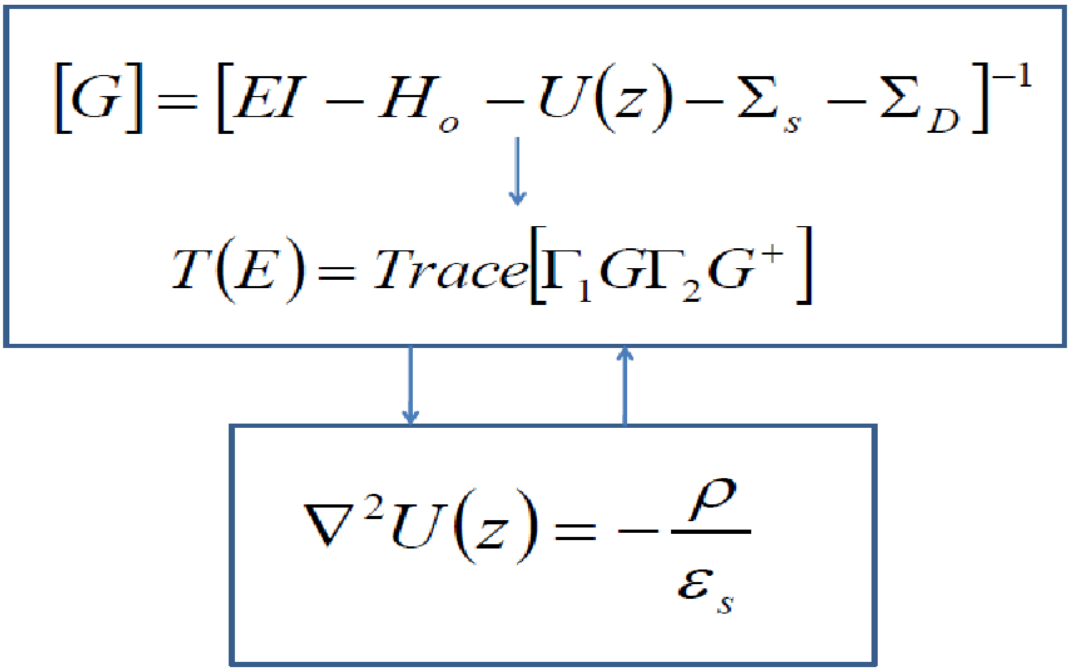

Figure 4.4: *The Self-Consistent Scheme for solving iteratively the Green's Function and the Poisson Equation inside the device for calculating T(E).*

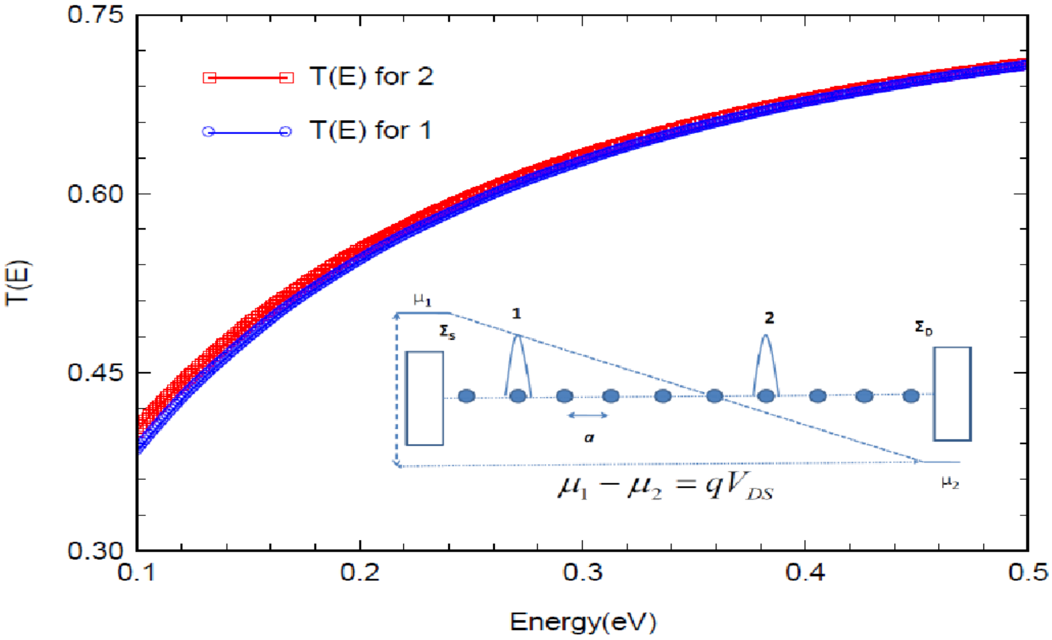

Figure 4.5: *T(E) for individual scattering centers 1 and 2. In some cases, the composite value of T(E) will exceed from the individual T(E)'s.*

4.3 Conclusions

We have seen the application of NEGF procedure to study the coherent transport of a low dimensional device with localized impurity scatterers. The transmission T(E) has been calculated and one can study the I-V characteristics of this low dimensional device from this. The phase breaking scattering in this low-dimensional system can be studied by incorporating additional energy dissipation in the device which will correspond to an additional self-energy term $\Sigma_{Dissipation}$ in the Green's function, [G]. We can calculate the transmission function T(E) through each individual scattering centers and compare it with the composite value of T(E) which we have calculated using NEGF method. When the scatterers are spaced by half a wavelength the reflections from the two scatterers interfere constructively, leading to a dip in the transmission. But if they are spaced by a quarter of wavelength, the reflections interfere destructively, leading to a peak in the transmission. This shows up as large oscillations in the transmission as a function of energy (which determines the de Broglie wavelength of the electrons)[66, 72, 73]. The oscillations occur in case of Fig.(4.1(b) & 4.2(b)) due to interference between two scatterers, while it does not happen in case of Fig.(4.5), because there is no interference. There is one scatterer at one time, so no interference occurs here and no oscillations are seen in this case.

Chapter 5

NEGF Formulation for Studying the Conductance and Transport in GNR under Ballistic Regime

5.1 Introduction

Advancements in the field of Nano-Scale technologies have resulted in the fabrication of GNR and CNT based devices. These novel devices may dominate the future of electronics and computer industries. Hence, it becomes extremely important to study the Physics and the Modeling of these GNR and CNT based devices. The most important thing that one should study first is the conductance of these novel materials which will take the role of the channel in the futuristic Nano-Scale devices. In this chapter, we have explained the NEGF procedure for studying the conductance in GNR.

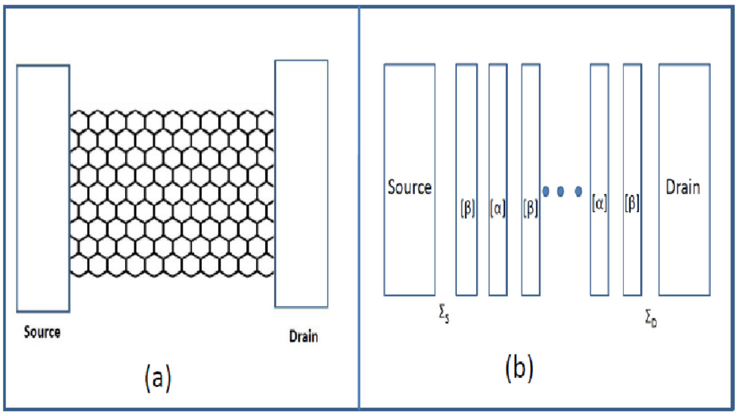

Figure 5.1: *(a) A simple two terminal device with zigzag GNR as channel (b) The discretization procedure involving [α], [β], [Σ_S] and [Σ_D] matrices.*

5.2 The Discretization Procedure

The discretization for the zigzag GNR can be very easily understood in terms of super cells and the matrices [α] and [β] for the zigzag GNR which is shown in Fig.(5.2).

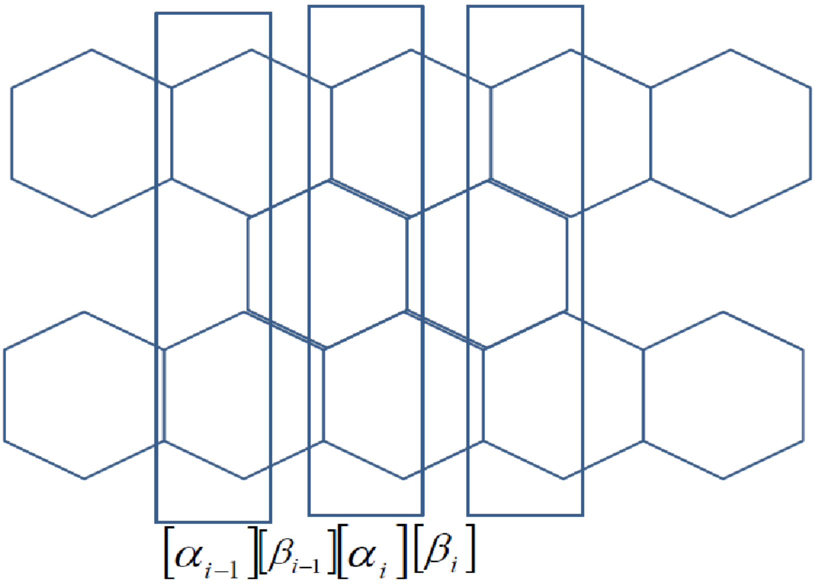

Figure 5.2: *Super cells for Zigzag GNR. [α_i] matrix corresponds to the discretization of a particular super cell and [β_i] corresponds to the coupling between the super cells.*

Now, by tight binding method, the matrices $[\alpha_i]$ and $[\beta_i]$ for the zigzag GNR which is shown are given as

$$[\alpha_i] = \begin{pmatrix} 0 & -t & 0 & 0 & -t & 0 & 0 & 0 \\ -t & 0 & 0 & 0 & 0 & -t & 0 & 0 \\ 0 & 0 & 0 & -t & 0 & 0 & -t & 0 \\ 0 & 0 & -t & 0 & 0 & 0 & 0 & -t \\ -t & 0 & 0 & 0 & 0 & 0 & 0 & 0 \\ 0 & -t & 0 & 0 & 0 & 0 & -t & 0 \\ 0 & 0 & -t & 0 & 0 & -t & 0 & 0 \\ 0 & 0 & 0 & -t & 0 & 0 & 0 & 0 \end{pmatrix} \tag{5.1}$$

$$[\beta_i] = \begin{pmatrix} 0 & 0 & 0 & 0 & -t & 0 & 0 & 0 \\ 0 & 0 & 0 & 0 & 0 & -t & 0 & 0 \\ 0 & 0 & 0 & 0 & 0 & 0 & -t & 0 \\ 0 & 0 & 0 & 0 & 0 & 0 & 0 & -t \\ 0 & 0 & 0 & 0 & 0 & 0 & 0 & 0 \\ 0 & 0 & 0 & 0 & 0 & 0 & 0 & 0 \\ 0 & 0 & 0 & 0 & 0 & 0 & 0 & 0 \\ 0 & 0 & 0 & 0 & 0 & 0 & 0 & 0 \end{pmatrix} \tag{5.2}$$

Now, the Hamiltonian obtained from the discretization of the zigzag GNR can be represented as a block-diagonal Matrix [H] which is shown below.

$$[H] = \begin{pmatrix} [\alpha_1] & [\beta_1] & \dots & \dots & [0] \\ [\beta_2] & [\alpha_2] & \dots & \dots & \dots \\ \dots & \dots & \dots & \dots & \dots \\ \dots & \dots & \dots & \dots & [\beta_{n-1}] \\ [0] & \dots & \dots & [\beta_{n-1}] & [\alpha_n] \end{pmatrix} \tag{5.3}$$

5.3 The Self Consistent Procedure

The Transmission function and the I-V characteristics for this device can be obtained by using a self-consistent procedure involving the NEGF method [74]. The transmission function T(E) and the I-V characteristics for the GNR based device can be obtained from iterative scheme shown below. Γ_1 and Γ_2 are the broadening terms of the two terminal device which describe the ease at which carriers can flow from the contact electrodes to the GNR channel of the device. The source and the drain contacts with the channel are manifested as the self energy terms which are given as Σ_s and Σ_D respectively. The Green's Function G(E) for the device is obtained in a self-consistent iterative manner with the Poisson equation. The potential U(z) takes into account the electron-electron interaction. The difference in the Fermi function is taken to be equal to the applied low bias across the device [75].

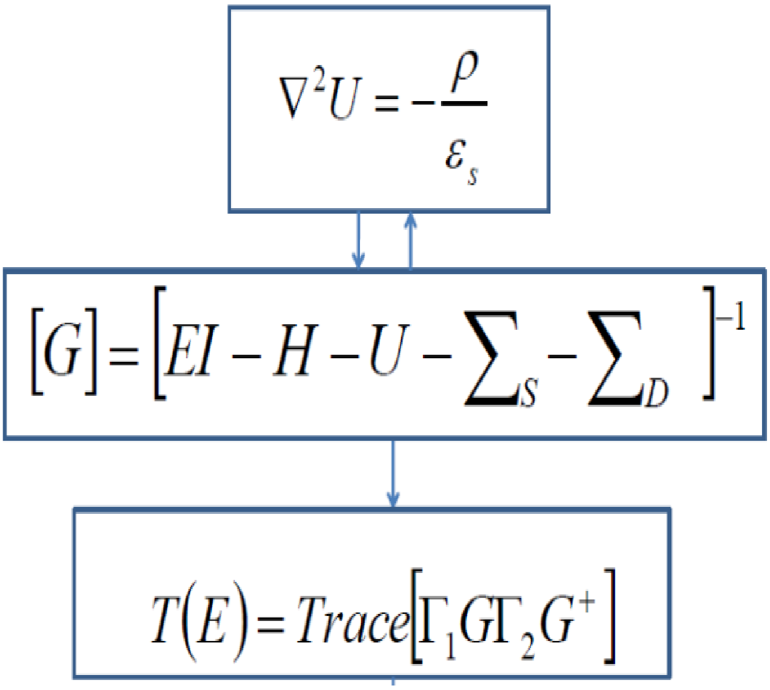

Figure 5.3:

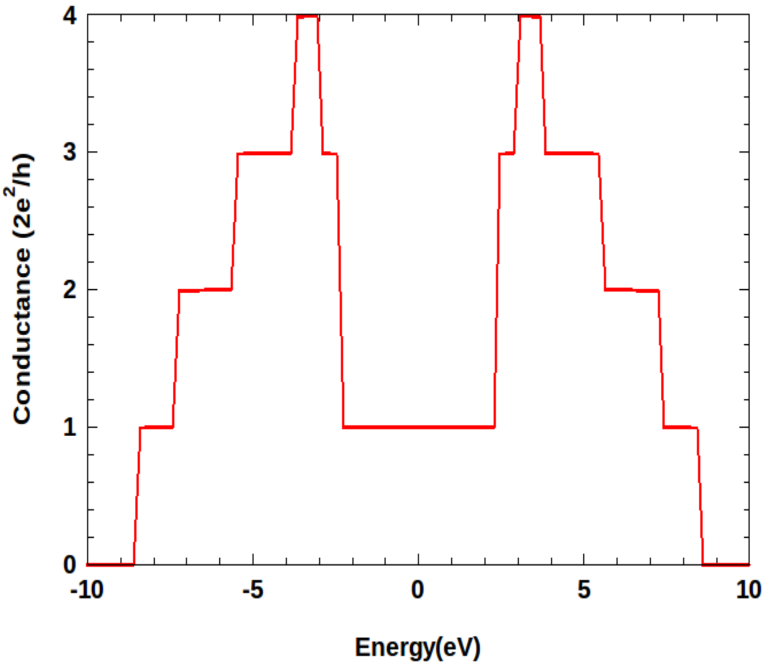

Figure 5.4: *Conductance of a zigzag nanoribbon obtained from the above self-consistent NEGF procedure.*

5.4 Ballistic and diffusive transport in GNR

The relationships between characteristic lengths determine the three transport regimes: ballistic, diffusive, and classic transport. Ballistic transport consists of single electron conduction with no phase and momentum relaxation. In a ballistic conductor, wavefunction of an electron is determined over the sample by solution of Schrödinger's equation. While in case of diffusive motion, many elastic scattering events occur. Since, the phase relaxation length is much longer than the mean free path in diffusive motion, localization of the wavefunction comes into picture. For ballistic transport we consider an ideal case where we have no electron scattering in the channel connected to two contacts. Elastic mean free path is the key parameter which dictates the crossover between ballistic and diffusive regime. The behavior of elastic mean free path in nanotubes and nanoribbons exhibit unique scaling features and can vary by orders of magnitude under a small Fermi level shift [76].

Systems which follow normal heat conduction also undergo a crossover from diffusive to ballistic regime when the length of the system is lowered. Length independent thermal current and linear dependence of thermal conductivity are considered as the signatures of ballistic transport. There are several experiments which show ballistic to diffusive crossover in low-dimension systems. In case of graphene nanoribbons it has been found that short, quarter-micron graphene samples approach the ballistic thermal conductance limit even at room temperature, due to the relatively large phonon mean free path (∼100nm) in substrate-supported graphene. However, patterning similar samples into nanoribbons leads to diffusive heat-flow [77]. Thus one observes a ballistic to diffusive heat transport as a function of the length (and also width) of the nano-ribbons. Different phenomenological approaches have been adopted in recent studies for the description of the ballistic to diffusive transport seen in many models and in experiments. People have used NEGF approach apart from other approaches like Boltzman transport equation, Buttiker formalism, Scaling theory etc. Thermal transport in atomistic systems with nonlinear interaction has been studied using the nonequilibrium Green's function which is quite powerful in mesoscopic systems and is applicable for both phonons as well as for electrons. However, we have not incorporated these interactions in our work. The nonlinearity is taken care of by using perturbative techniques or the mean field theory. This method works well for low temperatures but not for high temperatures and describes the quasi-ballistic transport in short carbon nanotubes at low temperature. This is in qualitative agreement with experiments [78].

5.5 Conclusions

We have presented the complete discretization and a NEGF based self-consistent procedure to simulate the conductance of a two terminal zigzag GNR based Nano-Scale device. This procedure can be extended for simulating armchair GNR and CNT based Nano-scale devices. We can also incorporate defects like atomic vacancies in our system and study its effect on the conductance and its I-V characteristics. The simulation procedure for defect related GNRs will be more challenging where we have to construct matrices for local $[\alpha]$ and $[\beta]$ by taking into account the vacancies. NEGF procedure has been discussed in detail to study the conductance in GNR. The discretization procedure for the GNRs and CNTs for zig-zag configurations has been discussed in detail. We have explained this with a block diagram where each block represents a block diagonal matrix. We have used tight-binding procedure to obtain the block diagonal matrices for GNRs. We have applied a recursive method to obtain the Green's function for GNR based channels.

Chapter 6

Transport properties of Zigzag Graphene Nanoribbons in the confined region of Potential well

6.1 Introduction

We report and adduced bandstructure by applying an external electrostatic potential inside the potential well or confined region, also outside the potential well. The local density of states (LDOS) has been shown in this chapter, how the Transmission occurs in zigzag graphene nanoribbon(GNR) inside the confined region of well. We want to study the confined (bound) states of an electron trapped inside the quantum well. We have studied the single subband in our system and calculated Transmission as well as the Local density of states and charge distribution. The nearest neighbour tight-binding model based on p_z orbital forms the Hamiltonian in our case. We have used Non equilibrium Green's function(NEGF) in our calculation to obtain the results. Transmission curves show oscillations with the increase of layers of unit cell in the confined region, as it happens in Fabry-Perot resonances. Charge distribution for the case of bound states has been discussed.

Quantum Transport in mesoscopic devices is becoming a topic of much research. We are interested in ZGNR since experimental-wise the zigzag GNR are relatively very easy to produce and their edges are very much favorable to form bonds with other atoms and as well with compounds [79–81]. Advancements in the field of Nano-Scale technologies have resulted in the fabrication of GNR and CNT-based devices. These novel devices may dominate the future of electronics and computer industries. Hence, it becomes extremely important to study Physics and the modeling of these GNR and CNT based devices. The most important thing that one should study first is conductance of these novel materials which will take the role of the channel in the futuristic nano-scale devices. As we know that nanoelectronics as well spintronics are rapidly emerging fields, and people have determined current corresponding to even a single molecule [2]. This is due to its application in diverse fields, so that our devices can become more efficient and powerful.

Graphene layers have honeycomb lattice of covalent-bond carbon atoms. It can be treated as two different sublattices, which can be labeled A and B as shown in Fig.(6.3).

Graphite-related materials have long been a subject of interest. Graphene has superb electrical properties as well as thermal properties. In case of graphene nanoribbon(GNR) people have observed band gap, which was not there in case of a graphene sheet, so that it can be used for as device purposes, since we know that band gap is inversely proportional to width of GNR [79]. Edge states of ZGNR has been discussed in this work, since finite graphite systems having a zigzag edge exhibit special edge states [82]. People have investigated the microscopic understanding of the conductance reduction [83]. Due to special bandstructure, it has not high mobility, but lot of other extraordinary properties. It has opened a new possibility in the fields of microelectronics, semiconductors and other novel applications.

Here, we study transport across a quantum dot created electrostatically by external potential as shown in Fig.(6.4). The red line indicates the energy of the quasi particle potential well. We have obtained the bandstructure in first Brillouin zone. The object of investigation is to study the transport properties of ZGNR of finite length/ZGNR based quantum dot is created electrostatically and which in principle is tunable.

Similar work has been done by applying gate voltage, where electric conductance of graphite ribbon with locally applied gate voltage has been studied in the form of Landauer approach. Nanographite ribbon with zigzag boundaries exhibits the single electronic transport channel due to the edge states with perfect transmission. In this work region, the region sandwiched by the barriers plays the role of a quantum dot, while in our work we have created potential well by fixing constant energy with red line Fig.(6.4) [84].

Researchers have studied GNR as bulk modes(BM), which are basis solutions to the Schrodinger equation. They have established a complete set of bulk modes for graphene ribbons at arbitrary energy within efficient electronic transport simulation of graphene based electronic devices [85]. They have also applied mode-matching approach to study the current blocking effect in GNR. It has been shown that the randomness of the interface tilting destroys the parity effect, if the spread of tilting parameter is larger than the lattice constant [86].

Our main motive is to show that GNR shows the metallic behavior inside the confined region of a potential well. We have also shown here that zigzag GNRs are metallic structures as it follows [87], but apart from that number of transmission peaks increases with the increase of number of layers of unit cells(M). Also it has been shown that proposed scheme matches with the ones already existing in literature, such as Fabry-Perot resonances curves.

We have studied only the single subband problem in our work. It has been shown in this chapter that graphite ribbon with a zigzag edge intrinsically possesses the edge states and it does not happen for the armchair case [87]. We have discussed only zigzag case and it matches with the above work. We have tried to study the bound states charge distribution of an electron trapped inside the quantum well. We have shown that maximum transmission occurs, when k.a=nπ, where n is the integer. We have investigated that number of peaks in transmission increases with the increase of a number of layers of unit cells(called M onwards). Van Hove singularities of the LDOS have been shown in the work. Furthermore latest studies proposed ZGNR as a strong candidate for application in spintronics devices [88]. We have investigated by using the TBGF(tight binding Green function) charge transport by calculating the low temperature conductance. To calculate the the wavefunction inside the well, we have used Eq.(6.3) where value of k is determined by the constant energy line that crosses the band structure as shown in Fig.(6.4) and also n which is called band number or transverse modes. The wavefunction ψ_{nk} is therefore the associated eigenstate corresponding to E(k,n). Now the overall wavefunction inside the quantum well is a linear combination of ψ_{nk} eigenstates whose energy is crossed by E=constant, it is the same energy which is shown with a red line in Fig.(6.4). Now the wavefunction becomes $\psi = \sum a_{nk}\psi_{nk}$ where sum runs over n and k quantum numbers of the crossed states. As shown in Fig.(6.4), e.g. in this figure E=constant line(red line) intersects 9 bands with n=1:5. Therefore for this E value, the overall wave function inside the quantum well is a linear combination of 9 ψ_{nk} eigenstates. GNR is a good one-dimensional structure, having low effective mass, smaller effective masses and momentum relaxation rates in the zigzag edge ribbons results in the electron mobility as much as an order of magnitude larger than the armchair edge ribbons [89] and also tunable band-gap. We have created a potential well by applying an external electrostatic potential like in our quantum mechanics potential barrier problem or finite potential well. Three regions have been created as shown in Fig.(6.4). We are only interested in a middle region called as confined region. We have used tight-binding method(TBM) in our work [90], since it gives atomic details and is also a real space approach. The low-energy band structure of graphene is gapless. We have studied in our work charge distribution for the case of bound states, when the bound states are formed in our system, instead of bandstructure, discrete energy levels will be formed, as we know from quantum dot case. We can see clearly from our charge distribution graphs that local charge distribution on the lattice is shown in color shapes, where the size of the circles is proportional to the amount of charge localized on the lattice points. We have compared in this work the results of a symmetric and asymmetrical cases(LDOS as well as Transmission). By using the TBGF (tight-binding Green's function) [82] formalism, we have tried to focus on the ballistic case, where no scattering plays any role and calculated the low-temperature conductance [91]. The electronic properties of GNR are sensitive to the geometry of their edges and the number of carbon atoms N across the ribbon [52]. The chapter is organized as follows. First we have shown the theoretical method including the Hamiltonian of the system, which is tridiagonal in form. We have shown the Quantum well in Fig.(6.4), how it is created by using an external potential and how the bandstructure differs in different regions of the potential well. We have tried to investigate the results of LDOS, transmission and charge distribution in the results and discussion section. In the last section, we have summarized the results.

6.2 Method

The geometry of the potential is given in Eq.(6.1) since

$$H_{tot} = H_{GNR} + V[\theta(x) - \theta(x - L)] \tag{6.1}$$

where $\theta(x)$ is the Heaviside function & V is constant. For V >0 the electrostatic potential takes the form of rectangular barrier, whereas for V <0 the potential is in the form of a quantum well. To model a quantum well, we assume that there is an external electrostatic potential, so that band-structure inside the well and outside will be different due to presence of external potential. We assume that there is an external potential in this form

$$V(x) = \begin{cases} V_0 & \text{if x <0 \& L<x ;} \\ 0 & \text{if } 0 \leq \text{x} \leq \text{L.} \end{cases} \tag{6.2}$$

Here, V_0 is the problem variable and its value is equal to 0.5eV. We have obtained the bandstrcuture by combining tight binding Hamiltonian with Bloch theorem. After diagonalizing the Hamiltonian and plotting the eigen values as a function of k yields the bandstrcuture as shown in Fig.(6.1). For the middle region (called confined region) V=0, so according to Bloch's theorem k-dependent Hamiltonian can be written as

$$H_k = H_{00} + H_{01}e^{ika} + H_{10}e^{-ika} \tag{6.3}$$

Which yields an energy and eigen states of the evanescent Bloch waves. Where H_{00} means when layer 0(inside confined region) is connected to 0 layer of the unit cells, similarly H_{01} is the layer 0 is connected to 1 of the unit cells and similarly for other layers of unit cells. Here lattice constant has been taken as $3.89A^0$. In the confined region general solution e^{ikx} and e^{-ikx} are the oscillatory solutions, where k indicates confined states. Going from one layer to next layer or previous one, wavefunction gains a shift in phase.

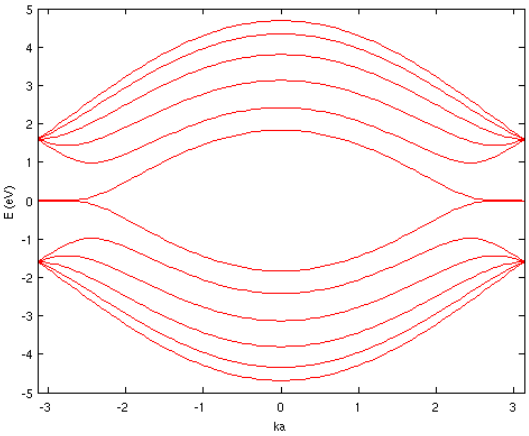

Figure 6.1: *The bandstructure of Graphene nanoribbon with terminated zigzag edges for number of atoms per unit cells=12.*

H_{00} in matrix form can be written as

$$[H_{00}] = \begin{pmatrix} 0 & -t & 0 & 0 & 0 & 0 & 0 & 0 & 0 & 0 & 0 & 0 \\ -t & 0 & -t & 0 & 0 & 0 & 0 & 0 & 0 & 0 & 0 & 0 \\ 0 & -t & 0 & -t & 0 & 0 & 0 & 0 & 0 & 0 & 0 & 0 \\ 0 & 0 & -t & 0 & -t & 0 & 0 & 0 & 0 & 0 & 0 & 0 \\ 0 & 0 & 0 & -t & 0 & -t & 0 & 0 & 0 & 0 & 0 & 0 \\ 0 & 0 & 0 & 0 & -t & 0 & -t & 0 & 0 & 0 & 0 & 0 \\ 0 & 0 & 0 & 0 & 0 & -t & 0 & -t & 0 & 0 & 0 & 0 \\ 0 & 0 & 0 & 0 & 0 & 0 & -t & 0 & -t & 0 & 0 & 0 \\ 0 & 0 & 0 & 0 & 0 & 0 & 0 & -t & 0 & -t & 0 & 0 \\ 0 & 0 & 0 & 0 & 0 & 0 & 0 & 0 & -t & 0 & -t & 0 \\ 0 & 0 & 0 & 0 & 0 & 0 & 0 & 0 & 0 & -t & 0 & -t \\ 0 & 0 & 0 & 0 & 0 & 0 & 0 & 0 & 0 & 0 & -t & 0 \end{pmatrix} \tag{6.4}$$

similarly H_{10} in matrix form can be written as

$$[H_{01}] = \begin{pmatrix} 0 & -t & 0 & 0 & 0 & 0 & 0 & 0 & 0 & 0 & 0 & 0 \\ 0 & 0 & 0 & 0 & 0 & 0 & 0 & 0 & 0 & 0 & 0 & 0 \\ 0 & 0 & 0 & 0 & 0 & 0 & 0 & 0 & 0 & 0 & 0 & 0 \\ 0 & 0 & -t & 0 & 0 & 0 & 0 & 0 & 0 & 0 & 0 & 0 \\ 0 & 0 & 0 & 0 & 0 & -t & 0 & 0 & 0 & 0 & 0 & 0 \\ 0 & 0 & 0 & 0 & 0 & 0 & 0 & 0 & 0 & 0 & 0 & 0 \\ 0 & 0 & 0 & 0 & 0 & 0 & 0 & 0 & 0 & 0 & 0 & 0 \\ 0 & 0 & 0 & 0 & 0 & 0 & -t & 0 & 0 & 0 & 0 & 0 \\ 0 & 0 & 0 & 0 & 0 & 0 & 0 & -t & 0 & -t & 0 & 0 \\ 0 & 0 & 0 & 0 & 0 & 0 & 0 & 0 & 0 & 0 & 0 & 0 \\ 0 & 0 & 0 & 0 & 0 & 0 & 0 & 0 & 0 & 0 & 0 & 0 \\ 0 & 0 & 0 & 0 & 0 & 0 & 0 & 0 & 0 & 0 & -t & 0 \end{pmatrix} \tag{6.5}$$

where H_{10} is the hermitian conjugate of H_{01}.

For the two end regions (first and third)

$$H_\alpha = H_{00} + H_{01}e^{\alpha a} + H_{10}e^{-\alpha a} \tag{6.6}$$

As it is clear from this equation that ik has been replaced by a pure real value say α. This guarantees that ψ will drop exponentially and α is called decaying constant.

Here we have taken the length of the well is 50nm and barrier height is 10meV.

Now the full Hamiltonian in the confined region becomes

$$[H] = \begin{pmatrix} [H_{00}] & [H_{01}] & \dots & \dots & [0] \\ [H_{10}] & [H_{00}] & \dots & \dots & \dots \\ \dots & \dots & \dots & \dots & \dots \\ \dots & \dots & \dots & \dots & [H_{01}] \\ [0] & \dots & \dots & [H_{10}] & [H_{00}] \end{pmatrix} \tag{6.7}$$

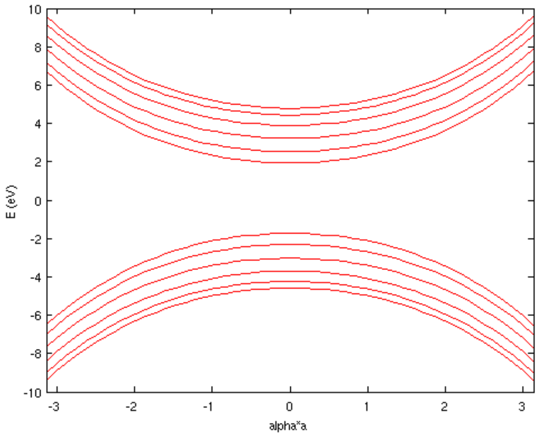

Figure 6.2: *The bandstructure in case of a Graphene nanoribbon in first and third region of quantum well, with terminated zigzag edges for number of atoms per unit cells=12.*

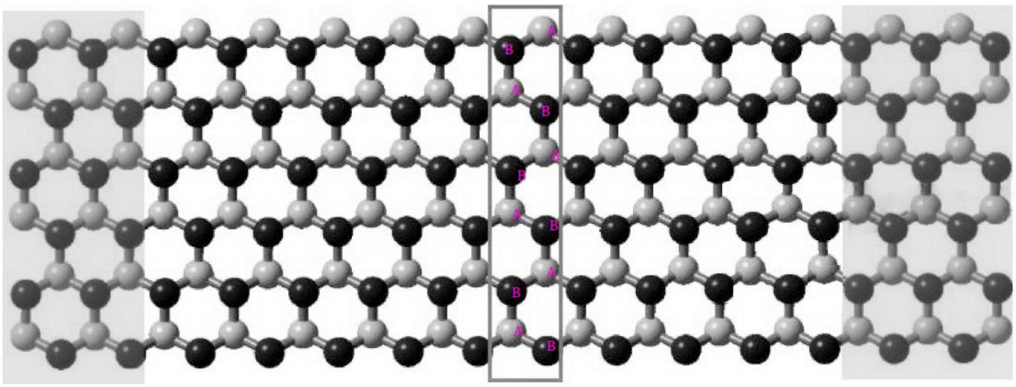

Figure 6.3: *Schematics of the transport channel connected to two semi-infinite Zigzag nanoribbons(shaded regions), in unit cell as shown in rectangle, having number of atoms per unit cells 12.*

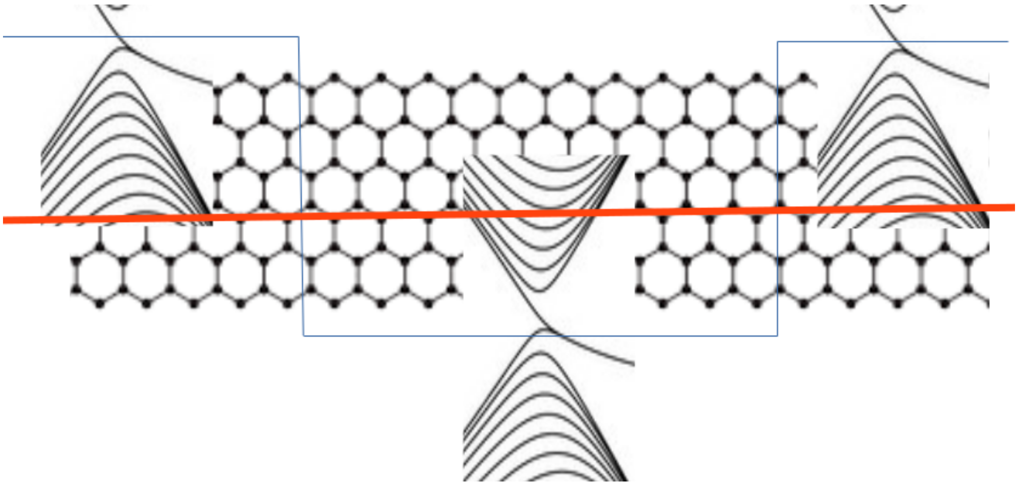

Figure 6.4: *Potential well created by applying an external potential, where red line shows the fixed energy.*

We have taken the distance between sublattices A and B to be equal to $0.46A^0$, as shown in Fig.(6.3). Configuration of our system is like iterative cells, where it is connected to two semi infinite zigzag nanoribbons towards left and right sides.
We use the non equilibrium Green function (NEGF) method for calculating DOS & the transmission function of our system. Here, the Green's function is calculated by using the method given in Datta's book [26],

$$G^r = (EI - H - \Sigma^r_{L,R})^{-1} \tag{6.8}$$

where G^r is the retarded Green function and G^a is the advance Green function. Also, $(G^r)^\dagger = G^a$. $\Sigma^r_{L,R}$ are the self energy matrices. At the ends, the surface Green's function includes the effect of semi-infinite surface layers and it is calculated by Lopez Sancho algorithm [92].

$$\Sigma^r_L = H^\dagger_{LC} G^0_L H_{LC} \tag{6.9}$$

Similarly for right side, we can write Σ^r_R which is the coupling matrix to the leads.

Transmission function can be written as [93]

$$T = Tr(\Gamma_L G^r \Gamma_R G^a) \tag{6.10}$$

which indicates transmission per energy channel between left and right leads and Γ_L and Γ_R are the broadening functions corresponding to left and right sides which are given as

$$\Gamma_L = i[\Sigma_L - \Sigma_L^\dagger] \tag{6.11}$$

$$\Gamma_R = i[\Sigma_R - \Sigma_R^\dagger] \tag{6.12}$$

6.3 Results And Discussion

DOS is equal to [94]

$$DOS = \frac{-Im(Tr(G))}{\pi} \tag{6.13}$$

where Im indicates the imaginary part.

As we can see clearly from Fig.(6.7) that Van Hove singularities occurs, which is non-smooth in the curve and reflect the onset of quasi-1D energy subbands, which have been observed experimentally. It is also observed in similar 1D structures such as for ordered case of grain boundaries of graphene [95] and also in case of carbon nanotubes [96]. Fermi energy of the structures has been taken equal to zero (reference point). The longest peak in the density of states indicates the localized edge states of zigzag nanoribbon, which does not occur in case of armchair. Fig.(6.5(a)) and Fig.(6.5(b)) shows the results for symmetric & asymmetric cases.

For symmetric case, the number of layers between left and right is M=20, while N (number of atoms per unit cell)=12 and $V_L = V_R$.

The number of layers for asymmetric case is also the same (M=20). The only

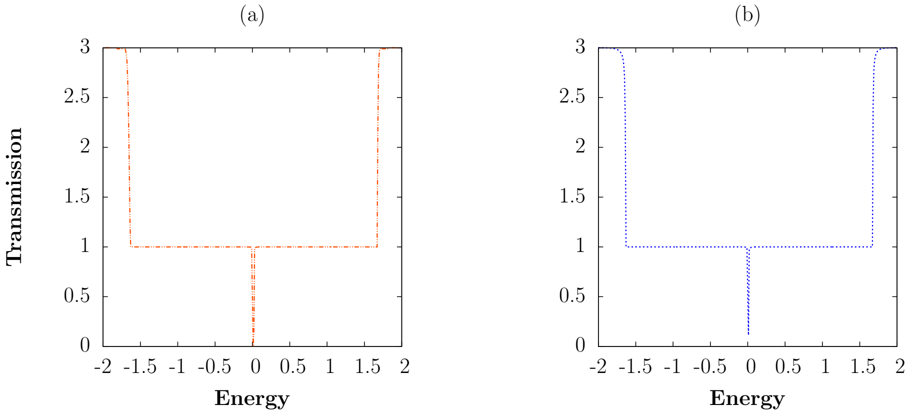

Figure 6.5: *Transmission in case of symmetric potential well (a)* $V_L = V_R$ *& asymmetric case (b)* $V_L \neq V_R$*, energy is in* eV*.*

difference is that here we have taken $V_L \neq V_R$.

We can show here also that how the charge distribution occurs in the confined case.

Fig.(6.6) shows the charge distribution results for symmetric case, where $V_L = V_R$. Here the size of circles is proportional to the amount of charge localized on the lattice points. Fig.(6.7(a)) show the LDOS in case of symmetric $V_L = V_R$ & Fig.(6.7(b)) show asymmetric case $V_L \neq V_R$.

When we increase N (number of atoms per unit cells) additional subbands (transverse modes) will contribute to electron transport and as a result the number of plateaus (step like conductance transition) increases. Conductance is quantized as one should expect, this curve has a type of step function and it also matches with the basic concept of quantum conductance. We see from Fig.(6.8) that number of oscillations is proportional to M (number of layers of unit cells). The transmission function oscillates with energy due to the resonance effect caused by confined states. This is similar to Ramsauer-Townsend effect [97]. We see that resonances give 100% transmission at certain energies. Resonances occur [97], when the distance covered by the particle in traversing the well back 2L is an integral multiple of the de-Broglie wavelength of the particle inside the potential.

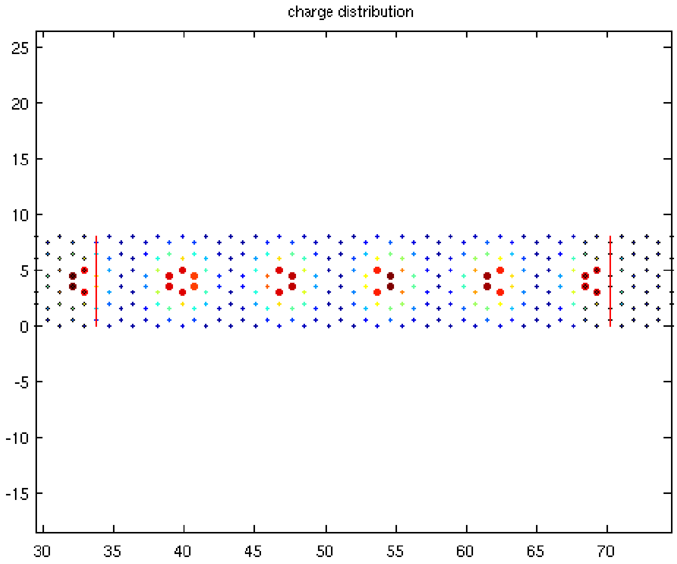

Figure 6.6: *Charge distribution in case of symmetric potential well, when N=12, M=20, tt=2.7eV(hopping), a = 2.46Å(lattice constant),* V_L *= 20 meV,* V_R *= 20 meV (x-axis=x-atoms, y-axis=y-atoms).*

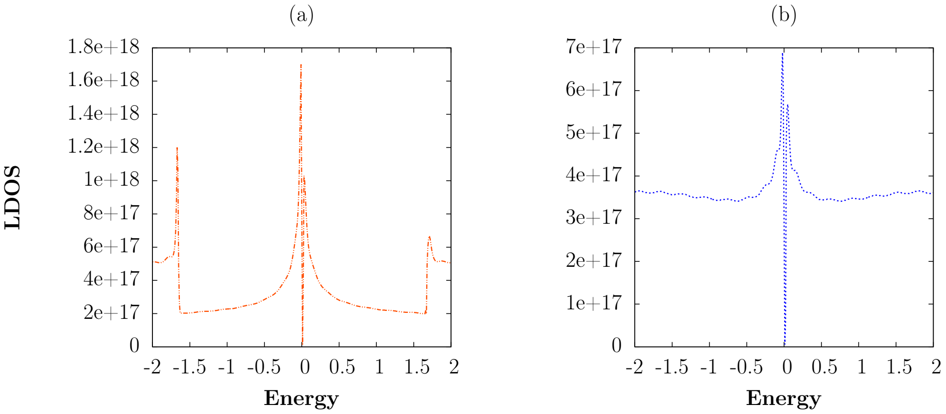

Figure 6.7: *LDOS in case of (a) symmetric and (b) asymmetric case, Energy is in eV.*

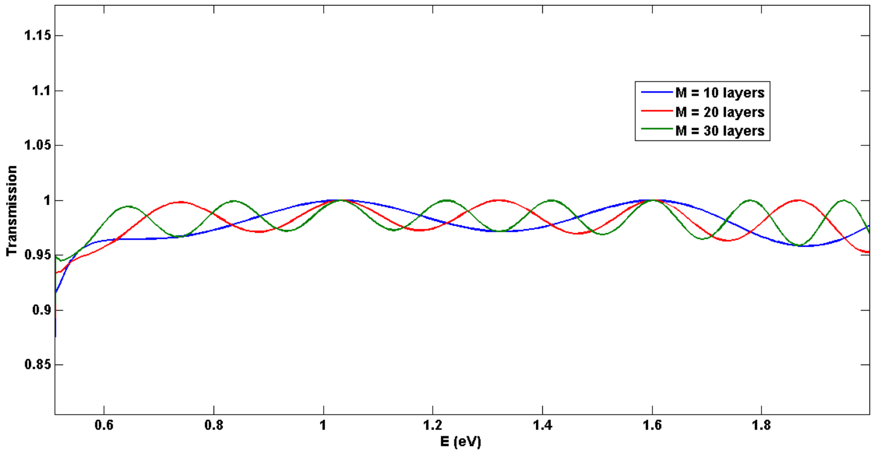

Figure 6.8: *Transmission oscillations increases with M.*

For E $>V_0$ reflections at potential discontinuities are not accompanied by any phase change. Therefore, the resonances correspond to formations of standing waves with in the potential well.

At resonance the waves incident on the potential at x=0, and the waves reflecting between the walls of the potential are in phase and reinforce each other. Far from resonances, standing waves can't be formed. Here, waves reflecting between both walls of the potential at x=0 and x=L, and the waves transmitted at x=0 are out of phase and corresponds to the destructive interference. The physics here is same as it used to happen in Fabry-Perot interferometer in optics, where the resonance condition and functional form of Transmission coefficient are the same.

Here T(E) and it is easy to know for which E values the transmission function is maximum. For n=1, k=1.884, so energy from this k value is E(6)=-1.043eV. From the above Fig.(6.9), we can see clearly that maxima occurs at E=-1.043 eV, which is also there in maximum transmission values as shown in Fig.(6.5). As shown in Fig.(6.9) with arrow also, upper arrow is for E(6)=-1.043, while lower arrow is for E(7).

In literature people usually know of a graphene quantum well as a p-n-p structure, as we have shown in Fig.(6.5-6.7), for symmetric as well as asymmetric case.

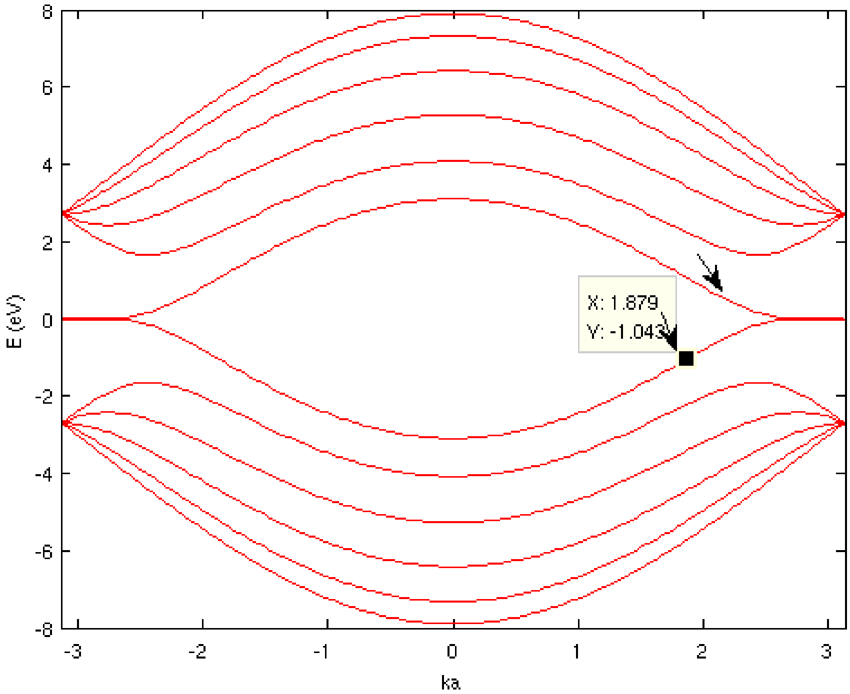

Figure 6.9: *Bandstructure a=2.46, N=12, M=12,* $V_L = V_R$*=10 mev.*

The local charge distribution is shown in Fig.(6.6) as well as in Fig.(6.10) in color scales. In Fig.(6.8) the oscillations in Transmission function mean that the probability of transmission is a function of energy. Physically speaking, it means that tunneling depends upon resonance like conditions. Here, we don't need to go beyond the energy limits (-2,2) as shown in Fig.(6.9), since it is single channel problem. Transmission function oscillates with E, so the maxima of these oscillations should coincide with the energies obtained through the Hamiltonian corresponding to

$$k = \frac{n\pi}{Ma} \tag{6.14}$$

where k is the wave vector, M is the number of layers of unit cell in transverse direction and 'a' is the lattice constant. Transmission is clearly positive and indicates the metallic behavior.

We have studied transport in the confined region of a potential well by giving

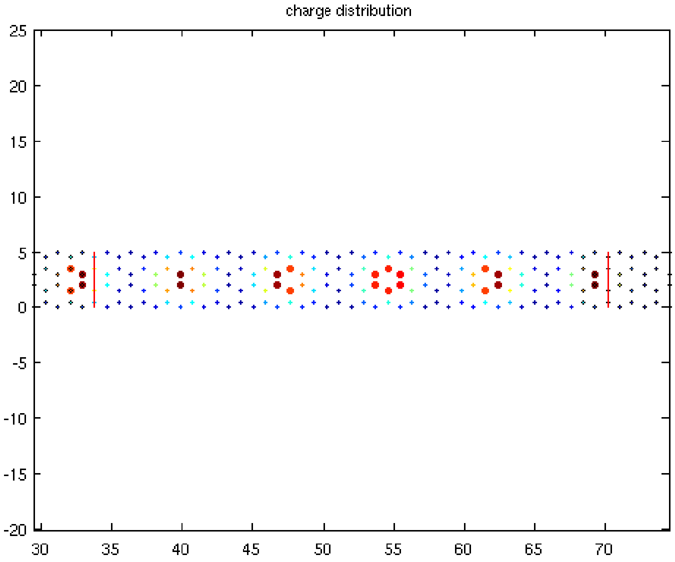

Figure 6.10: *Local charge distribution on the lattice points is shown in color and size is proportional to the amount of charge localized on the lattice points, when N=8, M=20,* $V_L = 20$, V_R*=10 mev(x-axis=x-atoms, y-axis=y-atoms).*

an external potential of 0.5 eV. Initially we have fixed the energy. We have created three regions in the graphene sheet. We have given left potential as well as right potential, including height of the barrier. We have focussed in the middle region of the well, where electrons have been confined. We have seen transport properties in the confined region. Edge states have been formed in this system. We have taken the number of atoms in the unit cell (N=12). These slices of unit cells are denoted M here onwards. We have seen in our transmission curves that when we are increasing M, number of peaks are increasing accordingly. Physically this happenes in case of Fabry Perot resonance curves. Where we have seen that resonance occurs at particular frequency [98]. At particular energy resonance occur in our system. It happens exactly like in the case of potential well. We can see from Eq.(6.14) that k is inversely proportional to M. For a fixed value of energy we have different k's in first Brillouin zone. Since it is a single subband problem, so we are not going for multi subbands. Perfect transmission occurs in our system. Bound states of the charge distribution have been shown at lattice points in the confined region of potential well.

The wavefunction outside the quantum well is exponentially damping, because we are only interested in confined states. When we are moving from one unit cell to the next in confined region, there is a phase shift in wavefunction. Phase shift is e^{ikx} in the forward direction and e^{-ikx} in the backward direction.

6.4 Conclusions

We have studied the electronic structure of ZGNR in a quantum well, which has been created by giving an external electrostatic potential. By using Tight binding Hamiltonian we first showed the band structure inside the middle region (confined region) of well, where stationary states have been formed. Later we have shown the behavior of LDOS, transmission as well as how the charge is distributed on the lattice points for symmetric and asymmetric cases. LDOS provided us the information about the distribution of electrons in the system. LDOS curve indicates that localized edge states make a sharp peak near the Fermi level, since there are few states near the Fermi level. Transmission and LDOS curves show that edge states clearly depend on the number of atoms in a unit cell, where electronic properties of the system are very sensitive to width and edges. The conducting behavior which we clearly show is also confirmed from the high transmission peak at the Fermi level peak in the LDOS. We can conclude from the Fig.(6.9) that spectrum is almost symmetric about the Fermi level and large transmission platforms continues until the energy reach +1.66eV and -1.66eV transmission coefficient undergoes drastic increase. Large peak is observed in the LDOS curves at the Fermi level and it corresponds to first quantized conductance band magnitude $\frac{2e^2}{h}$, while other peaks in the LDOS curves shows the quantized steps in the conductance curves.

In the limit of infinitely large number of atoms in the unit cell the conductivity of the system under consideration should converge to that of graphene. Although graphene has notoriously high conductivity, it is not a superconductor. It is known that intercalation by Ca is necessary to make it superconductive [99].

Chapter 7

Random Matrix Theory and Quantum Chaos

Random matrices first appeared in mathematical statistics in the 1930's, but got very less attention at that time. Inspite of huge success of statistical methods in describing the macroscopic thermodynamic behavior of physical systems, its relation to the underlying microscopic dynamics has remained a subject of debate [100]. It was very much clear since the beginning that we cannot directly apply the classical notion of chaos to quantum mechanical systems [101], for the simple reason that Schrodinger's equation is linear and cannot have exponentially departing trajectories. The theory became a cornerstone of modern physics. One should concentrate on the statistical properties of energy levels. Wigner's ideas were further extended by the seminal work of Dyson [102], who contributed towards the symmetry classification of Hamiltonians and showed the existence of three major symmetry classes of random matrices, orthogonal, unitary and simplectic. RMT was designed by Wigner to deal with the statistics of eigenvalues and eigenfunctions of complex many-body quantum systems [103]. In 1951, Wigner proposed the use of RMT to describe some properties of excited states of atomic nuclei and it was the first time this theory was used to model physical reality [103]. RMT became a powerful tool of mathematical physics in 1960's, notably given by Wigner, Dyson, Mehta and Gaudin. Mehta and Gaudin [104] developed the method of orthogonal polynomials. Mehta, Gaudin, Porter and Rosenzweig followed the ideas of Wigner. The idea behind it was to understand the statistics (particularly) of the distributions of spacings between energy levels of heavy nuclei, measured in nuclear reactions. In recent years there is huge interest in RMT mainly because of two reasons. Firstly, the Wigner-Dyson ensemble applies generally to chaotic systems [105, 106]. The RMT of quantum transport is a statistical theory of the transmitted eigenvalues of an open system [107], and RMT established by Wigner and Dyson addresses the statistics of energy levels in a closed systems.

7.1 Quantum Chaos-RMT

Chaos refers to the non-linear and irregular, deterministic behavior of a system that is very sensitive to the initial conditions. By chaos, we mean an irregular complex motion whose long behavior in detail is not predictable. The long term behavior in a non-linear system may become ultrasensitive to the initial conditions. Initial conditions play very important role in integrable motion, since we can predict the future path of the system with initial condition. Classical chaos is considered to be a property of bounded macroscopic systems. A small change in the initial conditions may completely change the future path of the system and hence the resulting motion is not predictable. Here, the system is classical and hence its motion is governed by the laws of classical mechanics. Thus, the motion is completely deterministic, but its long term behavior is chaotic. This is why the phenomenon of chaos is called deterministic chaos. Further in chaos, specific solutions change exponentially in response to small changes in the initial conditions. It is to be understood that the chaotic motion is not completely random. In a random sequence, the successive terms are governed by a definitive probability distribution, but are not completely determined. According to the Bohigas-Giannoni-Schmit (BGS) conjecture [108], classical chaos is a sufficient condition for the applicability of RMT. RMT describes the statistical fluctuations in the universal regime. Instead of trying to explain individual eigenfunctions, RMT discusses about the statistical behavior [103]. It took a large number of numerical studies to confirm the BGS conjecture. The BGS conjecture states that quantum spectra of classical chaotic systems are universally correlated according to the Wigner-Dyson random matrix ensemble [109]. In 1984, BGS gave proof that the quantum energy level sequence of systems with chaotic classical counterparts have statistical properties that fit the prediction of RMT [110].

The Kicked rotator is a model for chaos and quantum chaos studies. The model is described by the Hamiltonian

$$H(p,x,t)=\frac{p^2}{2}+K\cos(x)\sum_{n=-\infty}^{\infty}\delta(t-n) \tag{7.1}$$

Where δ is the Dirac delta function, x is the angular position, p is the momentum, K is the kicking strength as shown in Fig.(7.1) for different K's. Fig.(7.1) shows an area-preserving map for two canonical dynamical variables momentum and position (p,x) for different values of K [111], where large value of K green region is the main chaotic region of the map. Dynamics of K is described by the standard map

$$p_{n+1}=p_n+K\sin(x_n),\;\; x_{n+1}=x_n+p_{n+1} \tag{7.2}$$

With the caveat that p is not periodic as shown in the Fig.(7.1). Fig.(7.2) shows the system becomes more chaotic as dynamical symmetries are broken by increasing the quantum defect. Regular classical dynamics is manifested by a Poisson

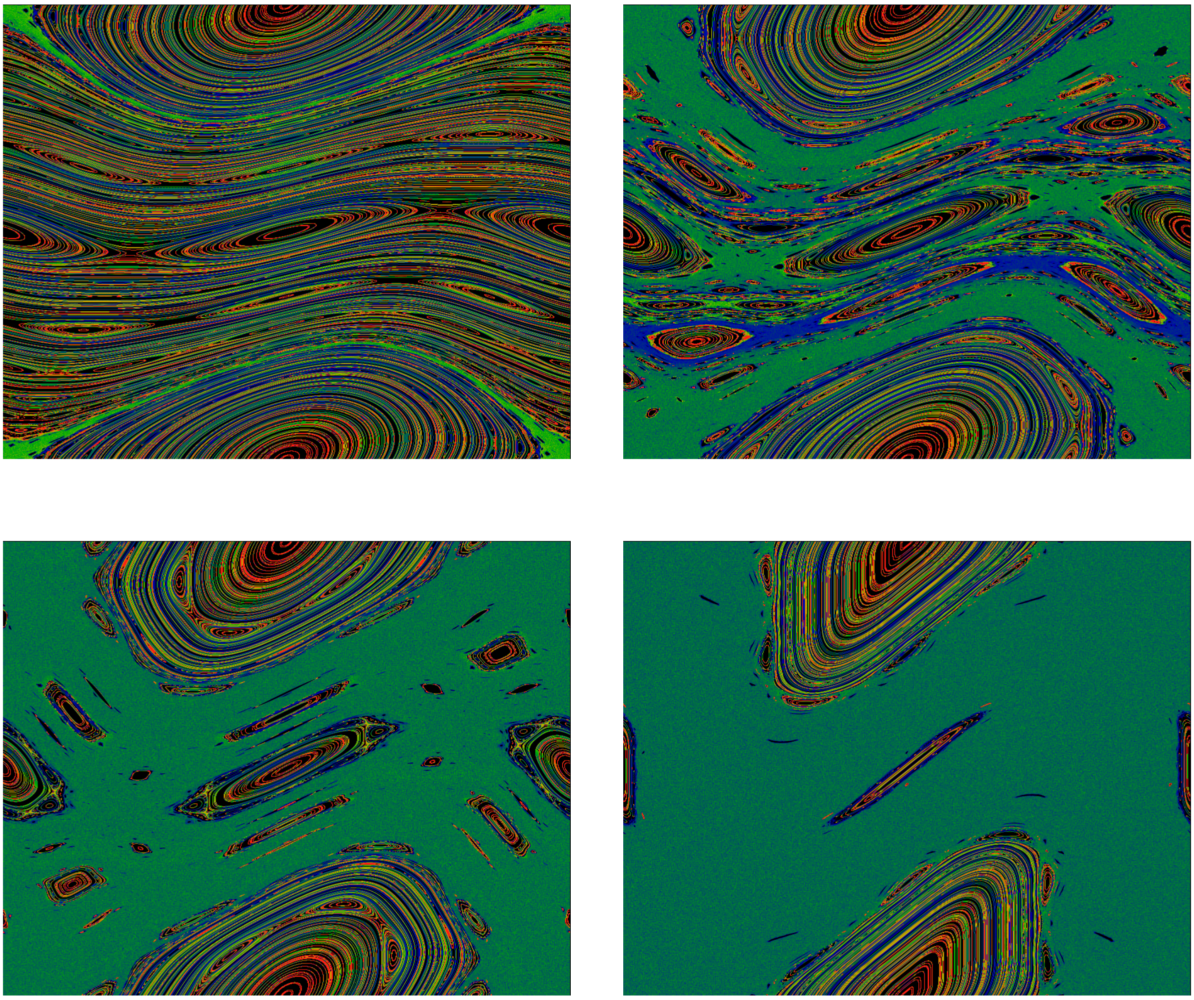

Figure 7.1: *Orbits of the standard map for K = 0.6(Top left), K=0.972(Top right), K=1.2(Bottom left), K=2(Bottom right) (Image taken from wikipedia commons)*

distribution of energy levels

$$P(s) = e^{-s} \tag{7.3}$$

the systems which show chaotic classical motion are expected to be characterized by the statistics of random matrix eigenvalues ensembles. If the normalized spacing between two energy levels is s, the normalized distribution of spacing is well approximated by

$$P(s) = \frac{\pi}{2} e^{-\pi \frac{s^2}{4}} \tag{7.4}$$

Although many Hamiltonian systems which are classically integrable (non-chaotic) have been found to have quantum solutions that exhibit nearest neighbor distributions. The systems which exhibit classical chaos have been found with quantum solutions yielding a Wigner quasiprobability distribution.

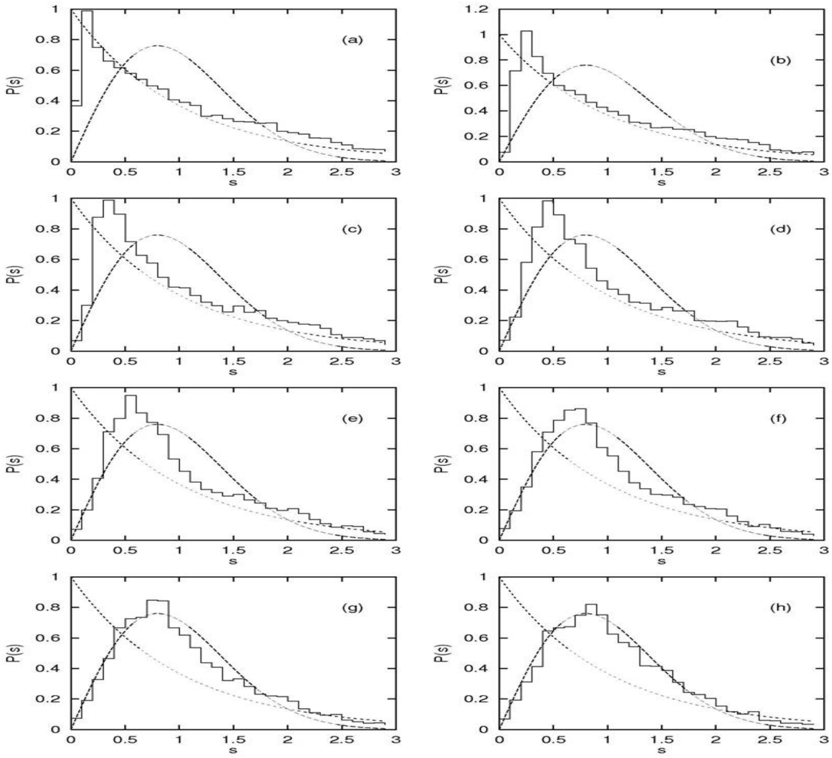

Figure 7.2: *Nearest neighbor distribution for Rydberg atom energy level spectra in an electric field as Quantum defect is increased from 0.04 (a) to 0.32 (h). The system becomes more chaotic as dynamical symmetries are broken by increasing the Quantum defect; consequently, the distribution evolves from nearly a Poisson distribution (a) to a quasiprobability distribution (h). (Image taken from wikipedia commons)*

Recently, there have been studies [112], where scattering of electromagnetic waves in a billiard like system has become a standard experimental tool for studying properties associated with quantum chaos. RMT describes statistics of eigenvalues and eigenfunctions in quantum mechanical language and remains one of the pillars of theoretical understanding of quantum chaotic systems. RMT is a natural tool for quantum information theory as well [113]. It is of importance for both its conceptual and its predictive powers. Many essential tools have been developed to analyze properties of random matrices.

Recently, more and more disciplines of science and engineering have found RMT valuable. RMT is rapidly progressing day by day and there are an increasing number of applications in the context of information theory and communication systems, especially in studying the properties of complex networks.

RMT aims to understand correlations between eigenvalues independently of the variations of level spacings. In random matrices, one is concerned with the question that given a large matrix whose elements are random variables with given probability laws, then what can be said about the probability of some of its eigenvalues and eigenvectors? This question is of pertinence to the understanding of the statistical behavior of slow neutron resonances in nuclear physics, where it was studied intensively by Physicists. This question gained importance later in other areas of physics and mathematics like characterization of chaotic systems, conductivity in disordered metals and many more areas of research. In case of bulk metals, at high temperature the electronic energy levels lie very near to each other and are broad enough to overlap and form a continuous spectrum. When we decrease the size of the sample, spectrum becomes discrete and when there is reduction in temperature, the width of the individual levels decreases. When the metallic particles are minute enough at low temperature, the spacing of the electronic energy levels may eventually become larger than the other energies, like the level widths and thermal energy k_bT. The thermal and electromagnetic properties of the fine metallic particles may deviate considerably from those of the bulk metal.

7.2 GOE and GUE

Wigner distributions for nearest neighbour level spacings are observed in a large variety of very different systems, ranging from the atomic nucleus to the microwave billiard. In random matrix theory this fact is accounted for by replacing the Hamiltonian by a matrix whose elements are randomly chosen. We are not completely free in fixing the matrix elements. The universality class restriction for the matrix elements have to be obeyed [22]. In a fully chaotic system one set of basis functions is a priori suited as well as the other. The correlated probability $p(H_{11}, ..., H_{NN})$ for the matrix elements should therefore not depend on the set of basis functions applied. This leads to the invariance property

$$p(H_{11}, ..., H_{NN}) = p(H^{'}_{11}, ..., H^{'}_{NN}) \tag{7.5}$$

$H^{'}$ is obtained from H by an orthogonal transformation $H^{'}$=OHO^{T} with OO^{T}=1. By means of Eq.(7.5) the number of possible forms for p($H_{11}, ..., H_{NN}$) is radically reduced. Functions of the H_{nm} being invariant under orthogonal transformations can depend only on the traces of powers of H. This is a consequence of the commutative property

$$Tr(OAO^{T}) = Tr(AO^{T}O) = Tr(A) \tag{7.6}$$

of the trace. Thus p($H_{11}, ..., H_{NN}$) can be expressed as

$$p(H_{11}, ..., H_{NN}) = f[Tr(H), Tr(H^{2}), ...]. \tag{7.7}$$

Moreover, we demand that the matrix elements are uncorrelated

$$p(H_{11}, ..., H_{NN}) = p(H_{11})p(H_{22})...p(H_{NN}) \tag{7.8}$$

The only possible functional form for $p(H_{11}, ..., H_{NN})$ obeying both Eq.(7.7) and Eq.(7.8) is given by

$$p(H_{11}, ..., H_{NN}) = Cexp[-BTr(H) - ATr(H^2)] \tag{7.9}$$

Without loss of generality we may take B=0 as it is always possible to shift the average energy, 1/N Tr(H), to be zero. The prefactor C is mixed with the help of the normalization condition

$$\int p(H_{11}, ..., H_{NN})dH_{11}...dH_{NN} = 1 \tag{7.10}$$

For the orthogonal case the nondiagonal matrix elements occur twice in the exponential function each yielding a normalization prefactor $\sqrt{2A/\pi}$, whereas the normalization factor for the diagonal elements is given by $\sqrt{A/\pi}$.

$$p(H_{11}, ..., H_{NN}) = (A/\pi)^{N/2}(2A/\pi)^{N(N-1)/2}exp(-A\sum_{n,m} H_{nm}^2) \tag{7.11}$$

The constant A may be expressed in terms of the variance either of the diagonal matrix elements

$$< H_{nm}^2 >= \sqrt{A/\pi}\int H_{nm}^2 exp(-AH_{nn}^2)dH_{nn} = 1/2A \tag{7.12}$$

for nondiagonal elements

$$< H_{nm}^2 >= \sqrt{2A/\pi}\int H_{nm}^2 exp(-2AH_{nm}^2)dH_{nm} = 1/4A \tag{7.13}$$

The set of all real random matrices with matrix elements obeying the distribution function (7.11) defines the Gaussian Orthogonal Ensemble (GOE). In complete analogy we obtain the Gaussian Unitary Ensemble (GUE) and the Gaussian Symplectic Ensemble (GSE) by the demand that the distribution of the matrix elements is invariant under unitary and symplectic transformations, respectively. For the correlated distribution of matrix elements of the GUE we get

$$p(H_{11}, ..., H_{NN}) = (A/\pi)^{N/2}(2A/\pi)^{N(N-1}exp\{-A\sum_{nm}[(H_R)^2_{nm} + (H_I)^2_{nm}]\} \quad (7.14)$$

where $(H_R)_{nm}$ and $(H_I)_{nm}$ are the real and imaginary parts of H_{nm}, respectively.

7.3 Applications

The theory has applications in biology, like in sequence matching, RNA folding, gene expression network. It also has applications in other fields of interest like in economics and finance, time series analysis, and in statistics, like in case of multivariate statistics, principal component analysis (PCA), image processing, data compression, Bayesian model selection. Random matrices are now used in fields such as condensed matter physics, statistical physics, chaotic system and many more areas [114]. RMT can be applied in number of fields including quantum dots (artificial atoms) quantum chaos, as well as application to Andreev billiards-quantum dots with induced superconductivity [115]. RMT has been widely used in physics in various areas like in disorder and localization, mesoscopic transport, optics, quantum entanglement, neutral networks, gauge theory, QCD, matrix models, cosmology, string theory, statistical physics (growth models) [116]. Applications of RMT to condensed matter physics search for universal features in the electronic properties of metals originating from the universality of eigenvalue repulsion [117]. In condensed matter physics applications of RMT fall into two broad categories. In the first case, one studies the thermodynamic properties of closed systems, such as metal grain or semiconductor quantum dots. The random matrix being the Hamiltonian (H), while in the second case one studies the transport properties of open systems, such as metal wires or quantum dots with point contacts. In this case the random matrix is the scattering matrix S. Both these categories have flourished with the development of nanotechnology. In case of quantum wires and quantum dots confinement of electrons at the nanoscale in wire geometries and box geometries respectively preserve their phase coherence [117], which is required for RMT to be applicable. Since RMT deals with the statistical properties of large matrices with randomly distributed element, it can be used to calculate the correlation functions of eigenvalues and eigenvectors from probability distributions [107]. Secondly, the discovery of a relation between universal properties of large matrices and universal conductance fluctuation [107], in disordered conductors [118, 119]. The RMT of quantum transport is concerned with the mesoscopic systems, which are at the borderline between the microscopic and macroscopic world [107]. RMT relates the universality of transport properties to the universality of correlation functions of transmission eigenvalues. It is worthwhile to recall the fundamental development of nuclear theory preceding it. In case of scattering of slow neutrons by medium-weight and heavy nuclei, narrow resonances had been observed. Each of these resonances corresponds to a long lived "compound state", in the famous paper of Niels Bohr, on the compound nucleus, as a system of strongly interacting neutrons and protons [120]. In this way, Bohr laid the ground for Wigner's work and RMT can be seen as a formal implementation of Bohr's compound nucleus hypothesis [103].

The relation between classical and quantum chaos was first identified in 1984 and stated that the statistical quantal fluctuations of a classically chaotic system are described by RMT. Statistical properties of chaotic systems follow the prediction of RMT [105]. RMT differs in a fundamental way from the conventional statistical approach. RMT has no scale, its physical parameter is determined by the mean level spacing and leads to universal predictions [108]. Just as, like charges repel each other, same thing happens in case of eigenvalues. To understand, the connections between classical and quantum physics, statistical analysis of the eigenvalues of quantum systems has become an important tool [110]. The eigenvalues of random hermitian matrices have some statistical properties like those of chaotic classical systems. As explained in [110], for the last 40 years researchers have been investigating whether there are any qualitative differences between quantum systems, whose classical counterparts are chaotic and those whose classical counterparts are regular. Most of the numerical techniques and experimental work supports these conjecture, although some researchers have taken the statistical properties of the spectra as the definition of quantum chaos, but this is not universally accepted. Quantum chaos, a mysterious counterpart of the classical dynamical chaos, is one of the most intriguing problems in contemporary physics, currently under extensive study by many researchers throughout the world [121]. The qualitative sequence has also found applications in areas outside physics like in mathematics. In number theory, e.g the sequence of prime numbers is statistically similar to a sequence of random numbers, while the imaginary part of nontrivial zeros of Riemann zeta functions have statistical properties that fit into the prediction of RMT [110, 122]. It indicates connections between quantum mechanics and number theory as well. The eigenvalues of a quantum system, whose classical counterpart is integrable, are not correlated at all and they exhibit level clustering and statistical properties similar to those of random numbers [110]. In contrast, the eigenvalues of a quantum system whose classical counterpart is chaotic as well as strongly correlated, exhibit level repulsion and are statistically similar to the eigenvalues of random matrices. RMT also describes statistical properties of interacting systems at high enough excitation.

In our 1D disordred system the Hamiltonian matrix is relevant for analyzing spectral statistics of disordered or classically chaotic systems. We have focussed in our work only on the disordered case. In our work, we are not going beyond 1D (disordered wire case), so we are not discussing here about 2D and 3D systems.

The description of RMT can be modified by the absence of complex phase factors. Random matrix is designed for an ensemble of chaotic scatterers and scattering is due to disorder, while all the different members of an ensemble have different disorder configurations [115]. RMT discusses many universal properties and there are a variety of systems to which it might be applied. We have shown in the next chapter that a 1D disordered system gives interesting properties in the mesoscopic regime.

Chapter 8

Mesoscopic fluctuations, two-parameter scaling and concommitant unusual level spacing distributions in finite 1D disordered systems

8.1 Introduction

As we discussed in the previous chapter, the Random Matrix Theory (RMT) deals with the statistical properties of very big matrices. We study the evolution of the random level spacing distribution in a finite-sized, disordered chain as it crosses over from a ballistic to the strongly localized regime (as a closed 1D quantum system). In a disordered chain with random but real-valued site-potentials, almost all the states are exponentially localized and hence an incident plane wave ($\sim e^{ikx}$) propagating in the positive x-direction is completely backscattered due to the well-known localization effects [123]. Because the hamiltonian is random, its eigenvalues (energy levels) are also random. There have been a lot of works [124] on the level spacing distribution (LSD) as well in such random disordered systems. The motivation for such studies come from the original works of Wigner [125], Dyson [126], and Mehta [127] on the nuclear level spectra of heavy elements, where the number of levels are so large that they warrant a statistical description. But, for a disordered system, whose hamiltonian may be represented by random matrices, randomness in the spectra and consequently the randomness in the level spacings come in a natural way.

It was known for a long time that in the disordered metallic regime, the LSD becomes one of the three Wigner-Dyson types (depending upon the three possible symmetry classes), whereas in the insulating regime it assumes a Poissonian form. These four *universal* behaviours were the only known ones to exist in the large length ('thermodynamic') limit. More recent works [128] indicate that asymptotically close to the critical disorder strength for the Anderson's metal-insulator (M-I) transition (which occurs only above 2D if the electrons are non-interacting and if there is no magnetic field), the LSD is neither Wigner-Dysonian on the metallic side, nor Poissonian in the insulating (localized) side, but it takes one of the *universal* forms as one renormalizes to the large infinite length limit. Further, the behaviour at the transition with a critical disorder, if there is one, is non-universal (i.e., none of the above four) even in the thermodynamic limit. As in these discussions, our studies below pertain to effectively non-interacting electrons.

One of the characteristic features of disordered mesoscopic systems is the statistics of its anomalously large conductance fluctuations and its universality in the diffusive regime. A lot of works [129] have been done in this area starting with the numerical work of Stone and Lee and the analytical work of Altshuler and others [130], to demonstrate that in the diffusive (disordered but metal-like) regime the sample-to-sample fluctuations of the two-probe conductance or the transmittance becomes universal. This is called the universal conductance fluctuation (UCF). The universality relates to the fact that the fluctuation (say, the standard deviation) is independent of the size of the system, the strength of disorder, the Fermi energy of the charge carriers, or the type of hamiltonian (say, Schrodinger with Kronig-Penney model, or the nearest neighbour tight binding one). Hence the UCF is expected to be independent of the specific material parameters, but does depend on the dimensionality of the system. For a long time, it was believed that, strictly speaking, the UCF occurs only in 3D, 2D and quasi-1D; but UCF cannot occur in 1D. But, in a series of recent works (starting with ref [131]), we have shown that an almost diffusive regime does occur even in 1-D (where $\xi = 4l_e$) and hence UCF is achieved in 1D as well starting from a length L of about $2l_e$ and persisting upto a length of about $5l_e$ (slightly larger than ξ). To put things in perspective, we quote the UCF values (in units of $2e^2/h$, considering electrons of two spin varieties): they are about 0.544, 0.431, 0.365 [130] and 0.30 [131] in three, two, quasi-1D, and exactly 1D respectively.

More interestingly, we observed [131, 132] an inadequacy of one parameter scaling [129] in 'finite-sized' 1D samples from the quasi-ballistic through quasi-diffusive to a mildly localized regime which we find to be about twice the localization length. The phrase 'mild localization' has been used to imply stronger than weak localization ('dirty' metallic or quasi-diffusive as discussed above) which appears in the length regime $l_e{<}L{<}\xi$.

In our previous work [133] (referred to as I from now on), we had reported that there are at least two relevant parameters for describing the conductance in this regime in the sense that the mean and the variance of the entity u=ln(1+$R_4(L)$)=-lnT(L), increase as a function of the length L with two distinct power-law exponents. Here T(L) is the transmittance and R_4(L) is the four-probe resistance of a sample of size L. Inside the mildly localized regime, $\langle u \rangle \sim$ L for any Fermi-energy (E_F), but var(u)$\sim L^{\kappa}$, where κ depends upon the E_F and is always greater than 1. Beyond this length scale (L > app. 7ξ in our work), the behaviour slowly crosses over towards the one parameter scaling behaviour in the thermodynamic limit in the sense that both $\langle u \rangle$ and var(u) diverge with the same exponent 1, irrespective of the E_F. In I, we had presented a typical case of W/V=1.0 and E_F/V=1.6 where V is the hopping term and found that κ =1.57. We give here the values of κ for some other Fermi energies (but the same W): (i) for E_F/V=0.1, κ=1.54, (ii) for E_F/V=0.5, κ=1.68, and (iii) for E_F/V=1.9, κ=1.39. Thus, it appears that from the quasi-ballistic to the mildly localized regime, the var(u) increases in an independent and faster power-law fashion than $\langle u \rangle$ does and that other than the disorder strength (or, equivalently, the Thouless energy) there is another relevant energy scale, namely the Fermi energy itself. We reiterate that our main focus is on the finite-size effects on the scaling and the level spacing distributions.

Next, one observes that conductance as a probe, samples the local LSD in the vicinity of the Fermi-energy. This is explicitly seen in the Kubo formula for conductivity which connects the properties of an open quantum system (conductance or reflectance) to those of a closed quantum system (spectrum of the allowed random energy levels). For transport to take place in a Fermi system, a particle from a state below the E_F, must be excited to a state above it, thereby creating a particle-hole pair. The steady-state dynamics of such pairs is responsible for the conduction (transmittance) in the sample. Since conductance in finite-sized systems is non-universal (beyond one-parameter scaling theory; as discussed above), we had conjectured in I that the LSD for finite-sized 1D systems should also be non-universal upto about the same length scale (i.e., about 2ξ) for the state with the largest ξ (usually the band centre E = 0 of a pure system obeying a tight binding hamiltonian). Thus, we focus on presenting the LSD of finite and closed quantum chains. The results presented below should amply support our conjecture in I. The other reason for focussing on finite chains is that many of the current experiments on mesoscopic fluctuations and quantum chaos are indeed done on low-dimensional and small-sized systems (even zero-dimensional, for a quantum dot).

8.1.1 Model

We consider a quantum chain of N lattice points (lattice constant unity), represented by the standard single band, tight binding equation:

$$(E - \epsilon_n)c_n = V(c_{n-1} + c_{n+1}) \tag{8.1}$$

Here E is the fermionic energy , V is the constant nearest neighbour hopping term, ϵ_n is the random site-energy, and c_n is the site amplitude at the n-th site. Without any loss of generality, we choose V=1 to set the energy scale. Further, we choose ϵ_n randomly from an uniform distribution with P(ϵ_n)=1/W only inside the real, symmetric interval [-W/2,W/2]. The N×N tridiagonal matrix (random in the diagonal entry) represented by the above equation is diagonalized using the standard procedures to obtain the N energy levels for various configurations with the same W. Since we are dealing with disorder, we have not used any periodic boundary condition and kept it free. Thus we get a set random energy-levels (E_n; n = 1, 2,....., N) for each configurations is then sorted in an increasing order. In the Figs.8.1(a)-8.1(j), we show the evolution of the density of states (DOS) with the size of the chain, for a fixed (mild) disorder of W = 1.0 and for N = 3, 5, 11, 21, 31, 41, 51, 101, 501, and 1001 respectively. It may be noted here that for this 1D tight binding model, one has a bounded spectrum within [-2,2] in the pure case. In an impure sample, the spectrum will have its bounds expanded since

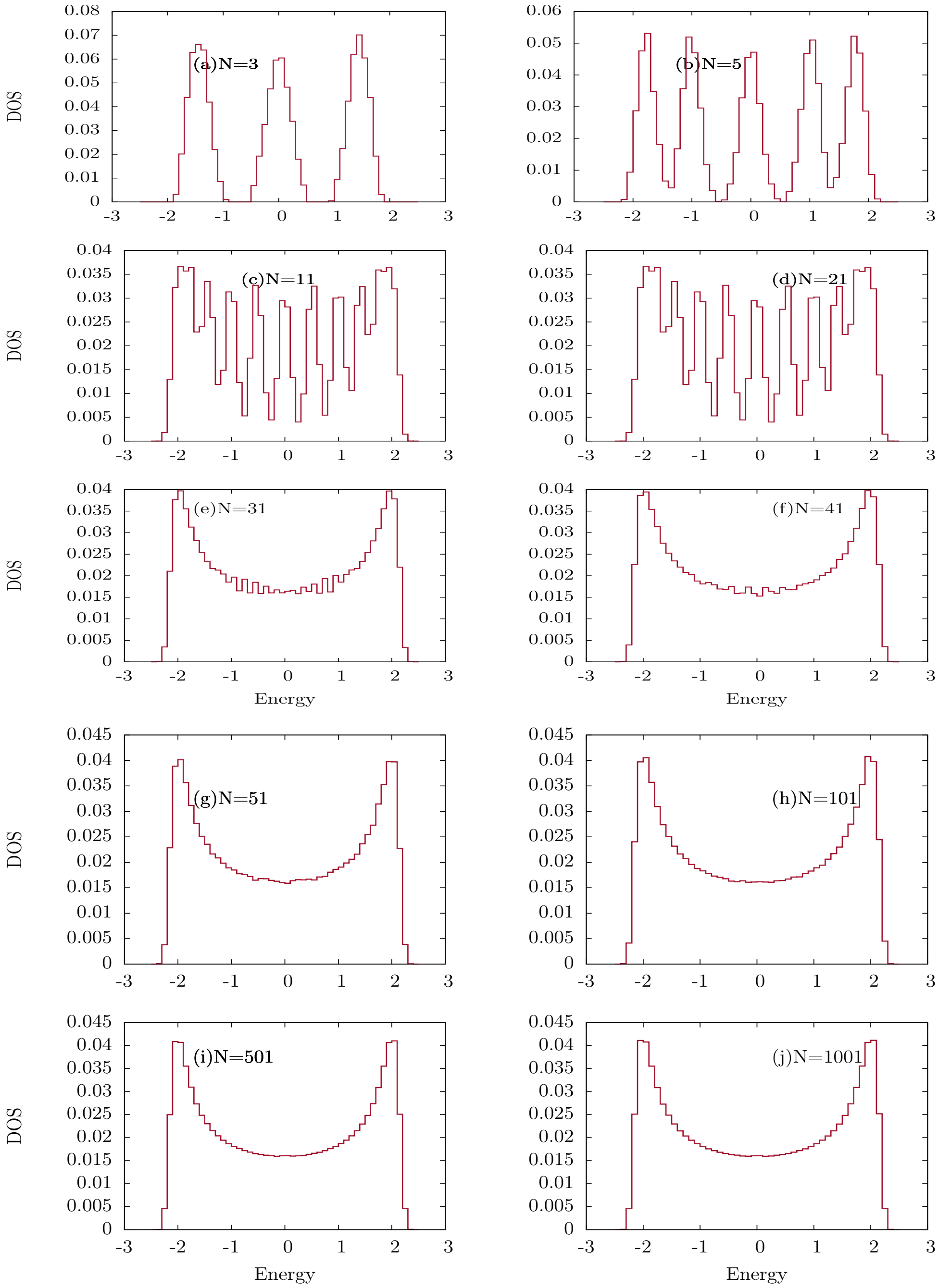

Figure 8.1: *Density of states (DOS) in arbitrary units for samples with a fixed, mild disorder of W=1.0 (in units of the hopping term V) and for different chains of sizes (N) equal to (a)3, (b)5, (c)11, (d)21, (e)31, (f)41, (g)51, (h)101, (i)501, and (j)1001.*

the localized states start appearing above or below the pure band depending on the sign, positive or negative, of the impurity potential. But still the width of these spectra remain bounded. For W=1.0, the width of the spectra remain bounded within [-2.5,+2.5], in units of V, in compliance with the *Gershgorin*'s theorem. Thus, it is clear that a particular realization of a sample of size N will have only N discrete eigenstates, and it will be very difficult to get an idea of the shape of the DOS for that finite size system. Indeed, to demonstrate a smooth enough curve for the DOS of a disordered chain of a small size, we should try to get the eigenstates of as many random realizations for that particular size as possible. In this particular problem, one is in a happy situation because one needs to use a very large number of configurations for a very small N, and a much smaller number of realizations for a large enough N. For example, for any fixed disordered chain of N=3, we have only three states in a energy-domain of width about 5 (in units of V), whereas for an arbitrary configuration with N=1001, we would have a random sample of 1001 states in about the same energy domain. Thus, in the first case of a randomly chosen sample of three possible energy eigenstates, we cannot get any idea of how the DOS, as a probability density function of the parent population, for N=3, looks like. But, in the latter case of one random sampling of 1001 possible energy eigenstates, inside an almost identical bounded energy domain, the shape of the probability density (DOS for N=1001) of the parent population is reasonably clear, even though some fluctuations do still remain prominent. For example, to obtain a reasonably smooth DOS (histogram), for a fixed disorder of W=1.0 (Fig.(8.1)), we have used, with hindsight, 5000 configurations for N=41 and 5000 configurations only for N=1001.

The DOS (in arbitrary units) for $N = 3$ as shown in the Fig.8.1(a), demonstrates that the three sharp energy eigenstates for the pure system has broadened substantially due to the mild disorder of $W = 1$, but there are still gaps in the spectrum between any two consecutive broadened levels. These gaps imply that the system certainly responds to the presence of a disorder by broadening each of the three sharp energy levels and yet it cannot ‘forget’ the predominant effects of order in this case, and reveals it through the finite gaps between any two consecutive broadened levels [as shown in Fig.8.1(a)]. In other words, the energy-states in this system, whose localization lengths are more than three (in lattice units) are much larger in number than those whose localization lengths are less than or equal to three. Thus most of the electronic states in this system of size three, are unaffected by disorder, and so they are almost ballistic in nature.

Fig.8.1(b) shows the DOS for N = 5 and one notices five very prominent peaks therein corresponding to five distinct energy levels in the pure case. But, disorder effects have started to show up somewhat more prominently in the sense that the level broadening is relatively larger and the overlap between two broadened levels are now large enough to rule out any energy-gap between them. The charge carriers are still quasi-ballistic though, since the five peaks are quite well-separated except near their bottommost parts. It may be stressed again that we are putting together the random spectra of many different configurations, not for any averaging process, just for a clearer visualization of the DOS.

The situation changes a little for N=11 [Fig.8.1(c)], since the overlaps are no more confined near the bottom of two consecutive levels. Instead, they move progressively upwards to the peaks themselves, as one moves away from the centre towards either end of the of the spectrum. Indeed, this disorder-induced broadening effect is so substantial near the edges of the spectrum (already for N = 11), that each pair of levels at the two ends of the spectrum have now almost completely merged to form one broad peak each. We know for the pure case, the sharp levels at the two ends of the spectrum cause vertical drops of the DOS to zero at the two band edges. But in the impure case, the levels at the ends of the spectrum (just like the others) do get broader, and the sharp drop of the DOS is softened by an exponential drop to zero.

Consequently, there is a concommitant increase of the spectral width (consistent with similar observations in many previous works). In this case, the exponential tails increases the spectral width from 4V to about 4.5V. The states around the middle of the spectrum, on the other hand, are much less affected by the disorder and, their localization lengths are still much larger than the system size (N = 11 here). Clearly, they are the ones to get localized much later (implying, at a larger disorder, as we keep on hiking up the W progressively). In any case, for N = 11, the system is still in the quasi-ballistic regime.

Next, for N=21 [Fig.8.1(d)], all the levels have become so much broadened, that they are not distinguishable any more. So, the quasi-ballistic behaviour has been completely defeated by the disorder effects, and the only remnants of the quasi-ballisticity of the 21 sharp energy levels for any arbitrary configurations (including the pure case) appear, collectively for a finite yet large number of configurations (used at least 5000 of them to make this histogram for N=21) in the form of large random fluctuations near the central one-third portion of the spectrum. So, the system is not quasi-ballistic anymore, but is in the weakly localized regime for the states around the centre of the spectrum and strongly localized for states near the edges. For example, using the Thouless formula (demonstrated to be quite reasonable in our previous works with such a mild disorder like W/V=1.0), we find the localization length, for an eigenstate with energies close to the band-centre, to be about 24. So, this is consistent with the behaviour we find in the Fig.8.1(d) with a system-size quite close to the maximum localization length of the system. The DOS shown in the Figs.8.1(e) and 8.1(f), for N = 31 and N = 41 looks only qualitatively similar and they show some small quantitative changes. From the Figs.8.1(g)-8.1(j), it is demonstarted further that the DOS as a probability density function changes even more imperceptibly for sizes beyond a few hundreds, and give us no further information about the localization (or lacks thereof) properties.

Next, we look at the level spacing distribution (LSD). We obtain (N-1) level spacings (s=$E_{n+1} - E_n$) for each configuration. Next we obtain the normalized histogram P(x) representing the LSD with the scaled dimensionless level spacings x=s/$\langle s \rangle$, where $\langle s \rangle$ is the average (nearest neighbour) level spacing. The more the number of configuration we choose, the smoother is the LSD. We would like to present our results in two different ways. In the former, keeping the length L = (N-1) fixed, we will keep on changing the disorder W from very small to quite large values. In the latter presentation we will do just the opposite, namely, that we will hold the disorder W fixed and change L from very small to fairly large values. As we find out, both the ways of presentation has some complementary aspects to display.

In the Figs.8.2(a)-8.3(j), we present the LSD for systems of size N = 51 using 5,000-10,000 configurations for various W starting from an almost pure (quasi-ballistic) sample with W=10^{-5} to a fairly strong disordered system with W = 10.0. In the case of the Fig.8.2(a), the system is almost periodic and the P(x) has a highly peaked structure with large gaps for small x. The gaps tend to disappear only near large x. All the peaks have the same height equal to 100, except a slightly smaller single one in the middle reminding us that there is minute disorder in the system. In the Fig.8.2(b), where W = 10^{-3}, the gaps are almost as before, but the maximum peak height is smaller (about 80), and hence the peaks have become broader (indeed at large x some of them have even merged together). Further, peak heights have become more random in response to the stronger disorder than in Fig.8.2(a). In the next Fig.8.1(c) for W=10^{-2}, the peak heights become even smaller but wider, with the largest peak very close to the upper bound of x, where P(x) drops down to zero with a very sharp band-edge like discontinuity.

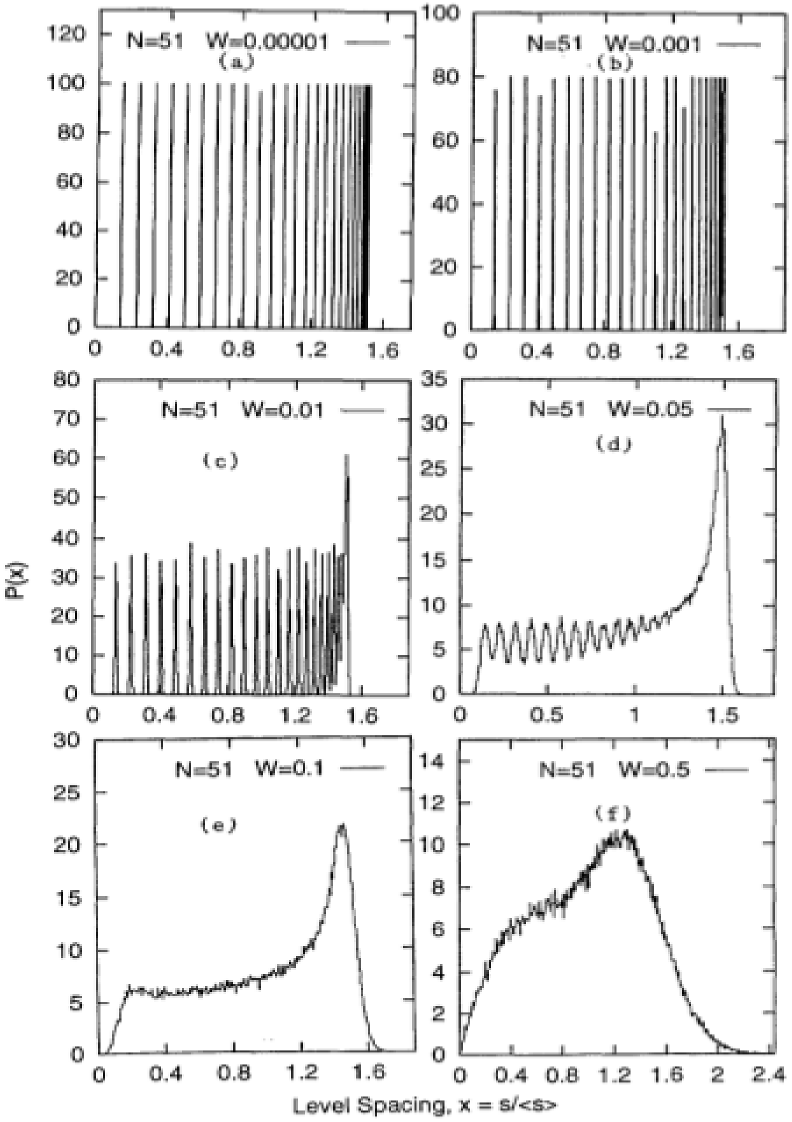

Figure 8.2: *Normalized level spacing distributions P(x) (as the function of a dimensionless level spacing x=s/⟨s⟩; where ⟨s⟩ is the level spacing for a particular case) of a 1-D disordered system of a fixed size N= 51 and varying disordered strengths (W/V) equal to (a) 0.00001, (b) 0.001, (c) 0.01, (d) 0.05,(e) 0.1,(f) 0.5.*

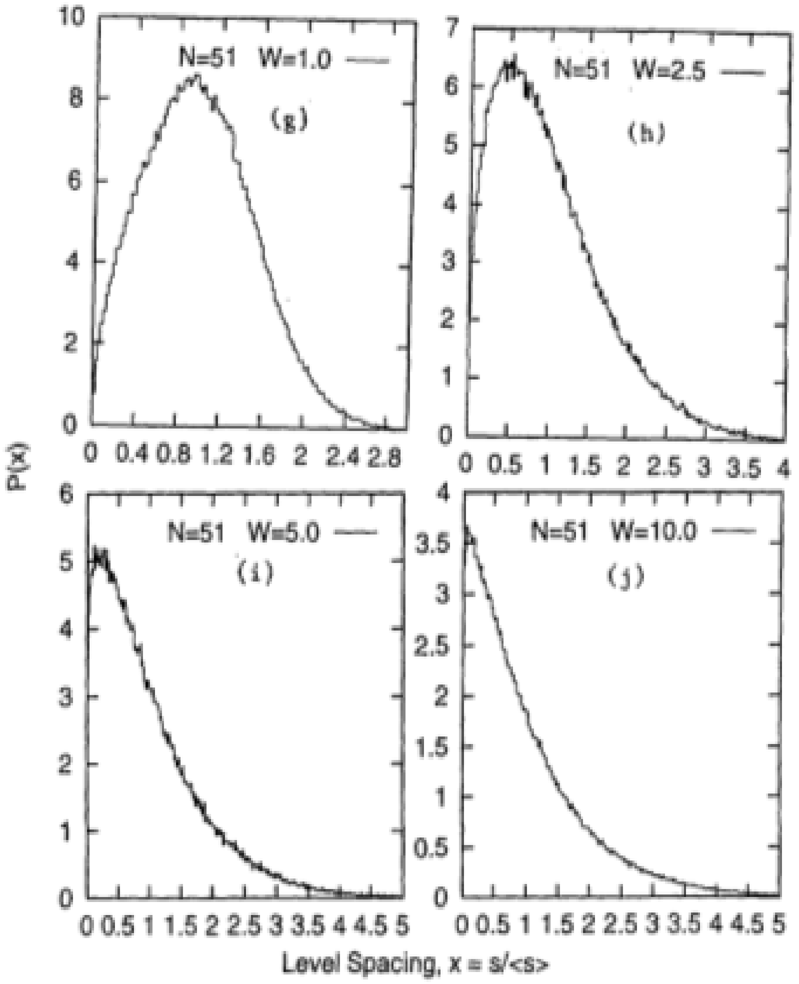

Figure 8.3: *Normalized level spacing distributions P(x) (as the function of a dimensionless level spacing* $x{=}s/\langle s\rangle$*; where* $\langle s\rangle$ *is the level spacing for a particular case) of a 1-D disordered system of a fixed size N= 51 and varying disordered strengths (W/V) equal to (g) 1.0, (h) 2.5, (i) 5.0, and (j) 10.0.*

But, it may be noted that the fragmented structure of P(x) still remains, as a memory of its relatively ordered situation. The concommitant gaps are the signatures of an almost ballistic regime, which implies that the localization lengths of almost all the states are larger than the system size chosen (L = 50). In Fig.8.2(d) for W = 0.05, the gaps between the peaks have completely disappeared, and the distribution at low x has a very interesting oscillatory form, but for a strong repulsion (gap) upto $x \leq x_0 \simeq 0.06$. This seems to be the typical behaviour of P(x) in the quasi-ballistic regime. In this regime, the band-edge like behaviour (at large x) beyond the largest peak has transformed into a less sharp decay. In Fig.8.2(e) for W = 0.1, the oscillatory pattern of P(x) has completely vanished, indicating that the localization effects have started becoming prominent. But, the behaviour is still metal-like in the sense that P($x = 0$) =0 (level-repulsion).

Yet, the LSD is qualitatively different from a Wigner-Dyson (WD) type, first because P(x) = 0 upto $x_0 = 0.03$ (note that x_0 is smaller than the same for W = 0.05) and next because a small hump appears near $x = 0.2$ followed by a relatively large quasi-flat region leading to a much larger second peak (at $x \simeq 1.5$) which finally decays very sharply quite close to zero near $x \simeq 1.7$. Thus this case still indicates a much stronger level repulsion than in the case of a Wigner-Dyson distribution, particularly because P(x) has an interesting double-peaked structure. This double peaked structure is more prominent in Fig.8.2(f) for W = 0.5. But, the peaks have come closer together with the smaller one at $x \simeq 0.5$ and the larger one at $x \simeq 1.2$. Further the decay beyond the larger peak is slower than before (P($x > 2.4$) $\simeq 0$), and while P($x = 0$) = 0, P($x > 0$) > 0. Clearly, this LSD is approaching a WD distribution, even though it is qualitatively very different from a WD form. For a mild disorder W = 1.0 as in Fig.8.3(g), the double-peaked structure has disappeared (the two peaks merge), and the LSD is qualitatively quite similar to a WD type. In the case of both the Fig.8.3(h) and Fig.8.3(i) for W = 2.5 and 5.0 respectively, again we have something very different from a WD in the sense that P($x = 0$) > 0 (level repulsion has disappeared), but on the other hand there is a single, broad peak at a finite $x > 0$, indicating the presence of some remnants of metal-like correlations. Thus these two P(x)'s seem to be a combination of a WD distribution and a Poisson distribution. Physically, this seems to indicate that some of the states are localized and others are extended for this finite sized sample. It is reminiscent of the existence of pre-localized states [134]. Finally, for a large disorder (W = 10.0) as shown in Fig.8.3(j), even the largest localization length at E = 0 is much smaller than the system size (L = 50). Hence all the states are strongly localized, and we get back the universal (Poisson) distribution in 1D in the thermodynamic (N $\rightarrow \infty$) limit.

Next, we would like to show pictorially in the Figs.(8.4-8.5), the evolution of the LSD as a function of the system size N, for a fixed, mild disorder strength W/V = 1.0 (V = 1.0 as stated before). Note that for this disorder, $\xi \simeq$100. In contrast with Figs.(8.2-8.3), all the LSD's are continuous here because we are probing the quasi-ballistic regime not with an extremely small disorder, but with a mild disorder and very small length of, say N = 3, as in Fig.8.4(a). The LSD shows no fragmentation or any oscillatory behaviour and is rather narrow with a single global peak at $x \simeq 1.0$ and a fast decay practically to zero beyond $x = x_0 \simeq 1.4$. Thus there is no sign of quasi-ballisticity and the effect of disorder is felt even at this small length. But the P(x) shows a much stronger level repulsion than in the WD case in the sense that P(x) = 0 upto any $x \leq x_0 \simeq 0.7$ [compare with the cases of Fig.8.2(d) and Fig.8.2(e)]. Almost similar is the case of Fig.8.4(b) for N = 11, where the very strong level repulsion is somewhat reduced in the sense that the initial gap in P(x) extends only upto an $x_0 \simeq 0.075$ (this is not so clear from the figure, but becomes evident on a log-log plot, which gives a power-law behaviour for small x: P(x) $\sim$ $(x - 0.075)^{\beta}$ with $\beta \simeq 2.2$).

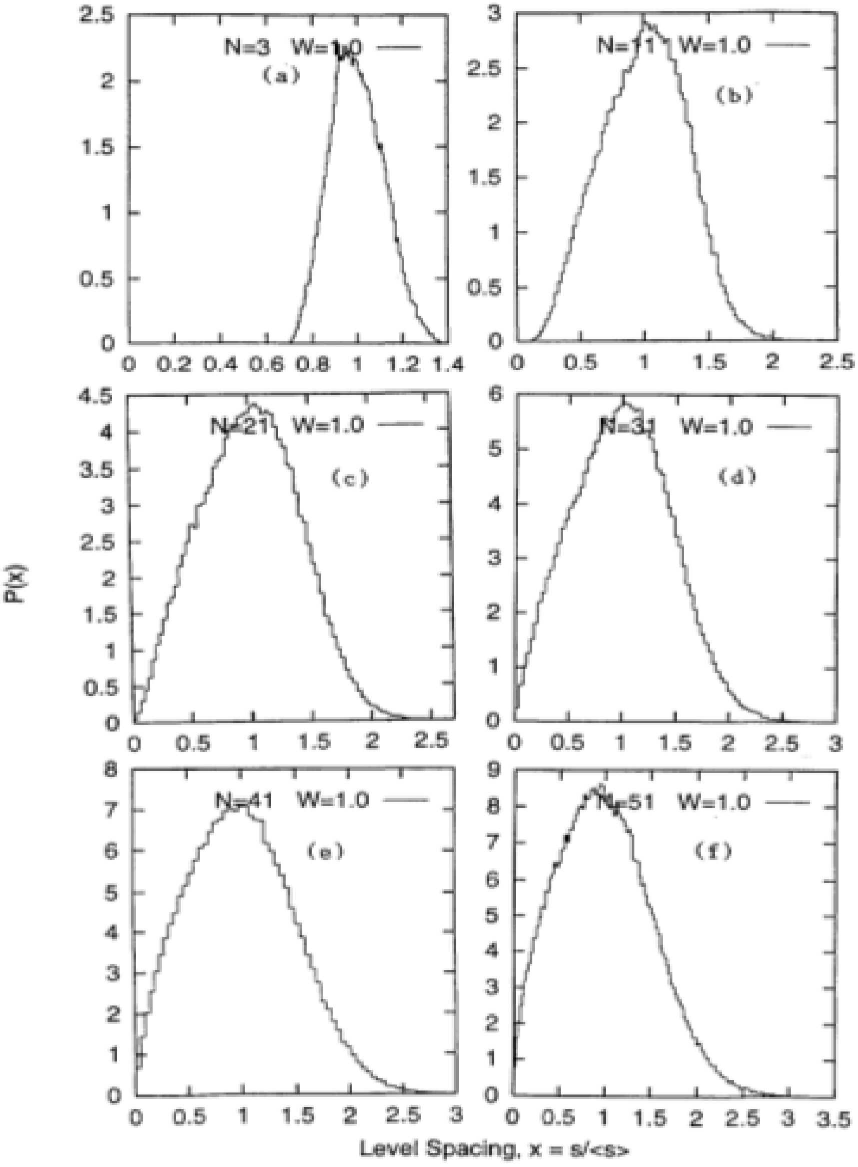

Figure 8.4: *Normalized level spacing distributions (as in fig.1) of a 1-D disordered system for a fixed and small disorder W/V = 1.0 and varying sizes (N) equal to (a) 3, (b) 11, (c) 21 ,(d) 31, (e) 41, and (f) 51.*

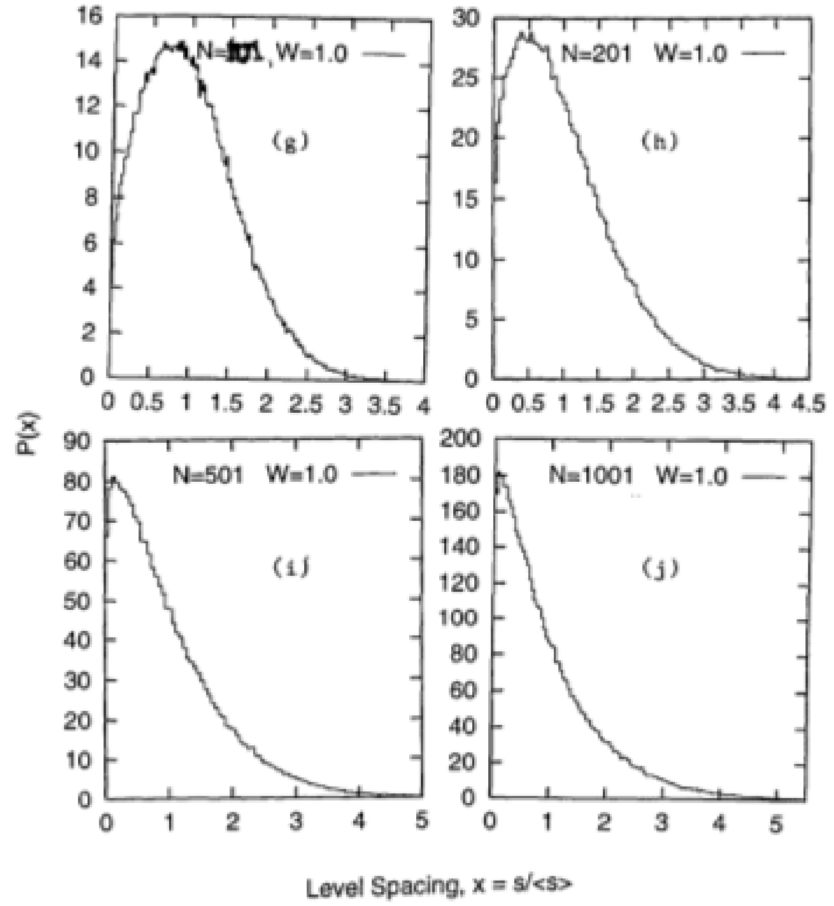

Figure 8.5: *Normalized level spacing distributions (as in fig.1) of a 1-D disordered system for a fixed and small disorder W/V = 1.0 and varying sizes (N) equal to , (g) 101,(h) 201, (i) 501, and (j) 1001.*

The cases of Figs.8.4(c-f) for N = 21, 31, 41 and 51 respectively, looks qualitatively like WD, but the exponent β keeps decreasing from about 2 to 0.58 for these cases. To be more explicit, we show in Fig.(8.6) the double-logarithmic plots of some of these P(s)'s for small s ≤ 0.1. While a $\beta < 1$ indicates a weaker level repulsion than in WD and hence seems surprising, one may find its origin in the Fig.8.2(e-f)

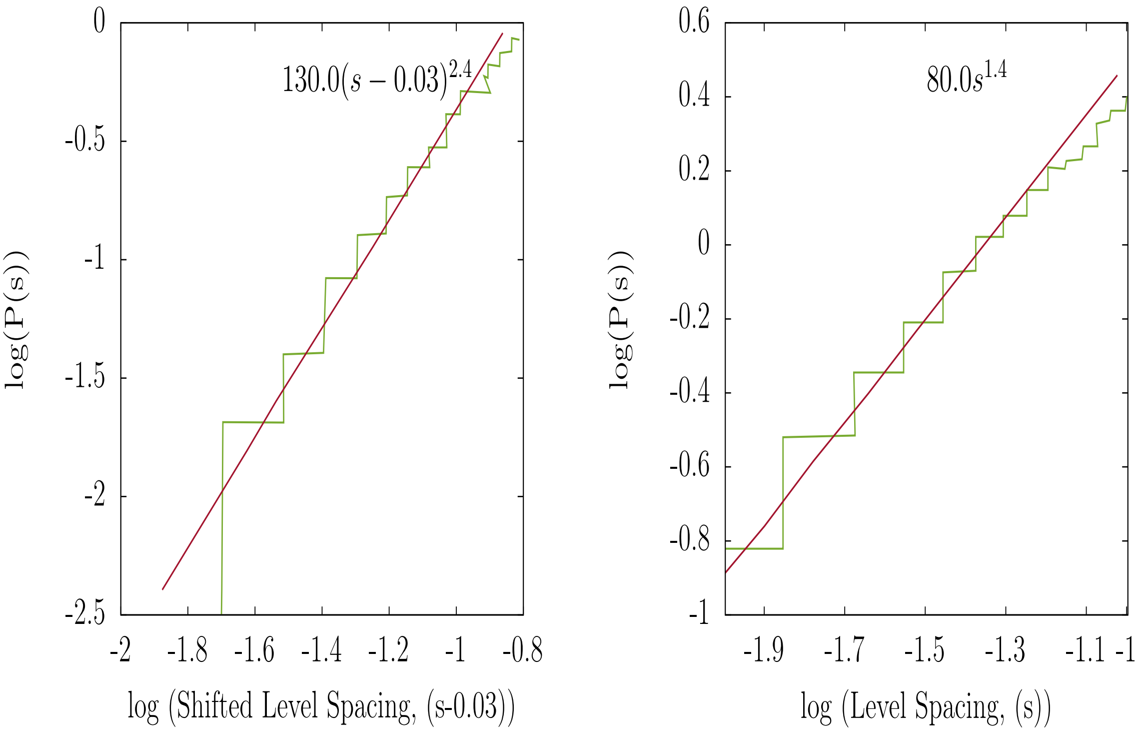

Figure 8.6: *Double-logarithmic plots of the level spacing distributions for small x.*

and Fig.8.3(g), where the weaker peak at small x slowly comes closer to the stronger peak and gives the LSD a convex shape upto the single global peak (implying a β < 1). For still larger sizes of N = 101, 201, and 501 as shown in the Figs.8.5(g-i) respectively, the LSD seems to be a mixture of WD and Poisson type distributions and hence seems to indicate the existence of pre-localized states [134] as in the cases of the Figs.8.3(h) and Figs.8.3(i). Finally, in the case of Fig.8.5(j) for N = 1001, L $\simeq 10\xi(\mathrm{E}=0)$, but the LSD does not yet seem to have reached the universal Poisson form (consistent with I). In contrast, for the case of Fig.8.3(j), L $\simeq$ 20 ξ (E = 0) and hence in conformity with our work in I, shows a Poisson distribution.

8.2 Conclusion and summary

To summarise and to draw some conclusions, we hope to have shown that finite-sized 1-D disordered systems do possess interesting properties in the mesoscopic regime (either for L$\rightarrow \infty$ at a temperature T $\rightarrow 0^+$, or L$< l_\phi$, where l_ϕ is the inelastic scattering length or the phase decoherence length due to scatterings with phonons at a T > 0). For example, we had already shown that a UCF of about $0.3e^2$/h does occur in the 1-D disordered system [131] around the quasi-diffusive to the weakly localized regime (L$\sim \xi/2$ to about ξ). Further, from the ballistic to the mildly localized regime ($\sim 2\xi$, independent of the Fermi energy E_F), we observe a two-parameter scaling [133], in the sense that the average $\langle u \rangle \sim$ L almost right from the quasi-ballistic regime onwards. But, as we show in I as well as with additional work here, var(u)$\sim L^\kappa$ where $\kappa = \kappa(E_F) >$1 is an independent exponent in the regime L=0 to L $\simeq 2\ \xi$. Of course, in the asymptotic limit L$\rightarrow \infty$ (indeed for L$\geq 20\xi$), the behaviour crosses over to $\kappa \rightarrow 1^+$, which is consistent with one-parameter scaling [129]. The reason for the above behaviour for finite size open quantum systems was found to be that the phase (coherent wave nature) ϕ of the electron's reflection co-efficient follows a distribution $P_L(\phi)$ which is most of the times far from uniform, and continues evolving as a function of L towards its stationary form $P_\infty(\phi)$ only for L$\gg 2\xi$. In the case of a finite, closed quantum system, we did look at the finite number of random energy eigenstates and the corresponding finite number of random nearest level spacings (s). Kubo formula indicates that the $P_L(s)$ (random LSD) should also be unusual in the same regime in which the mesoscopic conductance fluctuation is so, i.e., in the two-parameter scaling regime. Indeed, one observes a very strong level-repulsion (much stronger than in the case of Wigner-Dyson) in the quasi-ballistic regime. We have seen that the deviations from Wigner (mean LSD) in quasi-ballistic to quasi-diffusive domains, which means that quasi-UCF exists. Level spacing distribution crosses over to the regular Poisson (exponentially) distribution at large length limit. Typically, the exponent β in the power-law prefactor of $P_L(x)$ where x=s/$\langle s \rangle$ is the scaled level spacing, as obtained from small x is significantly larger than unity. As the system crosses over through the diffusive regime, β seems to decrease to values less than unity. In the mildly localized regime (L$\sim 2\xi$), there seems to be a non-zero probability of having x=0, and yet there is a Wigner-Dyson-like peak before the eventual decay of the $P_L(x)$ for large x. This is certainly quite unusual and seems to indicate that there are small clusters of pre-localized states [134] in some energy regime and some infinite clusters of extended states in another energy regime. Finally, in the large length/disorder limit, the extended states vanish, and one gets back the universal Poissonian behaviour for $P_{L\rightarrow\infty}(x)$. We have a disordered quantum chain (d=1):meso/nano system. E is the fermionic energy and ϵ is the random disorder. Our hamiltonian is random, so energy values are also random in this case. In our calculation we have worked out two cases. Firstly we changed disorder slowly and fixed the sample size. In the other case we have changed sample size slowly and fixed the disorder. In both the ways of presentation has some complementary aspects to display. In our observation we have seen that LSD shows WD distibution behavior for enough sample size and when sample size is large it shows PD behavior. For intermediate disorder or intermediate sample size we see that LSD seems to be a combination of a WD distribution and Poisson distribution. It is known that PD shows localized states and WD distribution shows extended states. Thus, in the intermediate regime level spacing statistics seems to indicate that some of the states are localized and others are extended for finite sized sample. It is reminiscent of the existence of pre-localized states, before the thermodynamic limit sets in. The problem of transition between localized and extended states in disordered system is analogous to the phase transition problem in several aspects. It may be expected that the state at the localization transition point should exhibit some critical behavior [135]. Since our system follows Power law behavior. It has been discussed in [134] that the multifractality is due to the existence of prelocalized states which are characterized by a power law form of statistically averaged. We have seen in our results that the deviations from Wigner in quasi-ballistic to quasi-diffusive domains, which means that quasi-UCF exists. Whereas pre-localized states exists when distribution is a mixture of WD distribution and PD.

Conclusions and Future Scope

In this thesis, we have investigated Nano-Scale physics using NEGF and RMT methods. Under NEGF method, we investigated the device channel, output characteristics and transmission of dual gate nanoscale MOSFETs and SWCNT based MOSFETs. We also studied the transmission of ZGNR using NEGF method. The device is modeled as an Open Quantum System and the Schrodinger equation for the channel gets modified as [EI-H-$\sum$](ψ)=S, which is responsible for the broadening of the channel density of states and for invoking eigenstates of finite lifetimes. The Physics of the Nano-Scale device is studied here using Density Matrix formalism. The device is first treated as a closed system and its channel density obtained as a function of gate voltages. Here, we see the role of the effective mass and how it is related to the size quantization. We apply a self-consistent scheme to solve the Schrodinger and Poisson equations in tandem. Next, we treated the device as a open quantum system and studied its output characteristics using NEGF method. We could reproduce all the relevant Physics of these devices. We also studied the transport properties of ZGNR based system. Under this, we studied its transport properties in the confined region of potential well.

In the second part of the thesis we have shown that finite-sized 1-D disordered systems do possess interesting properties in the mesoscopic regime. For example we had already shown that a UCF of about $0.3\frac{e^2}{h}$ does occur in the 1-D sytem [131] around the quasi-diffusive to the weakly localized regime. Further, from the ballistic to the mildly localized regime, we observe a two-parameter scaling [133], in the sense that the average $\langle u\rangle \sim$ L almost right from the quasi-ballistic regime onwards. But, as we show in I as well as with additional work here, var(u)$\sim L^{\kappa}$ where $\kappa = \kappa(E_F)$ > 1 is an independent exponent in the regime L=0 to L $\simeq 2\ \xi$. Of course, in the asymptotic limit L$\rightarrow \infty$ (indeed for L$\geq 20\xi$), the behaviour crosses over to $\kappa \rightarrow 1^{+}$, which is consistent with one-parameter scaling [129]. The reason for the above behaviour for finite size open quantum systems was found to be that the phase (coherent wave nature) ϕ of the electron's reflection co-efficient follows a distribution $P_L(\phi)$ which is most of the times far from uniform, and continues evolving as a function of L towards its stationary form $P_{\infty}(\phi)$ only for L$\gg 2\xi$. In the case of a finite, closed quantum system, we did look at the finite number of random energy eigenstates and the corresponding finite number of random nearest level spacings (s). Kubo formula indicates that the $P_L(s)$ (random LSD) should also be unusual in the same regime in which the mesoscopic conductance fluctuation is so, i.e., in the two-parameter scaling regime. Indeed, one observes a very strong level-repulsion (much stronger than in the case of Wigner-Dyson) in the quasi-ballistic regime. We have seen that the deviations from Wigner (mean LSD) in quasi-ballistic to quasi-diffusive domains, which means that quasi-UCF exists. Level spacing distribution crosses over to the regular Poisson (exponentially) distribution at large length limit. Typically, the exponent β in the power-law prefactor of $P_L(x)$ where x=s/$\langle s\rangle$ is the scaled level spacing, as obtained from small x is significantly larger than unity. As the system crosses over through the diffusive regime, β seems to decrease to values less than unity. In the mildly localized regime (L$\sim 2\xi$), there seems to be a non-zero probability of having x=0, and yet there is a Wigner-Dyson-like peak before the eventual decay of the $P_L(x)$ for large x. This is certainly quite unusual and seems to indicate that there are small clusters of pre-localized states [134] in some energy regime and some infinite clusters of extended states in another energy regime. Finally, in the large length/disorder limit, the extended states vanish, and one gets back the universal Poissonian behaviour for $P_{L\to\infty}(x)$.

References

[1] M. Lundstrom, *Fundamentals of Carrier Transport*, 2nd ed. (Cambridge University Press, 2009).

[2] S. Datta, *Quantum Transport: Atom to Transistor*, 2nd ed. (Cambridge University Press, 2005).

[3] R. Landauer, Journal of Mathematical Physics **37** (1996).

[4] R. Venugopal, M. Paulsson, S. Goasguen, S. Datta, and M. S. Lundstrom, Journal of Applied Physics **93**, 5613 (2003).

[5] R. Venugopal, S. Goasguen, S. Datta, and M. S. Lundstrom, Journal of Applied Physics **95** (2004).

[6] V. Vyurkov, I. Semenikhin, S. Filippov, and A. Orlikovsky, Solid-State Electronics **70**, 106 (2012), Selected Full-Length Papers from the {EUROSOI} 2011 Conference.

[7] Q. Gao, Y. Ouyang, and J. Guo, Journal of Applied Physics **109** (2011).

[8] H. Jiang and W. Cai, Journal of Computational Physics **229**, 4461 (2010).

[9] P. Vogl and T. Kubis, Journal of Computational Electronics **9**, 237 (2010).

[10] J. Maassen, F. Zahid, and H. Guo, Phys. Rev. B **80**, 125423 (2009).

[11] J. H. Oh, D. Ahn, Y. S. Yu, and S. W. Hwang, Phys. Rev. B **77**, 035313 (2008).

[12] R. Golizadeh-Mojarad and S. Datta, Phys. Rev. B **75**, 081301 (2007).

[13] R. Martel *et al.*, Phys. Rev. Lett. **87**, 256805 (2001).

[14] L. Zhuang, L. Guo, and S. Y. Chou, Applied Physics Letters **72** (1998).

[15] K. Hiruma *et al.*, Journal of Applied Physics **77** (1995).

[16] W. E. W. F. S. L. C. M. Dai, Hongjie, Nature **375**, 1920 (1995).

[17] T. Drkop, S. A. Getty, E. Cobas, and M. S. Fuhrer, Nano Letters **4**, 35 (2004).

[18] G. J. W. Q. L. M. D. H. Javey, Ali, Nature **424** (2003).

[19] P. L. McEuen, M. S. Fuhrer, and H. Park, IEEE Transactions on Nanotechnology **1**, 78 (2002).

[20] B. J. van Wees *et al.*, Phys. Rev. Lett. **60**, 848 (1988).

[21] F. J. Dyson, Journal of Mathematical Physics **3** (1962).

[22] H.-J. Stockmann, *Quantum chaos:an introduction*, 2nd ed. (Cambridge University Press, 1999).

[23] C. Porter, *Statistical Theories of Spectra: Fluctuations*, 1st ed. (Academic Press Inc, 1965).

[24] D. K. Ferry, S. M. Goodnick, and J. Bird, *Transport in Nanostructures*, 2 ed. (Cambridge University Press, 2009).

[25] A. Svizhenko, M. P. Anantram, T. R. Govindan, B. Biegel, and R. Venugopal, Journal of Applied Physics **91** (2002).

[26] S. Datta, *Electronic Transport in Mesoscopic Systems (Cambridge Studies in Semiconductor Physics and Microelectronic Engineering)* (Cambridge University Press, 1997).

[27] R. Venugopal, Z. Ren, S. Datta, M. S. Lundstrom, and D. Jovanovic, Journal of Applied Physics **92** (2002).

[28] S. Datta, Phys. Rev. B **40**, 5830 (1989).

[29] W. H. Press, B. P. Flannery, S. A. Teukolsky, and W. T. Vetterling, *Numerical Recipes in C: The Art of Scientific Computing, Second Edition* (Cambridge University Press, 1992).

[30] S. E. Laux, A. Kumar, and M. V. Fischetti, Journal of Applied Physics **95** (2004).

[31] B. Brar, G. D. Wilk, and A. C. Seabaugh, Applied Physics Letters **69** (1996).

[32] L. R. Ram-Mohan, K. H. Yoo, and J. Moussa, Journal of Applied Physics **95** (2004).

[33] J. Guo and M. S. Lundstrom, IEEE Transactions on Electron Devices **49**, 1897 (2002).

[34] J.-H. Rhew, Z. Ren, and M. S. Lundstrom, Solid-State Electronics **46**, 1899 (2002).

[35] S. Datta, Superlattices and Microstructures **28**, 253 (2000).

[36] G. Iannaccone, Microelectronics Journal **36**, 614 (2005), European Micro and Nano SystemsEMN 2004.

[37] A. Girdhar, C. Sathe, K. Schulten, and J.-P. Leburton, Proceedings of the National Academy of Sciences **110**, 16748 (2013), http://www.pnas.org/content/110/42/16748.full.pdf.

[38] Y. M. Lin *et al.*, IEEE Electron Device Letters **31**, 68 (2010).

[39] G. Liang, N. Neophytou, D. E. Nikonov, and M. S. Lundstrom, IEEE Transactions on Electron Devices **54**, 677 (2007).

[40] M. D. R Saito, G Dresselhaus, *Physical properties of CNT*, first ed. (Imperial college Press, 1998).

[41] R. Lake and S. Datta, Phys. Rev. B **45**, 6670 (1992).

[42] P. Havu, V. Havu, M. J. Puska, and R. M. Nieminen, Phys. Rev. B **69**, 115325 (2004).

[43] J. Wang, E. Polizzi, and M. Lundstrom, Journal of Applied Physics **96** (2004).

[44] H. Li and G. Li, Journal of Applied Physics **116** (2014).

[45] A. I. Khan, M. K. Ashraf, and A. Haque, Journal of Applied Physics **105** (2009).

[46] A. Trellakis, A. T. Galick, A. Pacelli, and U. Ravaioli, Journal of Applied Physics **81** (1997).

[47] T. Kubis and P. Vogl, Phys. Rev. B **83**, 195304 (2011).

[48] F. O. Heinz and A. Schenk, Journal of Applied Physics **100** (2006).

[49] G. S. H. Pau, Phys. Rev. B **78**, 155425 (2008).

[50] E. Polizzi and N. Ben Abdallah, Phys. Rev. B **66**, 245301 (2002).

[51] S. Datta, Nanotechnology **15**, S433 (2004).

[52] *Carbon Nanotubes: Advanced Topics in the Synthesis, Structure, Properties, and Applications .*

[53] S. Datta, *Lesson learn from nanoelectronics*, first ed. (Cambridge University Press, 2016).

[54] S. Datta, Superlattices and Microstructures **28**, 253 (2000).

[55] S. Barbastegan and A. Shahhoseini, Modern Physics Letters B **30**, 1650125 (2016).

[56] R. S. Muller and T. I. K. with Mansun Chan, *Device Electronics for Integrated Circuits*, 3 ed. (, 2003).

[57] T. Kerkhoven, A. T. Galick, U. Ravaioli, J. H. Arends, and Y. Saad, Journal of Applied Physics **68** (1990).

[58] I. Tan, G. L. Snider, L. D. Chang, and E. L. Hu, Journal of Applied Physics **68** (1990).

[59] Z. Wu and P. P. Ruden, Journal of Applied Physics **74** (1993).

[60] W. R. Frensley, Rev. Mod. Phys. **62**, 745 (1990).

[61] M. Dresden, Rev. Mod. Phys. **33**, 265 (1961).

[62] E. M. Conwell, *High field transport in semiconductors* (New York : Academic Press, 1967), Includes bibliographical references.

[63] R. Castagn, Physica B+C **134**, 55 (1985).

[64] L. Reggiani and M. Asche, *Hot-electron transport in semiconductors / edited by L. Reggiani ; with contributions by M. Asche ... [et al.]* (Springer-Verlag Berlin ; New York, 1985).

[65] H. U. Baranger and J. W. Wilkins, Phys. Rev. B **36**, 1487 (1987).

[66] S. Datta, *Quantum Transport: Atom to Transistor*, 2nd ed. (Cambridge University Press, 2005).

[67] C. Caroli, R. Combescot, P. Nozieres, and D. Saint-James, Journal of Physics C: Solid State Physics **5**, 21 (1972).

[68] R. Landauer, Physica Scripta **1992**, 110 (1992).

[69] S. Datta, Phys. Rev. B **40**, 5830 (1989).

[70] A. A. Yanik, G. Klimeck, and S. Datta, Phys. Rev. B **76**, 045213 (2007).

[71] S. Pratap and N. Sarkar, AIP Conference Proceedings **1724** (2016).

[72] S. Pratap and N. Sarkar, Studying the conductance and transport in low-dimensional graphene nano ribbon under ballistic regime, in *American Institute of Physics Conference Series*, , American Institute of Physics Conference Series Vol. 1728, p. 020267, 2016.

[73] A. Kumar and P. F. Bagwell, Solid State Communications **75**, 949 (1990).

[74] D. A. Areshkin and B. K. Nikolić, Phys. Rev. B **81**, 155450 (2010).

[75] H. Ren, Q.-X. Li, Y. Luo, and J. Yang, Applied Physics Letters **94** (2009).

[76] M. D. R Saito, G Dresselhaus, *Physical properties of CNT*, first ed. (Imperial college Press, 1998).

[77] D. Bagchi and P. K. Mohanty, Journal of Statistical Mechanics: Theory and Experiment **2014**, P11025 (2014).

[78] J.-S. Wang, J. Wang, and N. Zeng, Phys. Rev. B **74**, 033408 (2006).

[79] M. Y. Han, B. Özyilmaz, Y. Zhang, and P. Kim, Phys. Rev. Lett. **98**, 206805 (2007).

[80] M. P. Anantram and F. Lonard, Reports on Progress in Physics **69**, 507 (2006).

[81] charles kittel, *Introduction to solid state Physics* (Wiley, Boston, MA, October 2004).

[82] K. Nakada, M. Fujita, G. Dresselhaus, and M. S. Dresselhaus, Phys. Rev. B **54**, 17954 (1996).

[83] Y. Zhang *et al.*, Phys. Rev. B **78**, 155413 (2008).

[84] K. Wakabayashi and T. Aoki, International journal of modern physics B **16** (2002).

[85] H.-Y. Deng and K. Wakabayashi, Phys. Rev. B **90**, 045402 (2014).

[86] H.-Y. Deng, K. Wakabayashi, and C.-H. Lam, Journal of the Physical Society of Japan **82**, 104707 (2013), http://dx.doi.org/10.7566/JPSJ.82.104707.

[87] M. Fujita, K. Wakabayashi, K. Nakada, and K. Kusakabe, Journal of the Physical Society of Japan **65**, 1920 (1996), http://dx.doi.org/10.1143/JPSJ.65.1920.

[88] W. Zhang, Scientific Reports **4**, 1920 (2014), http://dx.doi.org/10.1038/srep06320.

[89] J. Kim, M. V. Fischetti, and S. Aboud, Electronic and transport properties of armchair and zigzag sp3-hybridized silicane nanoribbons, in *Computational Electronics (IWCE), 2012 15th International Workshop on*, pp. 1–4, 2012.

[90] S. Pratap, Superlattices and Microstructures **100**, 673 (2016).

[91] Y. Min *et al.*, Physica B: Condensed Matter **430**, 40 (2013).

[92] M. P. L. Sancho, J. M. L. Sancho, and J. Rubio, Journal of Physics F: Metal Physics **14**,

1205 (1984).

[93] R. S. Thomsen, C. and J. Maultzsch, *Introduction, in Carbon Nanotubes: Basic Concepts and Physical Properties* (wiley, 2004).

[94] S. Pratap, Superlattices and Microstructures **104**, 540 (2017).

[95] L. Rosales, C. D. Nunez, M. Pacheco, A. Latge, and P. A. Orellana, ArXiv e-prints (2013), 1306.6051.

[96] G. G. Naumis, M. Terrones, H. Terrones, and L. M. Gaggero-Sager, Applied Physics Letters **95** (2009).

[97] D. J. Griffiths, *Introduction to Quantum Mechanics, 2nd Ed. Prentice Hall, 2005.*, 2^{nd} ed. (Pearson, 2005).

[98] F. Hadjaj, A. Belghachi, A. Halmaoui, M. Belhadj, and H. Mazouz, International Journal of Mathematical, Computational, Physical, Electrical and Computer Engineering **7**, 1713 (2013).

[99] S. Yang *et al.*, Nature Communications **5**, 3493 (2014).

[100] G. E. Mitchell, A. Richter, and H. A. Weidenmüller, Rev. Mod. Phys. **82**, 2845 (2010).

[101] L. D'Alessio, Y. Kafri, A. Polkovnikov, and M. Rigol, Advances in Physics **65**, 239 (2016), 1509.06411.

[102] F. J. Dyson, Journal of Mathematical Physics **3** (1962).

[103] T. Guhr, A. MllerGroeling, and H. A. Weidenmller, Physics Reports **299**, 189 (1998).

[104] M. Mehta and M. Gaudin, Nuclear Physics **18**, 420 (1960).

[105] O. Bohigas, M. J. Giannoni, and C. Schmit, Phys. Rev. Lett. **52**, 1 (1984).

[106] M. V. Berry, **400**, 229 (1985).

[107] C. W. J. Beenakker, Rev. Mod. Phys. **69**, 731 (1997).

[108] Y. Alhassid, Rev. Mod. Phys. **72**, 895 (2000).

[109] A. M. García-García and J. Wang, Acta Physica Polonica A **112**, 635 (2007), 0710.5852.

[110] T. Timberlake, American Journal of Physics **74** (2006).

[111] B. Chirikov and D. Shepelyansky, Scholarpedia **3** (2008).

[112] Y. V. Fyodorov, ArXiv e-prints (2016), 1606.03124.

[113] B. Collins and I. Nechita, Journal of Mathematical Physics **57** (2016).

[114] A. M. Tulino and S. Verdú, Commun. Inf. Theory **1**, 1 (2004).

[115] C. W. J. Beenakker, Rev. Mod. Phys. **87**, 1037 (2015).

[116] D. F. P. Akemann G, Baik J, *The Oxford Handbook of Random Matrix Theory* (Oxford University Press, 2011).

[117] C. W. J. Beenakker, ArXiv e-prints (2009), 0904.1432.

[118] Y. Imry, EPL (Europhysics Letters) **1**, 249 (1986).

[119] P. A. Lee and A. D. Stone, Phys. Rev. Lett. **55**, 1622 (1985).

[120] Nature 137, 344-348 (29 February 1936) — doi:10.1038/137344a0 .

[121] B. Chirikov, F. Izrailev, and D. Shepelyansky, Physica D: Nonlinear Phenomena **33**, 77 (1988).

[122] A. M. Odlyzko, Math. Comp. 48 (1987), 273-308 **48** (1986).

[123] P. A. Lee and T. V. Ramakrishnan, Rev. Mod. Phys. **57**, 287 (1985).

[124] C. W. J. Beenakker, Rev. Mod. Phys. **69**, 731 (1997).

[125] E. P. Wigner, Annals of Mathematics **55**, 7 (1952).

[126] F. J. Dyson, Journal of Mathematical Physics **3**, 1199 (1962).

[127] F. J. Dyson and M. L. Mehta, Journal of Mathematical Physics **4** (1963).

[128] B. I. Shklovskii, B. Shapiro, B. R. Sears, P. Lambrianides, and H. B. Shore, Phys. Rev. B **47**, 11487 (1993).

[129] E. Abrahams, P. W. Anderson, D. C. Licciardello, and T. V. Ramakrishnan, Phys. Rev. Lett. **42**, 673 (1979).

[130] P. A. Mello, Phys. Rev. Lett. **60**, 1089 (1988).

[131] S. Gangopadhyay and A. K. Sen, Phys. Rev. B **46**, 4020 (1992).

[132] M. N. Ganguli and A. K. Sen, Phys. Rev. B **52**, 17342 (1995).

[133] A. K. Sen, Modern Physics Letters B **11**, 555 (1997).

[134] V. I. Fal'ko and K. B. Efetov, Phys. Rev. B **52**, 17413 (1995).

[135] H. Aoki, Journal of Physics C: Solid State Physics **16**, L205 (1983).

List of Publications and Presentations

Peer reviewed International Journals:

- *"Transport properties of Zigzag Graphene Nanoribbons in the confined region of Potential well"*
  Surender Pratap (Superlattices and Microstructures, volume 100(2016)673-682)
- *"Transmission and LDOS in case of ZGNR with and without magnetic field"*
  Surender Pratap (Superlattices and Microstructures, volume 104(2017)540-546)
- *"Comparison of the Self-Consistent Quantum and Semi-Classical Methods for Determining the Channel Electron density of a Dual Gate Nano-Scale MOSFET Under Symmetric and Asymmetric Gate Bias"*
  Surender Pratap and Niladri Sarkar, (Under review)
- *"Study of Physics and Modeling of Certain Technologically Important Nano-Scale MOSFETs as Closed and Open Quantum Systems"*
  Surender Pratap and Niladri Sarkar, (Communicated)
- *"Localization length in quasi one-dimensional case"*
  Surender Pratap and Asok K.Sen, (manuscript under preparation)
- *"Quantum chaos in one-dimensional disordered systems"*
  Surender Pratap and Asok k. Sen, (manuscript under preparation)

Peer reviewed Conference proceedings in Int. Journals:

- *"Application of the self-consistent quantum method for simulating the size quantization effect in the channel of a nano-scale dual gate MOSFET"*
  Surender Pratap and Niladri Sarkar, AIP Conf. Proc. **1665** 120036 (2015)
- *"Studying the conductance and transport in low-dimensional graphene nanoribbon under ballistic regime"*
  Surender Pratap and Niladri Sarkar, AIP Conf. Proc.**1728** 020267 (2016)
- *"Application of a self-consistent NEGF procedure to study the coherent transport with phase breaking scattering in low dimensional systems"*
  Surender Pratap and Niladri Sarkar, AIP Conf. Proc. **1724** 020096 (2016)

List of conferences/schools attended/participated:

- *"National Conference on Condensed Matter Physics"*,

  February 24-25, 2012, **BITS Pilani, INDIA**.

- *"Summer school on Condensed Matter Physics"*,

  April 01-13, 2013, BHU, **Varanasi, INDIA**.

- *"59th DAE Solid State Physics Symposium"*,

  December 16-20, 2014, VIT, **Tamilnadu, INDIA.**

- *"International Conference Condensed Matter & Applied Physics (ICC 2015)"*,

  October 30-31, 2015, GEC, **Bikaner, INDIA.**

- *"India Singapore Symposium in Condensed Matter Physics(8Th)"*,

  February 25-27, 2015, IIT **Kanpur, INDIA.**

- 2nd International Conference on *"ETMN 2015 Emerging Technologies Micro to Nano"*,

  October 24-25, 2015, Manipal University , **Jaipur, INDIA**.

Brief Biography of the Supervisor

Dr. Niladri Sarkar is Assistant Professor in Physics at Birla Institute of Technology & Science Pilani, Pilani Campus. He received his Ph.D. degree from School of Physical Sciences, JNU in 2006. He joined the Physics Department of BITS Pilani, Pilani Campus in December, 2006. He has published several highly cited papers in reputed international journals. His research interests are in the Physics of Quantum Transport. He is actively involved in the area of 'Semiconductor Device Physics' and 'Computational Electrodynamics'. Also, he is interested in 'History of Science'.

Brief Biography of the Student

Mr. Surender Pratap obtained his Masters degree in Theoretical Physics, Department of Physics Jamia Millia Islamia, Delhi in 2009. He cleared his JEST exam in 2010, then he joined Department of Physics, BITS Pilani as a research scholar in July, 2011. He is currently pursuing Ph.D. in the same Department in the area of Theoretical condensed matter physics. His research interests include the Quantum Transport in atomistic scale and localization in different dimensions, Quantum chaos in one-dimensional disordered system. He has published some papers in international journals and few are under review. In addition to this, he has participated and presented his work in several national and international conferences of high repute.